

PL-TR-97-2163

# CRUSTAL WAVEGUIDE EFFECTS ON REGIONAL PHASES IN CHINA AND SOUTHEAST ASIA

Thorne Lay  
Guangwei Fan  
Arthur Rodgers

University of California/Santa Cruz  
Earth Sciences Department & Institute of Tectonics  
Earth & Marine Sciences Building  
Santa Cruz, CA 95064

1 December 1997

Final Technical Report  
11 August 1995 - 11 November 1997

19980413 026

Approved for public release; distribution unlimited



DEPARTMENT OF ENERGY  
Office of Non-Proliferation  
and National Security  
WASHINGTON, DC 20585



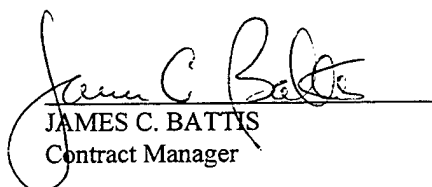
AIR FORCE RESEARCH LABORATORY  
Space Vehicles Directorate  
29 Randolph Road  
AIR FORCE MATERIEL COMMAND  
HANSCOM AFB, MA 01731-3010

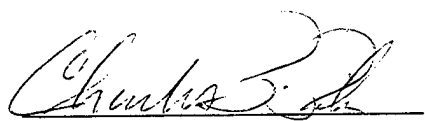
SPONSORED BY  
Department of Energy  
Office of Non-Proliferation and National Security

MONITORED BY  
Air Force Research Laboratory  
CONTRACT No. F19628-95-K-0014

The views and conclusions contained in this document are those of the authors and should not be interpreted as representing the official policies, either express or implied, of the Air Force or U.S. Government.

This technical report has been reviewed and is approved for publication.

  
JAMES C. BATTIS  
Contract Manager

  
CHARLES P. PIKE, Deputy Director  
Integration and Operations Division

This report has been reviewed by the ESD Public Affairs Office (PA) and is releasable to the National Technical Information Service (NTIS).

Qualified requestors may obtain copies from the Defense Technical Information Center. All others should apply to the National Technical Information Service.

If your address has changed, or you wish to be removed from the mailing list, or if the addressee is no longer employed by your organization, please notify AFRL/VSOS-IM, 29 Randolph Road, Hanscom AFB, MA 01731-3010. This will assist us in maintaining a current mailing list.

Do not return copies of the report unless contractual obligations or notices on a specific document requires that it be returned.

# REPORT DOCUMENTATION PAGE

Form Approved  
OMB No. 0704-0188

Public reporting burden for this collection of information is estimated to average 1 hour per response, including the time for reviewing instructions, searching existing data sources, gathering and maintaining the data needed, and completing and reviewing the collection of information. Send comments regarding this burden estimate or any other aspect of this collection of information, including suggestions for reducing this burden, to Washington Headquarters Services, Directorate for Information Operations and Reports, 1215 Jefferson Davis Highway, Suite 1204, Arlington, VA 22202-4302, and to the Office of Management and Budget, Paperwork Reduction Project (0704-0188), Washington, DC 20503.

1. AGENCY USE ONLY (Leave blank)	2. REPORT DATE 1 December 1997	3. REPORT TYPE AND DATES COVERED Final Report 11 Aug. 1995 - 11 Nov. 1997	
4. TITLE AND SUBTITLE  Crustal Waveguide Effects on Regional Phases in China and Southeast Asia		5. FUNDING NUMBERS  F19628-95-K-0014 PE 69120H PR DENN TA GM WU AA	
6. AUTHOR(S) Thorne Lay Guangwei Fan Arthur Rodgers		8. PERFORMING ORGANIZATION REPORT NUMBER	
7. PERFORMING ORGANIZATION NAME(S) AND ADDRESS(ES)  Earth Sciences Department and Institute of Tectonics University of California, Santa Cruz Earth and Marine Sciences Building Santa Cruz, CA 95064		10. SPONSORING / MONITORING AGENCY REPORT NUMBER  PL-TR- 97-2163	
9. SPONSORING / MONITORING AGENCY NAME(S) AND ADDRESS(ES) Air Force Research Laboratory 29 Randolph Rd. Hanscom AFB, MA 01731-3010  Contract Manager: James Battis/VSBI		11. SUPPLEMENTARY NOTES  This research was sponsored by the Department of Energy, Office of Non-Proliferation and National Security, Washington, DC 20585	
12a. DISTRIBUTION / AVAILABILITY STATEMENT  Approved for public release: distribution unlimited		12b. DISTRIBUTION CODE	
13. ABSTRACT (Maximum 200 words) This research program addressed the issue of reducing scatter in regional phase discriminant measures associated with waveguide irregularity. We empirically reduce discriminant measure variance, using along-path measures obtained from data bases for surface topography, crustal thickness, and sedimentary layer thickness. Several path-specific measures are found to have significant correlations with regional discriminant measurements, both before and after correction for propagation distance, for events in China and the Middle East. For station WMQ, in western China, variance reductions two to three times as large as those for distance corrections alone can be achieved by simple empirical models obtained by multiple-regression analysis. Multiple-regression analysis is applied for several path properties to all CDSN stations and broadband station ABKT in the Middle East under this contract. This final report presents four preprints: the first addresses variance reduction of discriminant measures at station WMQ, the second applies the same methodology to all stations in two sub-regions in China. The third applies an azimuthal sector analysis to data for station ABKT, and the fourth applies the multiple regression procedure to ABKT. Two earlier papers sponsored by this contract are now in press.			
14. SUBJECT TERMS  Regional seismic discriminants, regional phases, crustal propagation, nuclear discrimination		15. NUMBER OF PAGES 148	16. PRICE CODE
17. SECURITY CLASSIFICATION OF REPORT Unclassified	18. SECURITY CLASSIFICATION OF THIS PAGE Unclassified	19. SECURITY CLASSIFICATION OF ABSTRACT Unclassified	20. LIMITATION OF ABSTRACT  SAR



## Table of Contents

<b>PREFACE</b>	v
<b>MULTIVARIATE ANALYSIS OF WAVEGUIDE EFFECTS ON REGIONAL SEISMIC PHASES IN WESTERN CHINA</b>	1
Introduction	2
Data	4
Waveguide Path Effects for Model Parameterization	7
Model Results	11
Discussion	23
References	25
<b>REGIONALIZED WAVEGUIDE EFFECTS ON SEISMIC DISCRIMINANTS IN WESTERN CHINA</b>	27
Introduction	29
Data	31
Method	37
Regionalized Path Effects	42
Results of Multivariate Regressions	53
Summary and Conclusions	65
References	67
<b>CALIBRATION OF DISTANCE AND PATH EFFECTS ON REGIONAL P/S DISCRIMINANTS AT STATION ABKT (ALIBEK, TURKMENISTAN): AZIMUTHAL SECTOR REGIONALIZATION</b>	72
Introduction	73
Regional Waveform Data at ABKT and P/S Amplitude Ratio Measurements	76
Distance Corrections and Subdivisions of Data into Azimuthal Sectors	79
Discussion and Conclusions	91
References	95

<b>CALIBRATION OF DISTANCE AND PATH EFFECTS ON REGIONAL P/S DISCRIMINANTS AT STATION ABKT (ALIBEK, TURKMENISTAN): STATISTICAL ANALYSIS OF CRUSTAL WAVEGUIDE EFFECTS</b>	99
Introduction	101
Regional Waveform Data at ABKT and P/S Amplitude Ratio Measurements	103
Crustal Waveguide Profiles	105
Univariate Regressions of P/S Ratios on Crustal Waveguide Parameters	109
Multivariate Regressions of P/S Ratios on Crustal Waveguide Parameters	122
Multivariate Regression Results	124
Discussion and Conclusions	129
References	134

## Preface

This research is directed at improving the performance of regional seismic discriminants by developing new approaches for reducing the scatter in discriminant measures imparted by path-specific waveguide heterogeneity. Conventional procedures for regionalization of discriminant measures involve determining empirical distance-dependence of discriminants for regions that have relatively uniform propagation characteristics, with no blockage of phases. Such approaches essentially assume that the best propagation corrections that can be applied are those for a single, regionally averaged empirical distance trend. While this is a useful and necessary step, there is significant residual variance in all regional discriminants after distance correction, and this scatter intrinsically limits the performance of the discriminants, particularly at low frequencies.

Our previous work demonstrated that consideration of individual path properties allows further empirical reduction of discriminant measure variance, using along-path measures obtained from data bases for surface topography, crustal thickness, and sedimentary layer thickness. We extend this approach in this contract. Several path-specific measures are found to have significant correlations with regional discriminant measurements, both before and after correction for propagation distance, for events in China and the Middle East. For station WMQ, in western China, variance reductions two to three times as large as those for distance corrections alone can be achieved by simple empirical models obtained by multiple-regression analysis. We apply multiple-regression analysis for several path properties to CDSN stations and broadband stations in the Middle East under this contract. This final report presents four preprints: the first addresses variance reduction of discriminant measures at station WMQ, the second applies the same methodology to all stations in two sub-regions in China. The third applies an azimuthal sector analysis to data for station ABKT, and the fourth applies the multiple regression procedure to ABKT. Two earlier papers sponsored by this contract are now in press.

**Multivariate Analysis of Waveguide Effects on Regional Seismic  
Phases in Western China**

by Guangwei Fan and Thorne Lay

Institute of Tectonics, Department of Earth Sciences, University of California, Santa Cruz

submitted to *Bulletin of the Seismological Society of America*, July 31, 1997



**Abstract** Amplitude ratios of short-period regional seismic phases from earthquakes recorded at broadband station WMQ in western China are analyzed for dependence on path-specific crustal structure. Multivariate regression analysis is applied to  $Pg/Lg$ ,  $Pg/Sn$ ,  $Pn/Lg$  and  $Pn/Sn$  ratios in frequency bands of 0.75-1.5 Hz, 1.5-3.0 Hz, and 3.0-6.0 Hz using a suite of path properties, including path length, mean path elevation, variance of topography along the path, rms topographic slope variations, mean crustal thickness and mean sediment thickness. Optimal 3- and 4-parameter models all achieve reductions in variance of the measurements relative to conventional distance corrections alone, with more than factor of two improvements for the low frequency ratios involving  $Pg$ . Reduction in the amplitude ratio scatter is desirable for seismic discrimination applications, and it also provides insight into crustal structure controls on regional wave energy partitioning. Mean path elevation plays an important role for all short-period amplitude ratios, while crustal thickness and sediment thickness affect ratios involving  $Pg$ , and topographic variance and surface slope variations influence ratios involving  $Pn$ . In this instance, strong crustal variations associated with the structure of the Tibetan Plateau are responsible for part of the amplitude variations.

## Introduction

There is great interest in using regional distance seismic signals for monitoring the Comprehensive Test Ban Treaty (CTBT). Regional seismic signals can potentially be used to detect, locate and identify low magnitude sources. One of the primary strategies for source identification with regional signals involves characterizing the relative amounts of  $P$  and  $S$  energy released by a source (e.g.  $Pg/Lg$  ratios), as this reflects source radiation effects expected to differ for earthquakes and explosions. Ideally, such source identification would be based on the regional signals with the highest signal-to-noise ratio,

which is commonly in the 0.5-3 Hz passband. However, it has been found empirically that source discrimination is usually superior at frequencies above 3 Hz (e.g. Walter *et al.*, 1995; Taylor, 1996; Hartse *et al.*, 1997b). While this may be partly due to a lack of source type sensitivity in low frequency wave excitation for crustal events, it does appear that effects associated with source depth, earthquake focal mechanism, and crustal reverberations are more coherent for lower frequencies, with the resulting scatter reducing discriminant sensitivity. Unfortunately, paths in tectonically active regions that present acute CTBT monitoring challenges often have strong attenuation, which limits the bandwidth of regional phases to frequencies below 5 Hz. Improved methodologies for reducing scatter in regional phase *P/S* ratio measurements in the 0.5-3 Hz band are thus very desirable. In the context of event discrimination with a fixed monitoring network, new strategies for reducing the effects of propagation effects (independent of source type) are the primary need, as the only practical approach to reducing source related effects such as radiation pattern involves averaging of multiple station observations.

Propagation in a heterogeneous crustal waveguide is expected to give rise to path-specific variations in regional phase amplitude ratios (e.g., Kennett, 1989; Baumgardt, 1990; Zhang and Lay, 1994; Fan and Lay, 1997), but too little is known about the crust in most regions to accurately predict these effects. As a result, empirical methods are used, even in the calibration of standard distance dependent decay of phase amplitudes. This paper expands on a multivariate regression approach introduced by Zhang *et al.* (1994) and applied to data in Western China by Fan and Lay (1997), hereinafter called Paper 1. Regional phase discriminant measurements are empirically compared to waveguide parameters based on models of large scale crustal properties in western China including topography, crustal thickness and sedimentary basin extent. Multivariate regression models are obtained and can be used to reduce the path effects in the data for separate frequency bands. Paper 1 described the methodology and emphasized the results for *Pg/Lg* measurements. Here, we summarize the multiple regression models obtained for all four of

the common *P/S* discriminant measures, *Pg/Lg*, *Pg/Sn*, *Pn/Lg*, and *Pn/Sn* to further elaborate on this empirical path calibration strategy. Such procedures can be readily incorporated into CTBT monitoring operations. Hartse *et al.* (1997a) describe application of a similar strategy to a separate data set for explosions and earthquakes recorded at stations WMQ and AAK. The empirical relations that are obtained also provide a starting point for quantitative modeling efforts that can be pursued to quantify the underlying wave propagation effects.

## Data

The data set used in this paper involves 87 earthquakes with magnitudes of  $4.5 \leq m_b \leq 6.1$  that occurred between 1988 and 1995 in western China and its vicinity. These events were all recorded on the broadband vertical component at station WMQ, with the path coverage being shown in Figure 1. Observed seismograms show great variability in broadband waveform complexity on the different paths, as shown in Paper 1. To avoid ambiguity in regional phase recognition at very close distances, only events with epicentral distances greater than 240 km are used, with the most distant events being 2100 km from the station. The events are all large enough to have fairly well determined locations as a result of numerous teleseismic detections. For events prior to 1994 we use locations given by the International Seismological Centre (ISC) bulletins, and for events after 1994 we use locations from the USGS Preliminary Determination of Epicenters (PDE) catalog. Only events with focal depths less than 50 km are used in this study, but there are relatively large uncertainties in source depth due to the sparse regional station coverage and the complex crustal and upper mantle structures in the region.

Paper 1 describes the phase measurement procedure in detail. The *Pn* window begins at the onset of the signal (all events are at distances beyond the crossover distance) and ends at the start of the *Pg* window. The *Pg*, *Sn*, and *Lg* windows are between group velocities of 6.2 to 5.2 km/sec, 4.8 to 4.0 km/sec, and 3.6 to 3.0 km/sec, respectively.

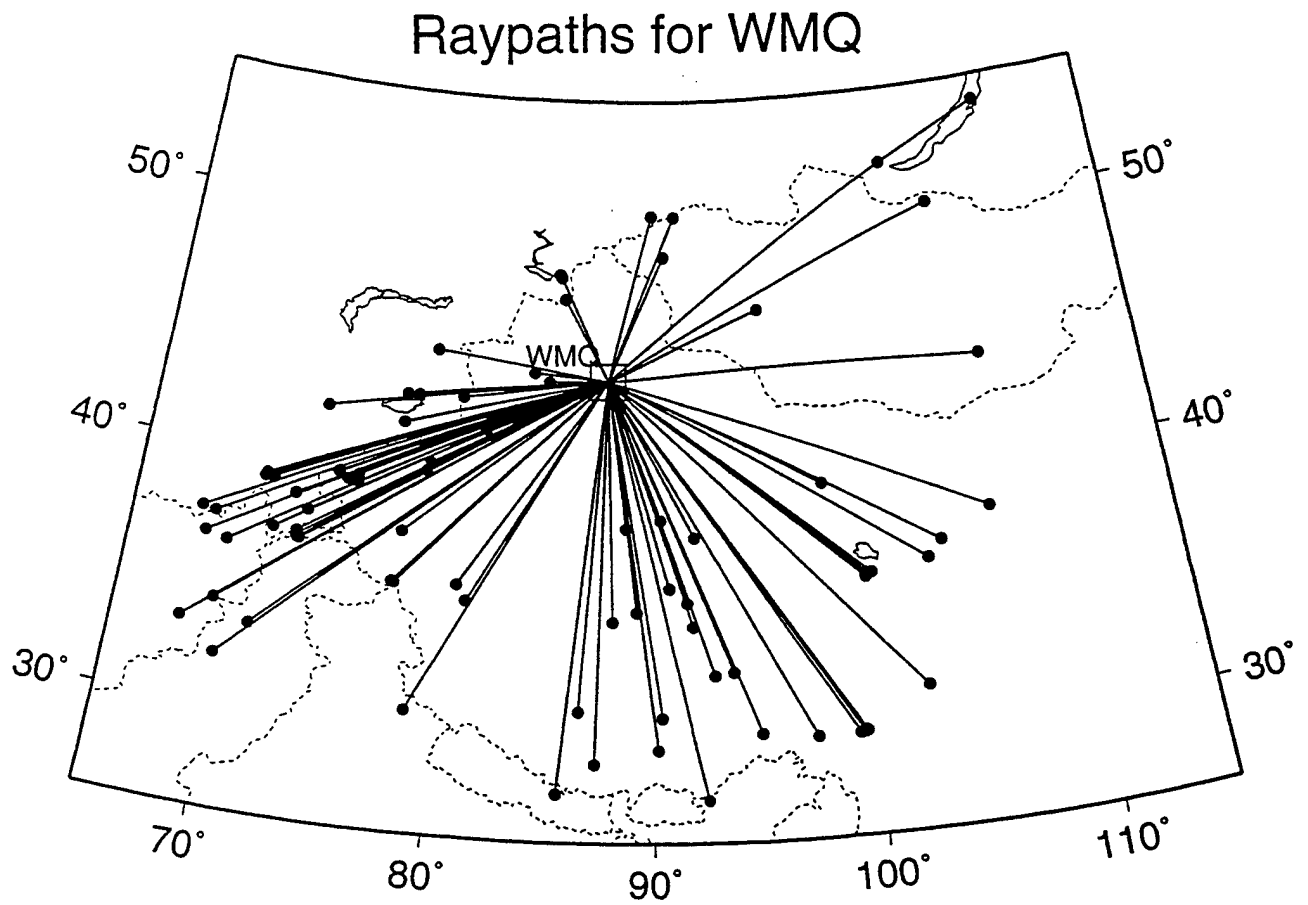


Figure 1. Ray paths from the epicenters of the 87 selected events to the station WMQ in western China.

For each phase, the vertical component broadband records (approximately proportional to ground velocity) were windowed and band pass filtered into four frequency bands: 0.75 to 1.5 Hz, 1.5 to 3.0 Hz, 3.0 to 6.0 Hz, and 6.0 to 9.0 Hz, using Butterworth filters, and rms amplitudes are computed. Noise levels are computed for the filtered seismograms using the rms amplitude in the 10 sec window preceding the manually picked first arrival time. Recordings with  $Pn$  signal-to-noise ratios greater than two are retained. For most of the events, the signal-to-noise ratios are between 10 to 100. We consider only ratios of phases in the same frequency band, which explicitly cancels the instrument effect.

Apart from path length, our knowledge of crustal properties for each path is limited to several independent data bases. The topographic relief data are from the GLOBE (Global Land One-km Base Elevation) project with a spatial resolution of 30 arc-second; relief is the most precisely known attribute of the regional crustal structure. Low resolution models of crustal thickness (Moho depth) and sediment thickness are available from the database compiled by Cornell University. These data were digitized from maps based on deep seismic sounding (DSS) profiles and gridded on a 10 km grid (Fielding *et al.*, 1992). There is no question that the accuracy of maps is limited, but these maps were derived independently from surface topography, and when averaged along any given ray path they probably provide first order average path properties that are not greatly in error in comparison with any point-wise property or local gradient in the properties in these models. Paper 1 shows maps of these crustal properties in the study area.

The great circle paths connecting the earthquake locations and WMQ (Figure 1) sample a large area in western China and its vicinity, with some of the most dramatic topographic features in the world, such as the Tibetan Plateau, and the Tien Shan, Pamir and Hindu Kush Mountains. Many paths project along or across the mountain belts, sedimentary basins or the margins of the Tibetan Plateau. Profiles of topography, Moho depth, and sedimentary layer thickness along each great circle path are extracted and a set of summary parameters for topography and waveguide irregularities calculated. The

topographic parameters are four path-specific measures: mean elevation, rms roughness (variance) of topography, rms slope of topography from point to point along the path, and topographic skewness. We also calculate minimum, maximum, and mean crustal thickness, and maximum and mean sediment thickness along each path. The minimum and maximum measures are local values, and hence subject to much greater uncertainties than the path-averaged mean values, but local extremes may be responsible for important effects such as blockage of phases. Figure 2 is a sample cross-section profile showing the topography and crustal structure along the path for the event of October 19, 1991, which is located in the southern margin of the Tibetan Plateau.

### Waveguide Path Effects and Model Parameterization

Path effects on all  $Pn/Lg$ ,  $Pg/Lg$ ,  $Pn/Sn$ , and  $Pg/Sn$  logarithmic ratios measured in different frequency bands for the 87 events recorded at WMQ have been explored. Paper 1 summarizes the inferred path effects for all of the regional phase ratios measured at WMQ detected using individual linear regressions. All of these regional discriminants show clear distance dependence, and apparently, the progressively accumulating relative attenuation and geometric spreading effects are primary factors controlling regional phase energy ratios. The highest correlations with propagation distance (more than 0.8) are found for the ratios involving  $Pn$ .  $Pg/Lg$ , and  $Pg/Sn$  also display significant distance dependence with the correlation coefficients ranging between 0.4 to 0.7 in the three passbands below 6 Hz. Strong correlations are also found for mean path elevation and surface roughness, with the ratios involving  $Pg$  having stronger correlations with these parameters than with distance. The correlations of  $\text{Log}(Pg/Lg)$  with mean crustal thickness and maximum crustal thickness are higher than those with distance or topography for the 0.75-1.5 Hz band, and comparable for the 1.5-3 Hz band, while  $\text{Log}(Pg/Sn)$  has similar correlations with crustal thickness, mean elevation and distance. Correlations of mean or maximum crustal thickness with ratios involving  $Pn$  are comparable to those with topography and lower than

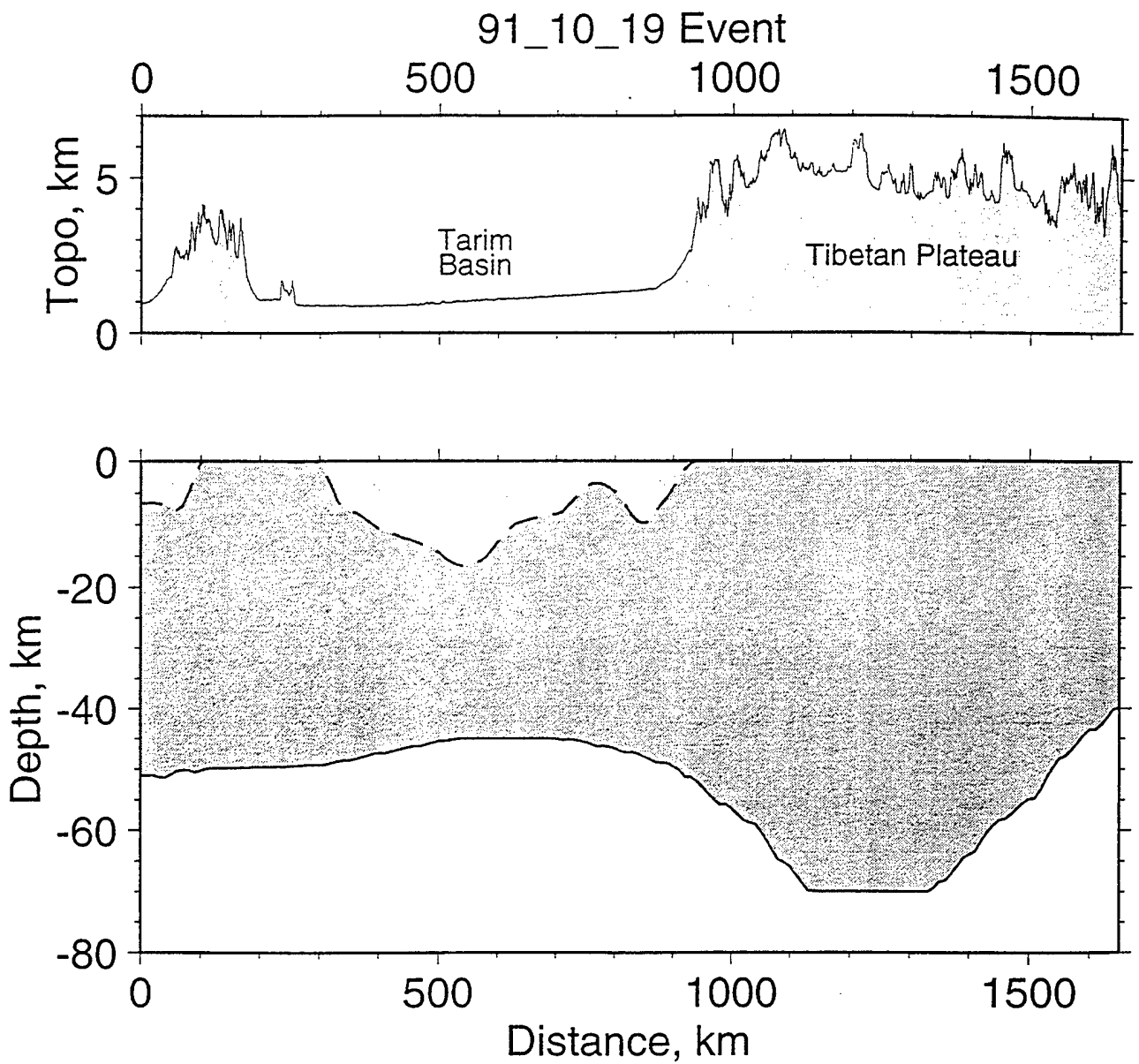


Figure 2. A sample cross-section profile for the raypath from station WMQ to the epicenter of the October 19, 1991 event, located in southern margin of the Tibetan Plateau. The scale for the topography is exaggerated by 5 times than the scale in depth.

those with distance. Weak correlations are found with rms slope of topography and sediment thickness for the WMQ data. Many of the crustal parameters show internal correlations that preclude identifying the waveguide properties affecting the amplitude ratios, and indeed it is likely that a combination of factors controls partitioning of energy in the regional wavefield.

Following Paper 1, we use multivariate regression to determine the best set of predictor variables from a set of parametric path properties giving an empirical model minimizing the variance in the data. An initial list of variables is defined, based on the separate correlation analyses in Paper 1, then an optimal combination is determined. Some variables are not used in the multivariate regression analysis such as maximum and minimum crustal thickness and maximum sediment thickness because they provide redundant information about the shape of the Moho discontinuity and basement structure. We keep rms slope in our initial list given its importance in variance reduction for the discriminant  $\text{Log}(Pn/Sn)$ . As a result, six parameters are used to characterize the path properties:  $x(1)$ , path length;  $x(2)$ , mean altitude;  $x(3)$ , rms roughness;  $x(4)$ , rms slope;  $x(5)$ , mean crustal thickness; and  $x(6)$ , mean sediment thickness. We construct a model in which these six parameters are initially assumed to influence a given frequency dependent regional phase ratio,  $Y$ , such as  $\text{Log}(Pn/Sn)$ , in the form

$$Y_i = b_0 + b_1x_{i1} + b_2x_{i2} + b_3x_{i3} + b_4x_{i4} + b_5x_{i5} + b_6x_{i6} + e_i \quad i = 1, 2, \dots, n, \quad (1)$$

where  $Y_i$  is the  $i$ -th observation that is assumed to be a linear combination of the  $x_{i1}$ ,  $x_{i2}$ , ...,  $x_{i6}$  predictor variables with linear coefficients  $b_0, b_1, b_2, \dots, b_6$ ,  $e_i$  is the random error associated with measurement of  $Y_i$ , and  $n$  is the number of observed values. If  $k$  is the number of independent variables considered, the model has  $m = k+1$  unknown parameters ( $m$  varies up to 7). We denote estimates of the  $b_j$  model coefficients as  $b_j$ .



As in Paper 1, we compute all possible linear regressions for our suite of six path parameters and then select a preferred set of best parameters for each data type based on statistical properties of the solutions. In addition to using the multiple coefficient of determination ( $R^2$ ) in selecting the best solution, two common criteria are used: (1) the mean square error (MSE) criterion, and (2) the  $C_p$ -statistic criterion. The MSE is the residual variance:

$$\text{MSE} = \frac{\text{SSE}}{n - m} = \frac{\sum_{i=1}^n (y_i - \hat{y}_i)^2}{n - m} \quad (2)$$

where SSE represents the sum of squared residuals,  $y_i$  are observed values, and  $\hat{y}_i$  are predicted values for the model. The MSE criterion minimizes the variance, taking into account the number of parameters in the model ( $m$ ), but it does not assess the resolution or contribution of each parameter. Mallows's  $C_p$ -statistic criterion is given by:

$$C_p = \frac{\text{SSE}_p}{S_k^2} - (n - 2p) \quad (3)$$

where  $\text{SSE}_p$  is the sum of squared errors for the model obtained for a subset of  $p$  variables out of a total of  $k$  predictor variables being considered; and  $S_k^2 = \text{MSE}(x_1, x_2, \dots, x_k)$  is the estimation variance based on all  $k$  predictor variables. After all possible regression combinations are determined,  $C_p$  is computed for each case. Since  $\text{SSE}_p$  represents the unexplained variation calculated from the model, we want  $\text{SSE}_p$  to be small, effectively, small  $C_p$ . Although adding even an unimportant independent variable to a regression model will decrease the unexplained variation  $\text{SSE}_p$ , it may result in an increase of  $C_p$ . Thus, the models that have  $C_p$  values close to  $p$  (i.e. low values) are the most desirable.

These criteria have proven to be very effective to justify goodness of fit in our model selection. Only a small number of models stand out with the desired features; high multiple coefficient of determination ( $R^2$ ), small residual variances, and small  $C_p$  values. Further, the estimate of the regression coefficient for individual variable has to be checked

against its standard deviation to ensure the coefficient is associated with a reasonably small standard deviation. As a whole, the preferred model should pass an F-test. In addition, all coefficients need to pass the partial F-test and t-test. For a specific coefficient the partial F-statistic  $F(b_j = 0)$  value must be greater than 3.96, the 5% right-tail point of  $F(0.95, 1, 81)$ , to pass the partial F-test. If a partial F-statistic value is smaller than 2.77, the 10% right-tail point of  $F(0.90, 1, 81)$ , then it implies that we cannot at the 90% confidence level reject the null hypothesis that  $b_j = 0$ . At the same time, all t-statistics should be substantially greater than rejection points with at least 95% confidence, in our case this corresponds to an absolute value of 1.664, indicating all  $b_j$  are nonzero and all model parameters selected are related to the amplitude ratio being considered.

## Model Results

In Paper 1, multivariate regression analysis of  $\text{Log}(Pg/Lg)$  for frequencies below 6 Hz yields preferred models which include four path parameters. In the frequency band 0.75-1.5 Hz, the preferred model involves distance, mean altitude, mean crustal thickness, and mean sediment thickness (see Table 1). This model explains 74% of the variance in the 87  $\text{Log}(Pg/Lg)$  measurements, while distance correction alone accounts for a 32% variance reduction. Variance reductions for the 1.5-3.0 Hz and 3-6 Hz bands are 70% and 35%, respectively, for 4-parameter models, and 43% and 20% for distance alone, respectively (Table 2). All of the  $Pg/Lg$  models involve distance and mean elevation. Surface roughness, mean crustal thickness, and sediment thickness are also important. The results for the 6-9 Hz frequency band show very little dependence on path parameters, possibly because the signal-to-noise ratios within the frequency band are marginal. After correction for the best model parameters, the residual variance distribution becomes an increasingly symmetric, normal distribution with decreasing standard deviation (see Figure 3).

Using the same multivariate regression method, we analyze the  $\text{Log}(Pn/Sn)$ ,  $\text{Log}(Pn/Lg)$ , and  $\text{Log}(Pg/Sn)$  observations. Our primary objective is to further explore the

TABLE 1. The best models for various discriminants observed at WMQ.

Discriminants	Frequency Band (Hz)	Distance	Mean Elevation	RMS Roughness	RMS Slope	Mean Crustal Thickness	Mean Sediment Thickness
Log(Pg/Lg)	0.75-1.5	X	X			X	X
	1.5-3.0	X	X	X			X
	3.0-6.0	X	X	X		X	
Log(Pg/Sn)	0.75-1.5	X	X		X		X
	1.5-3.0	X	X			X	X
	3.0-6.0		X			X	
Log(Pn/Lg)	0.75-1.5	X	X	X		X	
	1.5-3.0	X	X	X			
	3.0-6.0	X	X	X		X	
Log(Pn/Sn)	0.75-1.5	X	X		X		
	1.5-3.0	X	X		X		
	3.0-6.0	X	X		X	X	

TABLE 2. Variance reductions for various discriminants at WMQ after corrections for distance or a set of parameters from the best models.

Discriminants	Frequency Band (Hz)	Distance Correction (%)	Corrected using the Best Model (%)
Log(Pg/Lg)	0.75-1.5	31.8	74.8
	1.5-3.0	42.6	69.7
	3.0-6.0	19.7	35.0
Log(Pg/Sn)	0.75-1.5	23.4	46.4
	1.5-3.0	23.6	43.2
	3.0-6.0	7.0	13.4
Log(Pn/Lg)	0.75-1.5	64.2	86.9
	1.5-3.0	68.8	83.4
	3.0-6.0	47.6	59.4
Log(Pn/Sn)	0.75-1.5	76.4	86.6
	1.5-3.0	73.7	83.3
	3.0-6.0	54.5	63.1

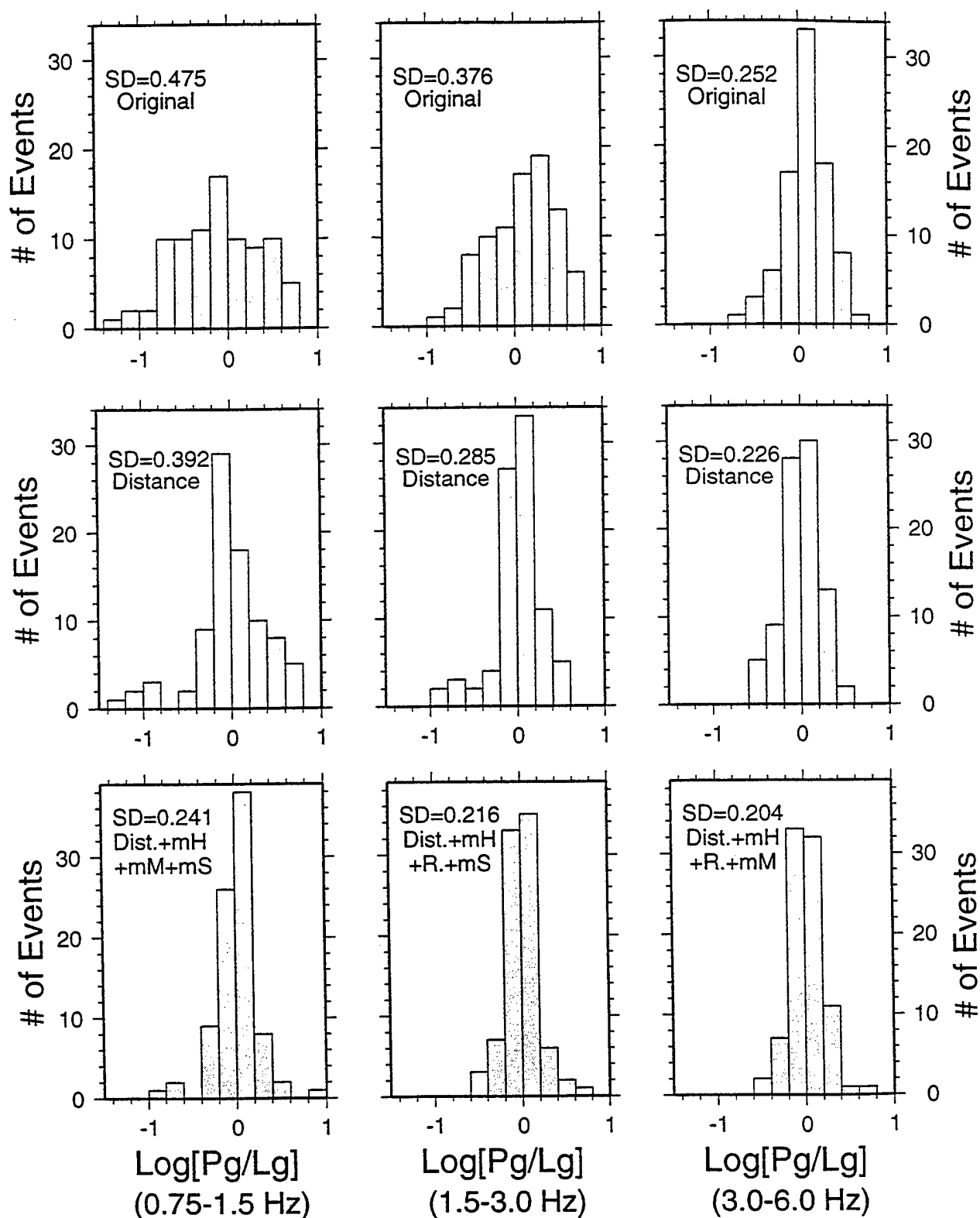


Figure 3. Histograms showing sample distributions for the  $\text{Log}(P_g/L_g)$  measurements. Top figures, for the raw data; middle figures, corrected for distance; bottom figures, corrected for the best models in the three frequency bands. Dist.+mH+mM+mS, corrected for a 4-parameter model involving distance, mean elevation, mean crustal thickness, and mean sediment thickness; Dist.+mH+R.+mS, corrected for a 4-parameter model involving distance, mean elevation, surface roughness, and mean sediment thickness; Dist.+mH+R.+mM, corrected for a 4-parameter model involving distance, mean elevation, surface roughness, and mean crustal thickness. The standard deviation of each population is given by SD.

empirical procedure for reducing variance in the regional phase data observed in a given region. Results are presented for these amplitude phase ratios in the passbands below 6 Hz, as the higher frequency data have inadequate signal-to-noise ratios.

We first consider the models obtained for  $\text{Log}(Pn/Sn)$ .  $Pn$  and  $Sn$  waves propagate mainly in the upper mantle lid just below the Moho discontinuity, and the  $Pn/Sn$  ratios shows the strongest correlations with path length as expected (up to 0.87) (Paper 1). Thus, distance correction is the most effective means for reducing the scatter in the data, with variance reductions of 74-76% for the two lower frequency bands, and about 54% for the 3-6 Hz band (Table 2). Further variance reduction can be achieved by including additional waveguide parameters, but the gains are not as large as for  $Pg/Lg$ . Mean path elevation consistently contributes to the variance reduction of  $Pn/Sn$ . A parameter which did not appear significant for  $Pg/Lg$ , but does contribute to multivariate regressions for  $Pn/Sn$  is rms slope of topography, even though rms slope alone shows very weak correlation with  $Pn/Sn$ .

In the frequency band 0.75-1.5 Hz, the residual variance in  $\text{Log}(Pn/Sn)$  is reduced from 0.216 for the raw data to 0.051 after just distance correction. It is reduced to 0.036 when a second parameter, mean elevation, is used simultaneously with distance. Adding a third parameter, rms slope, to the model further reduces the variance to 0.029. This 3-parameter model satisfies all criteria set by the statistical principles. All partial  $F(b_j=0)$  values are greater than 6.96 (Table 3), the 1% right-tail point of  $F(0.99, 1, 82)$ , thus the model passes all partial F-tests, indicating the null hypothesis ( $b_j=0$ ) can be rejected with 99% confidence. The 3-parameter model also passes all t-tests at 99% confidence level, suggesting  $b_j$ 's are nonzero and the three model parameters are related to the  $Pn/Sn$  amplitude measurements. This preferred model explains 87% of the total variation in the 87  $\text{Log}(Pn/Sn)$  amplitude ratios for the frequency band 0.75-1.5 Hz. Compared with the preferred 3-parameter model, a 4-parameter model, which involves distance, mean elevation, rms slope, and mean crustal thickness, was rejected because the fourth

parameter, mean crustal thickness, has a partial  $F(b_j=0)$  value of 3.08, which passes the partial F-test with 90% confidence, but fails the partial F-test at 95% confidence level. Because introducing the fourth parameter gives little improvement in variance reduction, we prefer the 3-parameter model over the 4-parameter model.

The same 3-parameter model, with all three parameters passing the partial F-tests and t-tests (Table 3), serves as the best model for the  $\text{Log}(Pn/Sn)$  data in the middle frequency band (1.5-3.0 Hz). It gives an 83% variance reduction, compared with a 74% variance reduction obtained from distance correction alone (Table 2). The 4-parameter model mentioned above is our preferred model for the 3-6 Hz frequency band. The variance reduction provided by the 4-parameter best model is 63%, a 9% improvement over that for standard distance correction. Table 3 provides information about the best models obtained for the  $Pn/Sn$  amplitude ratios in the three frequency bands. It is notable that the best model parameters are consistent in all three frequency bands of interest, and the improvements in variance reduction relative to standard distance correction are also similar for our preferred models. Figure 4 displays the scatter in the raw data, the data corrected for distance, and for the best models obtained from our multivariate regression for the  $\text{Log}(Pn/Sn)$  amplitude ratios.

The details of the best models from multivariate regressions for the  $Pn/Lg$  observations are shown in Table 4. In this case, distance is the best single parameter for correction, giving 64-68% variance reduction for the two low frequency bands and a moderate 47% variance reduction for the higher frequency band (3-6 Hz). This variance reduction by distance correction is lower than for the  $\text{Log}(Pn/Sn)$  measures, but higher than for the  $\text{Log}(Pg/Lg)$  ratio. A preferred 3-parameter model for the middle frequency band involves distance, mean elevation, and surface roughness. For the lower and higher frequency bands (0.75-1.5 Hz and 3-6 Hz) mean crustal thickness is included in preferred 4-parameter models. All coefficients in the best regression models have reasonably small

Table 3. The best set of predictor variables for the Log(Pn/Sn) data at WMQ.

		0.75-1.5 Hz	1.5-3.0 Hz	3.0-6.0 Hz
Distance	$b_j \pm s$	0.000706	0.000696	0.000487
	s	$\pm 0.0000501$	$\pm 0.0000563$	$\pm 0.0000622$
	F( $b_j=0$ )	198.2	152.6	61.35
	t( $b_j=0$ )	14.08	12.35	7.83
Mean Elevation	$b_j$	0.275	0.273	0.260
	s	$\pm 0.0342$	$\pm 0.0385$	$\pm 0.0591$
	F( $b_j=0$ )	64.33	50.42	19.44
	t( $b_j=0$ )	8.02	7.10	4.41
RMS Slope	$b_j$	-0.00197	-0.00170	-0.00145
	s	$\pm 0.000417$	$\pm 0.000469$	$\pm 0.000575$
	F( $b_j=0$ )	22.30	13.14	6.34
	t( $b_j=0$ )	-4.72	-3.62	-2.52
Mean Crustal Thickness	$b_j$	-	-	-0.0424
	s	-	-	$\pm 0.00967$
	F( $b_j=0$ )	-	-	19.19
	t( $b_j=0$ )	-	-	-4.38
Intercept		1.316	-1.146	1.417
R <sup>2</sup>		0.870	0.839	0.648
The Total Sum of Square (SST)		18.553	18.903	10.329
The Error Sum of Square (SSE)		2.411	3.044	3.632
The Error Mean Square (MSE)		0.0290	0.0367	0.0443
F( 3, 83)		185.256	144.160	
F( 4, 82)				37.793

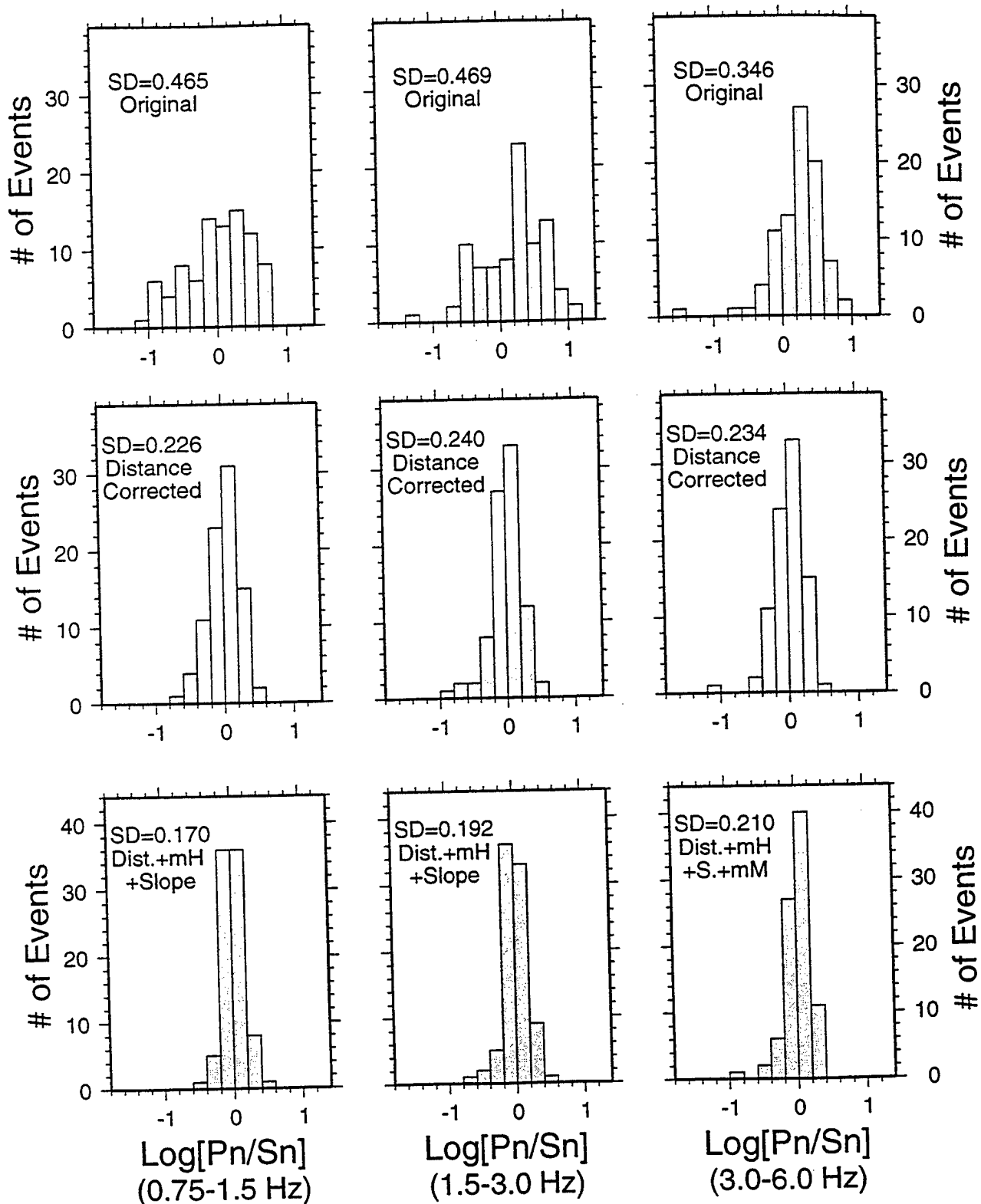


Figure 4. Same histograms showing sample distributions for the  $\text{Log}(P_n/S_n)$  measurements. All illustrations are the same as in Figure 3. Dist.+mH+Slope, corrected for a 3-parameter model involving distance, mean elevation, and rms slope; Dist.+mH+S.+mM, corrected for a 4-parameter model involving distance, mean elevation, rms slope, and mean crustal thickness.



Table 4. The best set of predictor variables for the Log(Pn/Lg) data at WMQ.

		0.75-1.5 Hz	1.5-3.0 Hz	3.0-6.0 Hz
Distance	$b_j$	0.000820	0.000875	0.000562
	$s$	0.0000800	0.0000830	0.0000932
	$F(b_j=0)$	104.9	111.2	36.31
	$t(b_j=0)$	10.24	10.54	6.03
Mean Elevation	$b_j$	0.253	0.222	0.196
	$s$	0.0614	0.0592	0.0715
	$F(b_j=0)$	17.02	14.03	7.55
	$t(b_j=0)$	4.12	3.75	2.75
Roughness	$b_j$	0.477	0.500	0.521
	$s$	0.117	0.100	0.136
	$F(b_j=0)$	16.67	24.72	14.63
	$t(b_j=0)$	4.08	4.97	3.82
Mean Crustal Thickness	$b_j$	0.0284	-	-0.0746
	$s$	0.0133	-	0.0155
	$F(b_j=0)$	4.53	-	23.11
	$t(b_j=0)$	2.13	-	-4.81
Intercept		-3.8739	-2.060	2.3851
$R^2$		0.875	0.840	0.613
The Total Sum of Square (SST)		45.693	40.230	20.032
The Error Sum of Square (SSE)		5.707	6.432	7.751
The Error Mean Square (MSE)		0.0696	0.0775	0.094
$F(3, 83)$			145.364	
$F(4, 82)$		143.643		32.479

standard derivations and pass the partial  $F(b_j=0)$  tests and t-tests with high confidence. The improvements in variance reduction obtained by correcting for the best model parameters relative to distance correction alone are between 12-22%, depending on the frequency band considered. Figures 5 and 3 show that the raw data of the  $\text{Log}(Pn/Lg)$  ratio span a wider range than the  $\text{Log}(Pg/Lg)$  measurements; however, after correction for the best regression models the variances of the data have reduced considerably and now are close to a Gaussian distribution. Total variance reductions achieved are 83-87% in the two lower frequency bands, comparable to those for the  $\text{Log}(Pn/Sn)$  ratio. Variance reduction is 4% less than that for the  $\text{Log}(Pn/Sn)$  ratio for the higher (3-6 Hz) frequency band.

Unlike the  $Pn/Sn$  and  $Pn/Lg$  amplitude ratios, the  $Pg/Sn$  ratios exhibit more diversity between the models fitting different frequency bands. Linear regressions indicate that distance is not the strongest controlling factor for the  $Pg/Sn$  ratio, compared with mean elevation, surface roughness, and possibly mean crustal thickness. From Figure 6 it is clear that the standard derivations for the original data are relatively small. Table 5 shows the detailed information for the best models obtained from multivariate regressions for these data. Although the partial  $F(b_j=0)$  values and t-statistics are not as high as those for the other three discriminants, all coefficients are greater than 3.96, indicating they have passed the partial F-tests at 95% confidence level. All coefficients also satisfy the t-tests with 97.5% confidence. Many multi-parameter models have small  $C_p$  statistic values, but often with one or two parameters failing the partial F-test or t-test, or standard derivations associated with one of the parameters being too large compared with the parameter value. Such factors result in exclusion of these models from our final analysis.

We find that the best model in the low frequency band 0.75-1.5 Hz involves distance, mean elevation, rms slope, and mean sediment thickness. Among all two-parameter models, a model with mean elevation and rms slope gives the highest multiple coefficient of determination ( $R^2$ ) and the smallest unexplained variation ( $SSE_p$ ), in contrast to the cases for the  $Pn/Sn$ ,  $Pn/Lg$ , and  $Pg/Lg$  ratios, where distance always is one of the

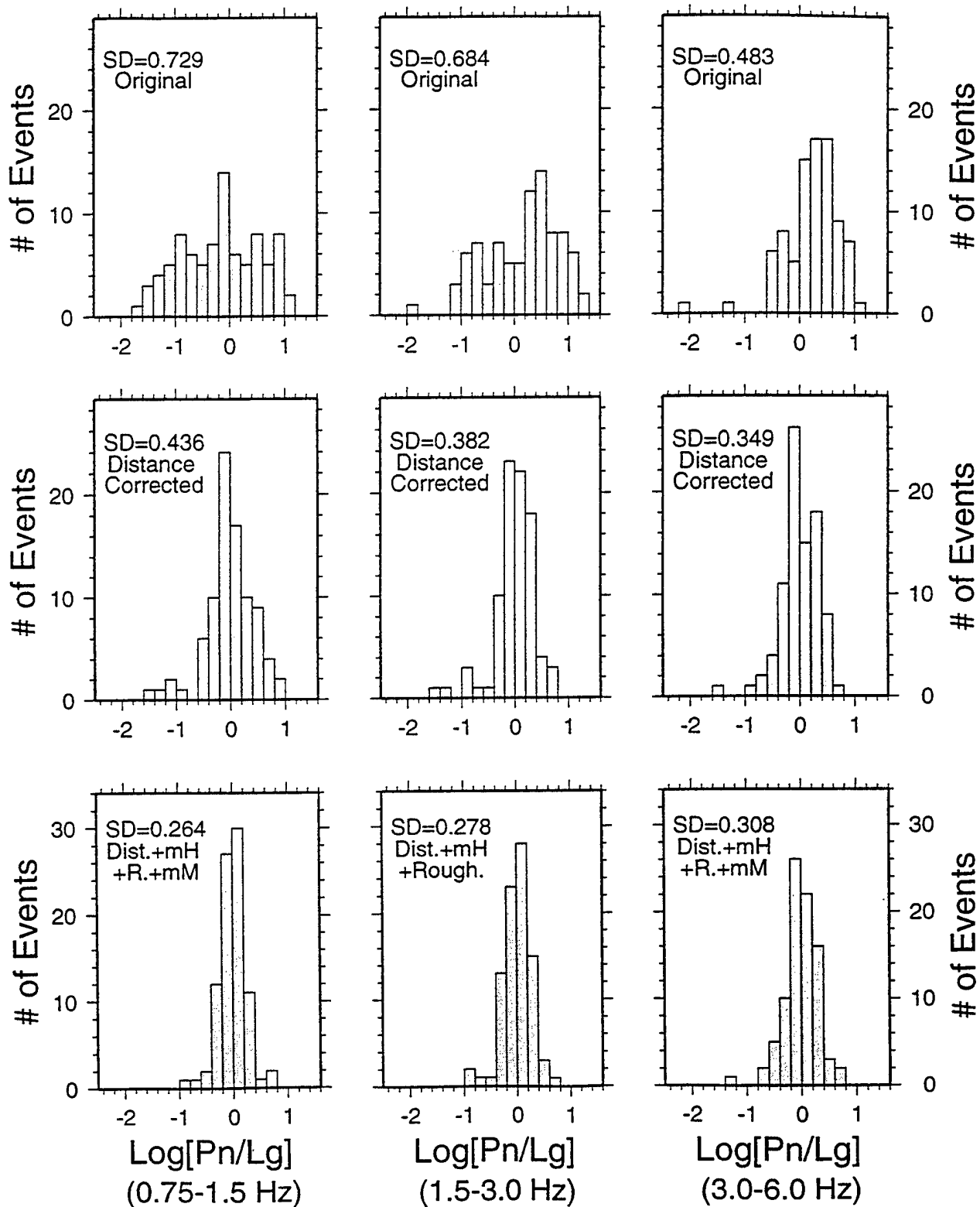


Figure 5. Same histograms showing sample distributions for the  $\text{Log}(P_n/L_g)$  measurements. All illustrations are the same as in Figure 3. Dist.+mH+Rough., corrected for a 3-parameter model involving distance, mean elevation, and surface roughness; Dist.+mH+R.+mM, corrected for a 4-parameter model involving distance, mean elevation, surface roughness, and mean crustal thickness.

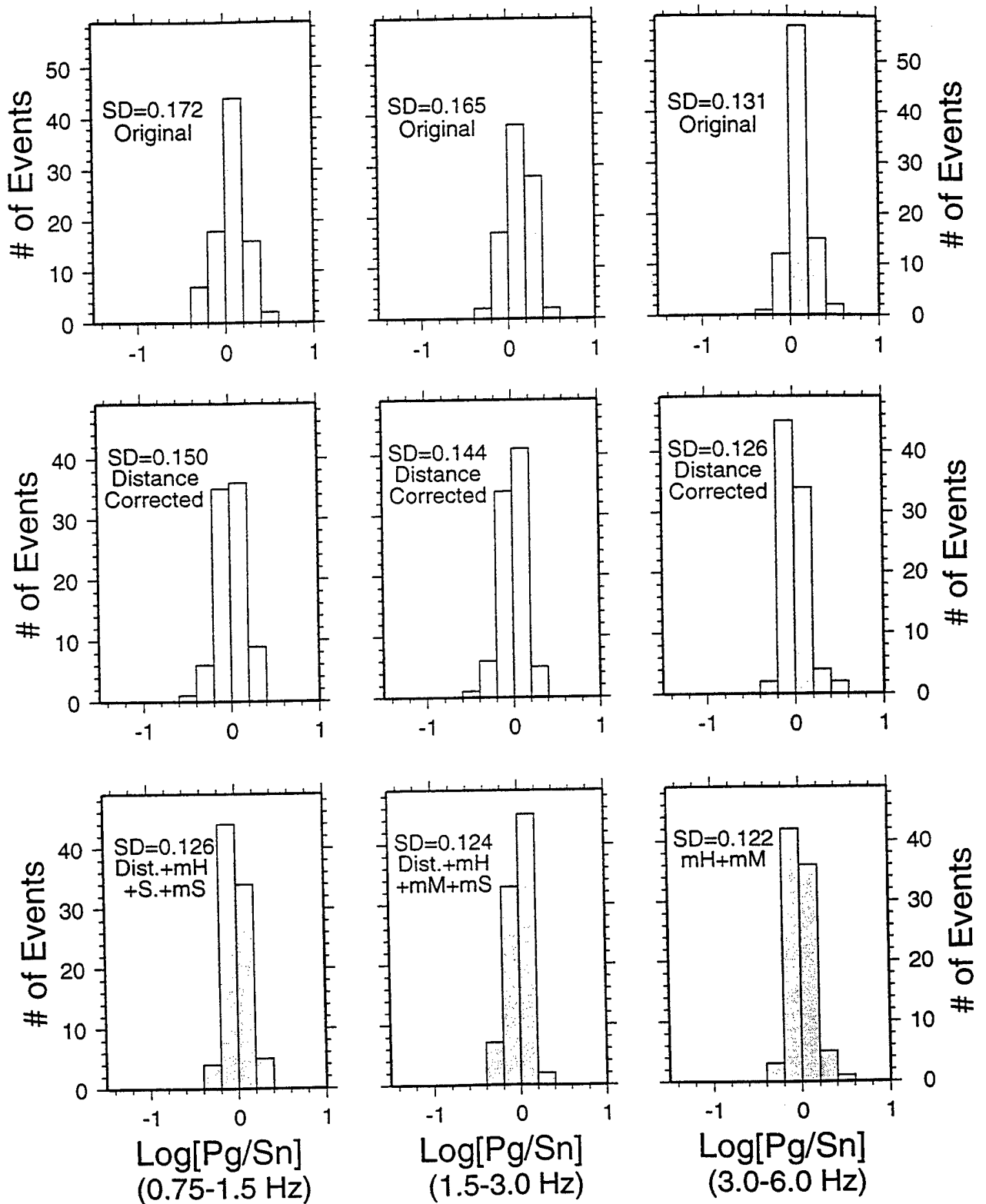


Figure 6. Same histograms showing sample distributions for the  $\text{Log}(\text{Pg}/\text{Sn})$  measurements. All illustrations are the same as in Figure 3. mH+mM, corrected for a 2-parameter model involving mean elevation and mean crustal thickness; Dist.+mH+S.+mS, corrected for a 4-parameter model involving distance, mean elevation, rms slope, and mean sediment thickness; Dist.+mH+mM+mS, corrected for a 4-parameter model involving distance, mean elevation, mean crustal thickness, and mean sediment thickness.

Table 5. The best set of predictor variables for the Log(Pg/Sn) data at WMQ.

		0.75-1.5 Hz	1.5-3.0 Hz	3.0-6.0 Hz
Distance	$b_j$	0.000112	0.000131	-
	$s$	0.0000383	0.0000378	-
	$F(b_j=0)$	8.50	12.05	-
	$t(b_j=0)$	2.92	3.47	-
Mean Elevation	$b_j$	0.154	0.0714	0.0956
	$s$	0.0258	0.0290	0.0248
	$F(b_j=0)$	35.54	6.07	14.93
	$t(b_j=0)$	5.96	2.46	3.86
RMS Slope	$b_j$	-0.00118	-	-
	$s$	0.000312	-	-
	$F(b_j=0)$	14.22	-	-
	$t(b_j=0)$	3.77	-	-
Mean Crustal Thickness	$b_j$	-	0.0106	-0.0104
	$s$	-	0.00513	0.00500
	$F(b_j=0)$	-	4.25	4.28
	$t(b_j=0)$	-	2.06	-2.07
Mean Sediment Thickness	$b_j$	0.0292	0.0305	-
	$s$	0.0107	0.0105	-
	$F(b_j=0)$	7.38	8.42	-
	$t(b_j=0)$	2.72	2.90	-
Intercept		-0.3648	-0.8395	0.4310
$R^2$		0.489	0.458	0.155
The Total Sum of Square (SST)		2.534	2.333	1.469
The Error Sum of Square (SSE)		1.294	1.265	1.242
The Error Mean Square (MSE)		0.0158	0.0154	0.0148
$F(2, 84)$				7.676
$F(4, 82)$		19.642	17.312	

two factors for the best two-parameter models. The 4-parameter model constructed from multivariate regression provides 46% variance reduction of the data, a 23% improvement in variance reduction relative to that by distance correction alone. The best model for the middle frequency band is also a 4-parameter model, involving distance, mean elevation, mean crustal thickness, and mean sediment thickness. This model satisfies all selecting criteria with the smallest  $C_p$  value, high multiple coefficient of determination ( $R^2$ ), and all coefficients passing partial  $F(b_j=0)$  tests and  $t(b_j=0)$  tests. Although variance reduction by the distance correction approximately equals that for the lowest frequency (24%), the variance reduction improves by about 20% after correction for the best model. In the frequency band 3-6 Hz, variation in the original amplitude ratio data is relatively small (see Figure 6), and the variance reductions achieved by correcting for distance or for the best model, 7% and 13%, respectively, are the smallest values among all cases studied. The preferred best model is a 2-parameter model, involving mean elevation and mean crustal thickness, without distance. A number of multiple parameter models have a higher multiple coefficient of determination ( $R^2$ ) and comparable  $C_p$  values; however, one or two coefficients of the models fail the partial F-test or t-test.

## Discussion

All of the regional phase amplitude ratios considered,  $Pn/Lg$ ,  $Pg/Lg$ ,  $Pn/Sn$ , and  $Pg/Sn$ , exhibit frequency-dependent variations with propagation distance, and correction for this effect is valuable for discrimination applications. However, the uncorrected data sometimes correlate better with specific path properties than they do with distance. The WMQ data exhibit significant Lg blockage, and much of the value of correction for path-specific wave guide properties stems from effects of the Tibetan Plateau. Our multivariate regression analysis clearly indicates that the scatter of various discriminants can be reduced considerably by correcting for other path specific parameters. While the reduction in variance associated with the multiple regression analysis for  $Pg/Lg$ ,  $Pg/Sn$ ,  $Pn/Sn$ , and

*Pn/Lg* phases recorded at WMQ is encouraging, it must be emphasized that the corresponding model is empirical, is unlikely to generalize because of the extreme path complexity in the region, and is only useful for the specific frequency bands. The systematic relationships observed in this study between regional discriminants and parameters of the wave guide structure suggests that blockage effects involve a continuum of effects rather than bimodal behavior. The empirical nature of the model implies that the best models obtained only serve as tools for the variance reduction, and the physics behind the scene is not fully revealed.

We often will have only a few stations in tectonically complex regions and must have procedures that account for the path complexity effects on regional phase amplitudes. This multivariate regression analysis method can be easily applied in other regions, and reductions in the scatter of discriminant measures for an earthquake population should help directly to improve the performance of discrimination. However, we do expect that different waveguide parameters may emerge as the most important ones in regions of less crustal heterogeneity, and in some cases standard correction for path length may be all that is warranted.

In addition to path length, a generalized topographic parameter, mean elevation, occurs in every preferred models in the three frequency bands for all discriminant ratios considered (Table 1). Because precise topographic data are available for all major continents in the world and isostasy theory suggests that mean elevation is associated with the deep crustal structure, it seems reasonable to use topographic parameters, including mean elevation, to seek variance reduction of regional phase amplitude ratios. This leaves open the issue of what are the controlling effects on regional phases, with factors that are probably important being geometric spreading, attenuation, scattering, sedimentary basins, changes in Moho depth, rough surface topography, and internal crustal structure. There is a need for extensive modeling of realistic (3-dimensional) crustal waveguides with structure

at a wide variety of scale lengths, if we are to fully understand the nature of these regional phases.

### Acknowledgments

We thank the IRIS DMC for providing access to seismic data used in this study. We thank Dr. Tian-Run Zhang for discussions and for providing some software. Dr. Hans Hartse provided a preprint of a related study. This research was supported by Phillips Laboratory Contract No. F19628-95-K-0014, and by IGPP-LANL UCRP grant #609. This is the contribution #336 of the Institute of Tectonics, University of California, Santa Cruz.

### References

- Baumgardt, D. R. (1990). Investigation of teleseismic Lg blockage and scattering using regional arrays, *Bull. Seism. Soc. Am.*, 80, 2261-2281.
- Fan, G.-W., and T. Lay (1997). Statistical analysis of irregular waveguide influences on regional seismic discriminants in China, submitted to *Bull. Seism. Soc. Am.*
- Fielding, E. J., B. L. Isacks, and M. Barazangi (1992). A geological and geophysical information system for Eurasia, Tech. Report 2, F29601-91-K-DB08, Philips Lab., Hanscom Air Force Base, Mass.
- Hartse, H. E., R. A. Flores, and P. A. Johnson (1997a). Correcting regional seismic discriminants for path effects in western China, *Bull. Seism. Soc. Am.*, submitted.
- Hartse, H. E., S. R. Taylor, W. S. Phillips, and G. E. Randall (1997b). A preliminary study of regional seismic discrimination in central Asia with emphasis on western China, *Bull. Seism. Soc. Am.*, 87, 551-568 .
- Kennett, B. L. N. (1989). On the nature of regional seismic phases - I. Phase representations for Pn, Pg, Sn, Lg, *Geophys. J.*, 98, 447-456.



- Taylor, S. R. (1996). Analysis of high-frequency Pn/Lg ratios from NTS explosions and western U.S. earthquakes, *Bull. Seism. Soc. Am.* 86, 1042-1053.
- Walter, W. R., K. M. Mayeda, and H. Patton (1995). Phase and spectral ratio discrimination between NTS earthquakes and explosions. Part I: Empirical observations, *Bull. Seism. Soc. Am.*, 85, 1050-1067.
- Zhang, T.-R., and T. Lay (1994). Analysis of short-period regional phase path effects associated with topography in Eurasia, *Bull. Seism. Soc. Am.*, 84, 119-132.
- Zhang, T.-R., S. Schwartz, and T. Lay (1994). Multivariate analysis of waveguide effects on short-period regional wave propagation in Eurasia and its application in seismic discrimination, *J. Geophys. Res.*, 99, 21,929-21,945.

**Regionalized Waveguide Effects  
on Seismic Discriminants in Western China**

by

Guangwei Fan and Thorne Lay

Institute of Tectonics

Department of Earth Sciences

University of California, Santa Cruz

Santa Cruz, CA 95064

submitted to BSSA

November 20, 1997

## ABSTRACT

Regional seismic signals play an important role in identifying low magnitude explosion and earthquake sources for monitoring the Comprehensive Test Ban Treaty (CTBT). To enhance the performance of seismic discriminants, regional phases need to be corrected for the influence of large- and intermediate-scale crustal waveguide heterogeneity. Multivariate regression analysis using parametric path characteristics has shown promise for reducing the propagation-induced scatter in short-period regional phase amplitude ratios. While path length is a dominant parameter for most seismic phase amplitudes, other parametric features of crustal waveguide structure are often significantly correlated with regional amplitude ratios of P wave energy ( $P_n$ ,  $P_g$ ) to S wave energy ( $S_n$ ,  $L_g$ ). We investigate regionalized waveguide effects on regional seismic discriminants in central Asia and Southwest China. Linear regressions indicate that specific path parameters extracted from available crustal models vary in significance from one station to another and from one sub-region to another. Single station and multiple station data are analyzed to assess strategies for regional calibration of path effects. In general, corrections for optimal combinations of waveguide parameters obtained from multivariate regression reduce the data variance more than conventional corrections for path length alone. However, in central Asia several stations show path dependence with opposite sign, so regional calibration with combined stations does not perform well. This is due to highly path specific effects. In Southwest China, there is greater commonality in behavior amongst stations, and robust regional calibration can be achieved. However, the resulting variance reduction is less than for individual station analysis because some path effects appear to be highly direction dependent. Our results indicate that individual station calibration is the preferred procedure, but this should include corrections for path effects beyond simple distance correction.

## Introduction

In monitoring the Comprehensive Test Ban Treaty (CTBT), seismic signals recorded at regional distances play a critical role for discriminating low magnitude explosion sources from earthquakes. Amplitude ratios of short-period P wave energy ( $P_n$ ,  $P_g$ ) to S wave energy ( $S_n$ ,  $L_g$ ) have emerged as particularly promising discriminants, especially at frequencies above 3 Hz (Walter *et al.*, 1995; Taylor, 1996; Hartse *et al.*, 1997a). Regional seismic waves from crustal events are mainly influenced by shallow Earth structure and the source radiation. These waveforms are very complicated as a result of multiple reflections and phase conversions within the crustal and lithospheric waveguide, particularly in the short period range ( $< 1$  sec) for which high signal-to-noise ratios are observed. The regional phases  $P_n$  and  $S_n$  propagate just below the Moho discontinuity within the upper mantle, while  $P_g$  and  $L_g$  propagate within the crust. The shape and properties of the crustal and upper mantle waveguide which affect these phases vary greatly from one region to another. Thus, large- and intermediate-scale heterogeneities within the shallow waveguide play a key role in shaping regional waveforms (e.g. Kennett, 1989; Zhang *et al.*, 1994).

As a consequence of large-scale variation in waveguide properties, regional seismic phases show systematic characteristics in different geologic regions.  $L_g$  blockage is often associated with specific crustal structure, such as oceanic crust (Press and Ewing, 1952), margins of the Tibetan Plateau (Ruzaikin *et al.*, 1977; Ni and Barazangi, 1983; McNamara *et al.*, 1996; Fan and Lay, 1997a), and the Alpine mountains (Campillo *et al.*, 1993).  $L_g$  blockage is related to changes in crustal waveguide structure, including shallow sedimentary basins (Kennett, 1988; Baumgardt, 1990; Bostock *et al.*, 1990; Zhang and Lay, 1995). Meanwhile,  $S_n$  waves are strongly attenuated along paths across the northern Tibetan Plateau (Ni and Barazangi, 1983) and across some areas in the Middle East (Kadinsky-Cade *et al.*, 1981; Rodgers *et al.*, 1997a). Strong attenuation and low velocity

gradients in the mantle lid appear to be responsible for these effects. In Scandinavia,  $P_n$  is observed to be related to the relief in the Moho discontinuity (Kvaena and Doornbos, 1991). Recent studies further indicate that topographic features, which reflect the shape and tectonic history of the crustal waveguide, are correlated with the scatter in regional phase amplitude ratios (Zhang and Lay, 1994; Zhang et al., 1996; Fan and Lay, 1997a, b). These effects are not readily characterized by standard geometric spreading models for one-dimensional structures.

The lack of detailed knowledge about the crustal waveguide in most regions has impeded quantitatively modeling of propagation effects on regional phases. As a result, empirical methods are being pursued for calibration of distance decay and other path-specific propagation effects for regional discriminants. The objective is to develop robust propagation corrections to reduce the data variance. This is important for isolating source radiation effects that lie at the heart of seismic discrimination. The empirical calibration method has been demonstrated in the western U.S. and central Eurasia (e.g. Zhang and Lay, 1994; Zhang et al., 1996; Fan and Lay, 1997a, b; Hartse et al., 1997b) and the Middle East (Rodgers et al., 1997c). However, the simple empirical relationships appear to vary regionally, and it is not clear whether or not one can transport relationships between stations in a given region. Multicollinearity between the available path-related parameters makes the situation complicated, as it is important to minimize the number of parameters while reducing the variance in the observations.

We apply multivariate regression to analyze path specific influences on regional discriminants in two provinces: one in central Asia, the other in southwest China. By separately analyzing single station data and combined data from multiple stations, we compare variance reduction in different frequency passbands to assess regional calibration methods. We demonstrate the pitfalls of regional calibration, and conclude that individual station calibration is preferred to multi-station calibration, and that it is important to account for path specific effects for frequencies less than 6 Hz. The empirical relationships

obtained also provide a starting point for quantitative modeling efforts that can be pursued to quantify the underlying wave propagation effects.

### Data

The central Asia study region includes the Tien Shan, the Pamirs, the Hindu Kush, and the western portion of the Tibetan Plateau (Figure 1a). This area is tectonically complex, with many earthquakes related to the ongoing continental collision/subduction process. Many events in the region have source depths well below the Moho discontinuity (e.g. Roecker et al., 1980; Fan et al., 1994), and these intermediate-depth earthquakes were not included in our analysis as they can be discriminated on the basis of the source depth. Gravity and regional Pnl waveform modeling indicate that the crustal thickness is from 63 to 67 km beneath the Hindu Kush, Pamirs, and Karakorum regions (Mishra, 1982; Holt and Wallace, 1990), thus we used 50 km as a depth threshold for selecting crustal events. We analyze 58 earthquakes (Table 1) with magnitudes of  $4.8 \leq m_b \leq 6.5$ , that occurred between 1988 and early 1996. These events are recorded at the regional broadband seismic stations, AAK, GAR, NIL, WMQ, and WUS, and provided 101 vertical component signals satisfying our data selection criteria (following Fan and Lay, 1997a).

Our second study area is in southwest China (Figure 1b), where one broadband seismic station, LSA, is located within the Tibetan Plateau at an elevation of 3780 m, and four seismic stations, ENH, KMI, LZH, and XAN, are located outside of the plateau. The diffuse seismicity provides ray paths covering a large portion of the eastern Tibetan Plateau and an arcuate transition zone from the high plateau to the surrounding lowlands. Intermediate-depth seismicity occurs beneath the Indo-Burman ranges in the southwestern corner of the study area and is mainly associated with underthrusting Indian plate and overriding Burman platelet (Le Dain et al., 1984; Ni et al., 1989). The crustal thickness

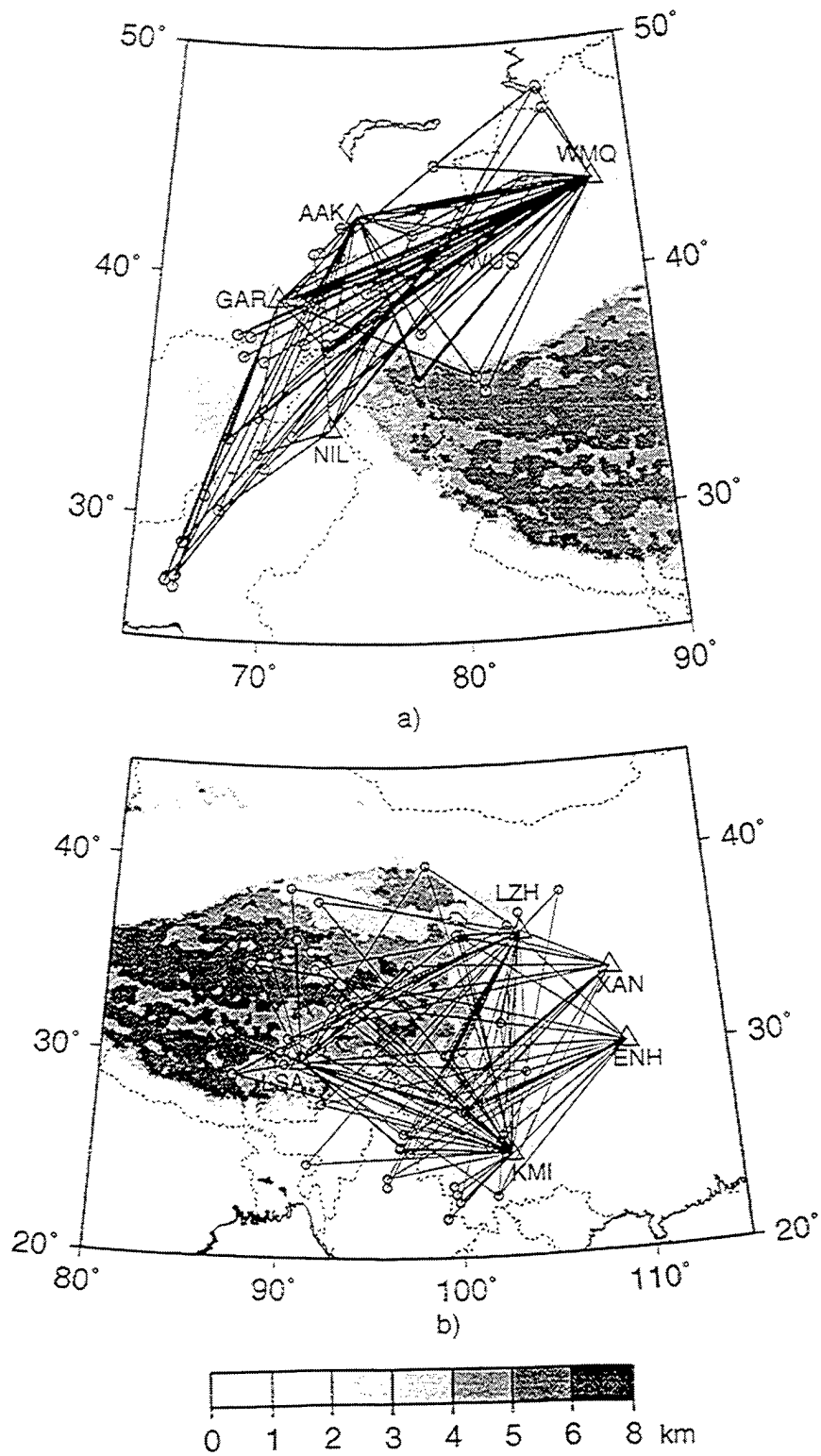


Figure 1. Topography in our two study areas: a) central Asia; b) southwest China. The circles represent the epicenters of the 58 events used; the labeled triangles are the seismic stations used. Lines indicate great circle paths.

Table 1. Parameters of the selected 58 earthquakes used in central Asia

Date (mon/day/yr)	Origin Time (hour:min:sec)	Focal Depth* (km)	$m_b$	Latitude (N°)	Longitude (E°)
1/6/88	15:31:15.1	48.	5.0	39.63	75.53
1/9/88	3:55:05.9	38.	5.3	39.10	71.50
6/17/88	13:30:43.2	18.	5.2	42.92	77.49
7/20/88	6:20:53.5	15.	5.4	37.01	72.94
8/12/88	18:58:34.2	15.	5.2	39.64	74.53
9/23/88	4:46:41.4	38.	5.2	39.60	74.56
9/25/88	20:52:14.9	11.	5.4	37.17	71.81
3/4/90	19:46:19.5	10.	5.8	28.91	66.37
3/5/90	20:47:06.6	18.	5.7	36.90	73.02
3/6/90	18:07:08.4	33.	5.0	36.92	73.07
3/6/90	21:39:53.7	17.	5.2	36.88	73.10
4/2/90	19:06:14.8	37.	5.1	33.18	68.19
4/17/90	1:59:30.0	15.	5.9	39.38	75.03
4/19/90	22:41:30.7	23.	5.3	34.09	69.59
4/27/90	5:29:30.0	47.	5.3	28.87	66.32
6/14/90	12:47:28.5	36.	6.1	47.85	85.06
6/17/90	4:51:45.9	15.	5.9	27.45	65.74
7/26/90	6:53:56.6	19.	5.8	27.34	65.68
8/3/90	9:15:04.0	16.	6.0	47.97	84.97
8/14/90	0:50:39.4	21.	5.2	27.09	66.05
9/8/90	19:33:15.0	1.	5.6	27.55	66.13
10/24/90	23:38:15.0	20.	5.2	44.11	83.88
11/3/90	16:39:56.8	43.	5.5	39.05	71.44
11/12/90	12:28:50.0	9.	5.8	42.94	78.07
12/1/90	18:09:29.0	30.	5.0	40.89	73.59
2/25/91	14:30:27.6	21.	5.5	40.36	78.98
4/18/91	9:18:29.0	22.	5.4	37.49	68.29
4/26/91	22:24:00.0	4.	5.3	39.04	71.04
8/19/91	6:05:51.0	25.	5.5	47.00	85.31
1/4/92	3:35:21.5	26.	5.0	32.00	70.00
4/5/92	7:47:48.0	18.	5.5	35.77	80.68
4/24/92	7:07:23.8	25.	5.8	27.52	66.09
5/10/92	4:04:32.9	33.	5.5	37.17	72.93
5/20/92	12:20:32.9	16.	5.9	33.35	71.33
6/27/92	13:21:21.0	31.	4.9	35.16	81.15
8/19/92	2:04:37.4	27.	6.5	42.12	73.60
11/23/92	23:11:06.9	43.	5.6	38.57	72.65
12/17/92	17:43:12.0	33.	5.3	37.40	68.94
4/8/93	3:49:33.2	38.	5.0	35.69	77.64
6/15/93	23:12:26.2	42.	4.8	35.65	77.76
11/16/93	15:52:49.0	31.	5.4	30.81	67.22
11/30/93	20:37:13.0	13.	5.1	39.32	75.52
12/30/93	14:24:2.0	1.	5.7	44.74	78.80



Table 1. (Continued)

Date (mon/day/yr)	Origin Time (hour:min:sec)	Focal Depth* (km)	$m_b$	Latitude (N°)	Longitude (E°)
3/5/94	4:3:52.5	33.	5.1	36.58	68.66
8/23/94	14:18:31.6	15.	5.0	40.04	78.82
10/21/94	5:6:21.0	15.	5.4	36.39	69.71
2/20/95	4:12:23.2	27.	5.4	39.17	71.12
2/20/95	8:7:34.2	33.	5.0	41.07	72.45
5/2/95	11:48:11.6	18.	5.5	43.78	84.66
5/31/95	13:51:19.4	15.	5.2	30.23	67.94
6/11/95	21:55:49.1	16.	5.1	32.56	69.62
9/26/95	4:39:6.4	43.	5.3	41.81	81.59
10/8/95	8:55:49.9	20.	5.9	40.99	72.12
11/1/95	12:29:28.7	15.	5.5	42.99	80.31
12/23/95	10:31:59.1	33.	5.2	38.01	73.33
12/24/95	9:36:7.4	33.	4.9	37.64	77.89
1/9/96	6:27:54.4	33.	5.2	43.70	85.65
1/18/96	9:33:51.2	20.	5.2	41.83	77.48

\*Focal depths are determined by the ISC or from Harvard CMT solutions.

varies greatly from a upper bound of 70 km in the Tibetan Plateau (Hirn et al., 1988) to 34-35 km and 50-60 km in the surrounding areas (Holt and Wallace, 1990). A total of 57 earthquakes with focal depths less than 45 km and magnitudes of  $4.8 \leq m_b \leq 6.1$  were selected (see Table 2), providing 144 useable signals.

We limit our attention to observations at epicentral distances greater than 240 km and less than 2100 km. The event locations are from the International Seismological Centre (ISC) bulletins prior to 1994, and from the USGS Preliminary Determination of Epicenters (PDE) catalog from 1994 on. The vertical component broadband records (approximately proportional to ground velocity) were windowed and bandpass filtered into four frequency bands: 0.75 to 1.5 Hz, 1.5 to 3.0 Hz, 3.0 to 6.0 Hz, and 6.0 to 9.0 Hz, using Butterworth filters. We did not deconvolve the instrument response, as we consider only ratios of phases in the same frequency band, which explicitly cancels the instrument effect. Root-mean square (rms) amplitudes are used for all phases because of the stability that results from averaging of multiple arrivals (Gupta et al., 1992). The  $P_n$  window begins at the

onset of the signal and ends at the start of the  $P_g$  window. The  $P_g$  and  $L_g$  windows are between group velocities of 6.2 to 5.2  $\text{km s}^{-1}$  and 3.6 to 3.0  $\text{km s}^{-1}$ , respectively. The  $S_n$  window is between group velocities of 4.8 to 4.0  $\text{km s}^{-1}$  for central Asia and between 4.8 to 3.9  $\text{km s}^{-1}$  for southwest China. All waveforms are visually screened to ensure that these windows capture the primary energy for each signal. Noise levels are computed using rms measures of the filtered seismograms in a 10 sec window preceding the manually picked first arrival time. Events with  $P_n$  signal-to-noise ratios lower than two are excluded from analysis. For most of the events, the signal-to-noise ratios are between 10 and 100. For the passband of 6.0-9.0 Hz, the signal-to-noise ratio is relatively low, thus the results for this passband are not presented here.

Topography reflects gross tectonic features of the crust, with high topography in areas of tectonically thickened crust, and laterally variable topography in areas of rapidly changing crust and mantle structure. Surface topography is the most precisely known attribute we will ever have for regional crustal structure, thus it is very attractive to explore its use in correcting for wave propagation effects. Of course, topography is not a perfect surrogate for internal crustal structure. Our topographic relief data are from the GLOBE (Global Land One-km Base Elevation) project with a spatial resolution of 30 arc-second (one-km), developed by the National Imagery and Mapping Agency (NIMA) and the National Geophysical Data Center (NGDC) of NOAA. Topography and ray path coverage in our two sub-regions are illustrated in Figure 1.

We also use largely independent models of the crustal thickness (Moho depth) (Figure 2) and sediment thickness (Figure 3) provided by the database compiled by Cornell University (Fielding et al., 1992). Although the accuracy of these data is very limited, these models provide additional characterizations of the crustal structure, which are probably valid in some average sense. Given the limited accuracy of the models, we prefer path average values instead of point-wise parameters. As regional seismic wave energy tends to average the waveguide structure along the path, mean crustal thickness is expected

Table 2. Parameters of the selected 57 earthquakes used in Southwest China.

Date (mon/day/yr)	Origin Time (hour:min:sec)	Focal Depth* (km)	$m_b$	Latitude (N°)	Longitude (E°)
1/3/88	21:32:24.0	4	5.4	38.10	106.34
1/25/88	1:12:22.2	36	5.4	30.16	94.87
2/6/88	14:50:45.4	33	5.8	24.67	91.56
9/3/88	12:52:46.0	22	5.0	29.95	97.33
11/5/88	2:14:30.0	5	5.8	34.35	91.85
11/15/88	10:28:14.6	18	5.0	23.15	99.65
11/27/88	4:17:56.4	16	5.0	22.73	99.86
11/30/88	8:13:30.0	15	5.5	22.76	99.84
1/18/89	18:22:47.0	28	5.1	30.18	100.21
2/3/89	17:50:00.0	19	5.4	30.19	89.94
2/12/89	7:55:46.0	20	5.1	26.20	96.90
4/15/89	20:34:10.1	21	6.0	29.97	99.23
4/25/89	2:13:20.9	8	6.1	30.01	99.43
5/3/89	05:53:03.0	25	6.0	30.07	99.49
5/3/89	15:41:30.0	0	5.8	30.04	99.53
5/7/89	0:38:18.6	33	5.4	23.54	99.54
5/13/89	23:19:39.7	15	4.9	35.27	91.58
7/21/89	3:09:15.0	25	5.5	30.02	99.46
9/22/89	2:25:49.0	4	6.0	31.54	102.45
1/14/90	3:03:19.2	12	6.1	37.80	91.97
3/8/90	18:57:00.0	24	4.8	25.45	96.64
5/7/90	5:17:33.0	1	5.5	36.10	100.36
5/15/90	22:29:59.2	13	5.5	36.09	100.16
6/2/90	0:32:36.0	17	5.5	32.45	92.81
10/20/90	8:07:27.7	12	5.5	37.07	103.8
1/5/91	14:57:11.2	18	6.1	23.55	95.96
1/12/92	0:12:27.3	22	5.4	39.67	98.34
6/15/92	2:48:56.1	17	5.8	24.00	95.97
7/30/92	8:24:49.0	31	5.8	29.57	90.18
12/22/92	16:42:37.0	31	5.0	34.55	88.06
1/18/93	12:42:04.5	10	5.7	30.84	90.38
1/26/93	20:32:06.8	32	5.4	23.01	101.10
3/20/93	14:51:59.7	12	5.7	29.03	87.33
3/20/93	21:26:40.0	21	4.9	29.01	87.34
7/17/93	9:46:34.1	26	5.2	27.99	99.62
8/14/93	14:30: 4.8	33	4.9	25.42	101.54

Table 2. (Continued)

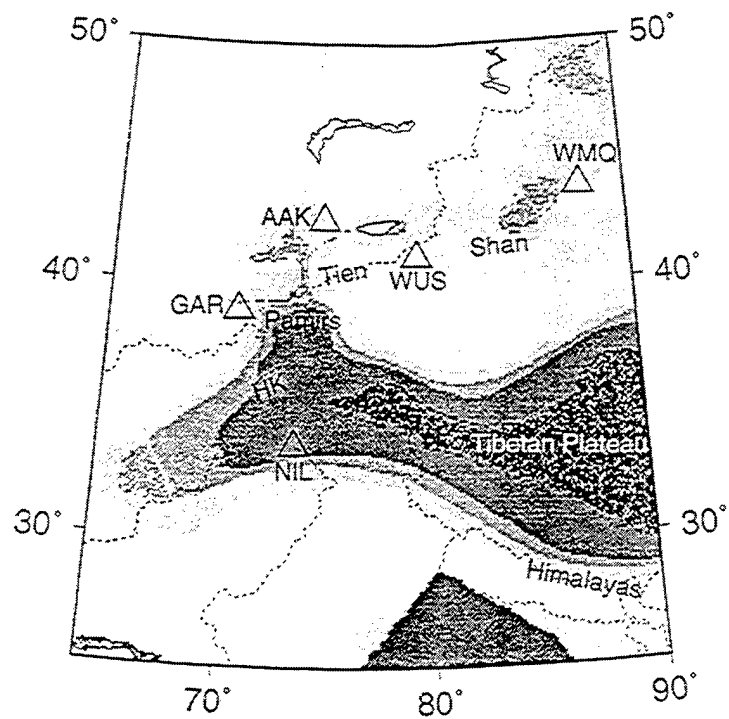
Date (mon/day/yr)	Origin Time (hour:min:sec)	Focal Depth* (km)	$m_b$	Latitude (N°)	Longitude (E°)
1/3/94	5:52:27.7	15	5.7	36.03	100.12
1/11/94	0:51:56.4	32	5.9	25.21	97.21
4/6/94	7: 3:27.6	15	5.6	26.19	96.87
6/29/94	18:22:33.5	15	5.9	32.57	93.67
6/30/94	0:48:32.5	15	5.1	32.54	93.68
7/23/94	20:57:59.0	17	5.1	31.07	86.55
8/14/94	7:38:27.3	33	4.5	34.93	89.21
9/4/94	14:50:34.3	15	5.3	35.94	100.08
9/7/94	13:56:25.2	33	5.1	38.49	90.35
9/23/94	19:15:44.4	15	5.1	36.05	100.15
10/10/94	14: 7:57.3	33	5.0	36.06	100.16
11/21/94	8:16:34.0	43	5.6	25.54	96.66
12/28/94	3:56:17.4	33	4.9	35.84	90.69
12/29/94	18:58:30.4	33	5.3	29.08	103.79
2/17/95	2:44:25.0	35	5.2	27.64	92.37
7/9/95	15:56:28.5	33	5.2	36.04	100.07
7/21/95	22:44: 7.6	15	5.7	36.44	103.11
10/23/95	22:46:50.4	15	5.5	26.00	102.27
12/18/95	4:57: 5.1	33	5.2	34.53	97.29
2/4/96	16:58:05.9	15	5.6	27.04	100.30
2/6/96	7:36:13.7	15	5.3	27.19	100.28

\*Focal depths are determined by the ISC or from Harvard CMT solutions.

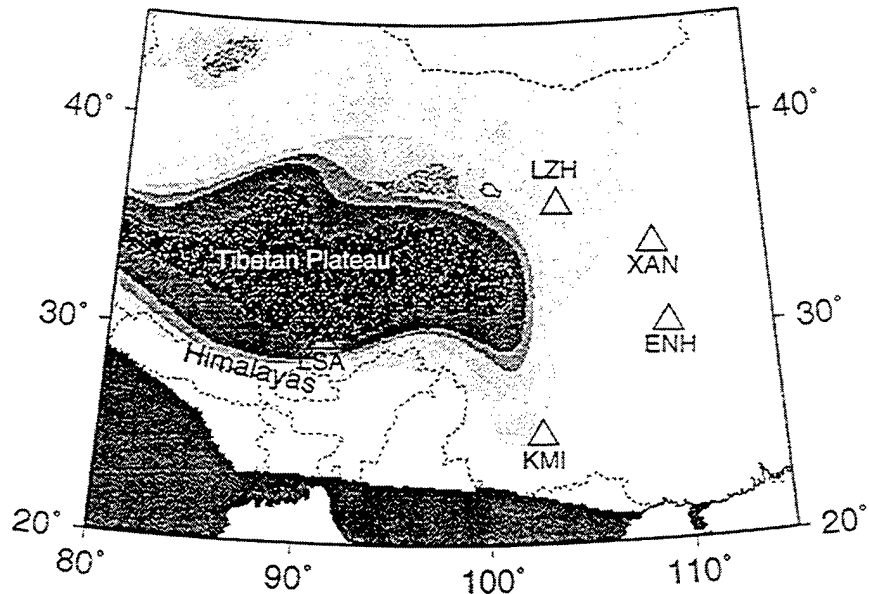
to be a better path parameter than a point-wise property, such as minimum and maximum Moho depth. As we shall see, this path averaging leads to limitations in regionalization efforts.

### Method

We parameterize our models with several path-specific parameters for waveguide properties, such as mean elevation, rms roughness (variance) of topography, rms slope of topography from point to point along the path, mean Moho depth, and mean sediment thickness. These parameters have been shown to provide effective path corrections in previous work (Fan and Lay, 1997a, b; Rodgers et al, 1997c). Topographic skewness, or the third moment of topography, and minimum and maximum measures for crustal thickness and sediment thickness are subject to much greater uncertainties and provide



a)



b)

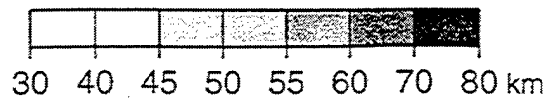


Figure 2. Depth to the Moho discontinuity for: a) central Asia; b) southwest China. HK, Hindu Kush. The labeled triangles are the seismic stations used. The blackened areas represent regions where there are no data for the Moho depth.

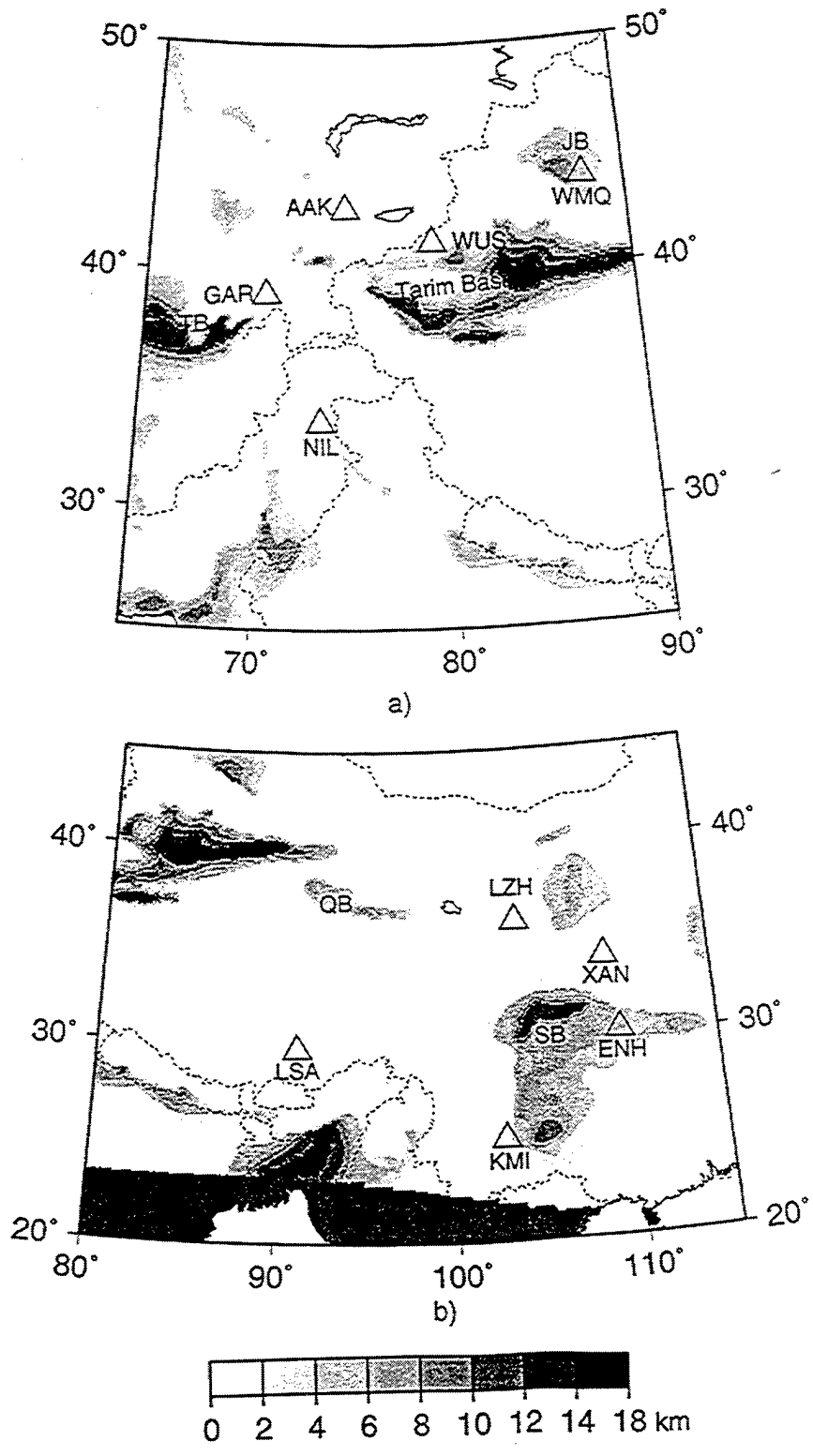


Figure 3. Sedimentary basin thickness for: a) central Asia; b) southwest China. TB, the Tadjik Basin; JB, the Junggar Basin; SB, the Sichuan Basin; QB, the Qsaidam Basin. The blackened area represents the region where there are no data for sediment thickness.

largely redundant information about the shape of the Moho discontinuity and basement structure, thus they are not used here. Other databases, such as frequency-dependent path attenuation models, may also be considered, but at present these are even less reliable for western China than the gross crustal models, so we restrict our attention to the measures listed above.

To reduce the scatter in regional discriminant measures we use multivariate regression to determine the best set of predictor variables from a set of parametric path properties giving an empirical model minimizing the variance in the data. Our initial list of variables includes the six parameters:  $x(1)$ , path length;  $x(2)$ , mean altitude;  $x(3)$ , rms roughness;  $x(4)$ , rms slope;  $x(5)$ , mean crustal thickness; and  $x(6)$ , mean sediment thickness. We construct a model in which these six parameters are initially assumed to influence a regional phase ratio,  $Y$ , such as  $\text{Log}(P_g/L_g)$ , for a given frequency band in the form

$$Y_i = \beta_0 + \beta_1 x_{i1} + \beta_2 x_{i2} + \beta_3 x_{i3} + \beta_4 x_{i4} + \beta_5 x_{i5} + \beta_6 x_{i6} + e_i \quad i = 1, 2, \dots, n, \quad (1)$$

where  $Y_i$  is the  $i$ -th observation that is assumed to be a linear combination of the  $x_{i1}$ ,  $x_{i2}$ , ...,  $x_{i6}$  predictor variables with linear coefficients  $\beta_0, \beta_1, \beta_2, \dots, \beta_6$ ,  $e_i$  is the random error associated with measurement of  $Y_i$ , and  $n$  is the number of observed values. If  $k$  is the number of independent variables considered, the model has  $m = k+1$  unknown parameters ( $m$  varies up to 7). We seek to identify and retain in the model only those parameters that are statistically significant. We denote estimates of the  $\beta_j$  model coefficients as  $b_j$ .

To overcome the drawbacks from multicollinearity in application of parameter elimination techniques, we compute all possible linear regressions for all combinations of the six path parameters and then select a set of preferred parameters based on statistics of the solutions. High multiple coefficient of determination ( $R^2$ ) and two other criteria are used in selecting the best solution: (1) the mean square error (MSE) criterion, and (2) the

$C_p$ -statistic criterion. The MSE criterion minimizes the variance, taking into account the number of parameters in the model ( $m$ ), but it does not assess the resolution or contribution of each parameter. Mallows's  $C_p$ -statistic criterion is defined to be:

$$C_p = \frac{SSE_p}{S_k^2} - (n - 2p) \quad (2)$$

where  $SSE_p$  is the sum of squared errors for the model obtained for a subset of  $p$  variables out of a total of  $k$  predictor variables being considered; and  $S_k^2 = MSE(x_1, x_2, \dots, x_k)$  is the estimation variance based on all  $k$  predictor variables. After all possible regression combinations are determined,  $C_p$  is computed for each case. Since  $SSE_p$  represents the unexplained variation calculated from the model, we want  $SSE_p$  to be small, which means we want  $C_p$  to be small. Although adding even one unimportant independent variable to the regression model would decrease  $SSE_p$ , it may increase  $C_p$ . Thus, models that have  $C_p$  values close to  $p$  (i.e. low values) are the most desirable.

To judge goodness of fit in selection of the models, the estimate of the regression coefficient for an individual variable has to be checked against its standard deviation to ensure that error associated with the coefficient is small. The preferred model must pass an F-test for the complete model and pass partial F-tests for each individual model parameter. As a double check, the individual t-statistics should be greater than rejection points with at least 95% confidence such that we can accept a hypothesis that a given parameter is non-zero. These combined statistical tests then indicate that all model parameters retained are indeed related to the amplitude ratio being considered at a confidence level of at least 95%.

After the best model is selected for a specific discriminant in a given frequency band, we calculate the variance reduction for the distance-corrected data and the data corrected with the best models relative to the uncorrected original data. The numerical values of variance reduction are measures of how well the scatter in original data is reduced. We recognize, of course, that reducing the scatter will not necessarily result in



enlarged separation between the populations of earthquakes and explosions (Hartse et al., 1997b). However, there is no question that propagation effects should be fully suppressed before testing discriminant performance. We use variance reduction here to evaluate strategies for correction for propagation effects, comparing corrections applied on a station basis or on a regional basis.

### Regionalized Path Effects

We initially analyze the path effects on the  $P_g/L_g$  ratios measured in different frequency bands for individual seismic stations and for all stations combined in each of the two sub-regions. Linear correlation coefficients are calculated for the six path-related predictor variables along with two compound parameters, involving multiplication of path length with mean elevation or rms roughness (motivated by the results of Zhang et al., 1996). Simple linear correlation analysis provides guidance as to which parameters are likely to be important, but of course it does not address possible collinearity. We begin to address that by directly correlating the waveguide measures.

Correlations among various waveguide parameters vary between the different geologic regions. For previously analyzed data at station WMQ, mean elevation, rms roughness and mean Moho depth all show moderate correlations with path length (Fan and Lay, 1997a). For our paths in central Asia and southwest China only rms roughness is moderately correlated with distance. The correlation between path length and mean sediment thickness is also weak for these two sub-regions. Among variables directly related to the crustal waveguide, mean elevation exhibits strong correlation with rms slope in central Asia (Figure 4a), while it is most strongly correlated with mean crustal thickness in southwest China (Figure 4b). Individual station correlations can be stronger than

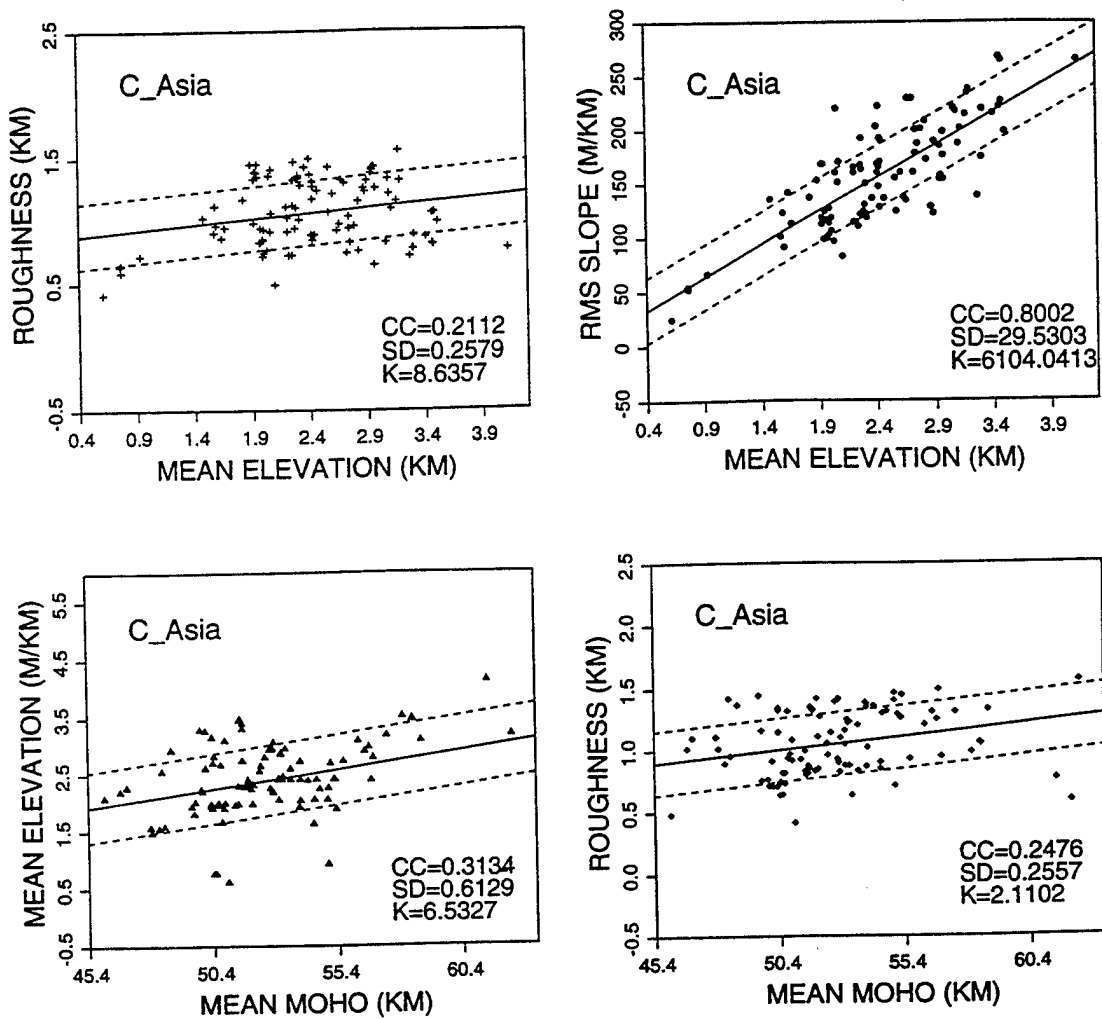
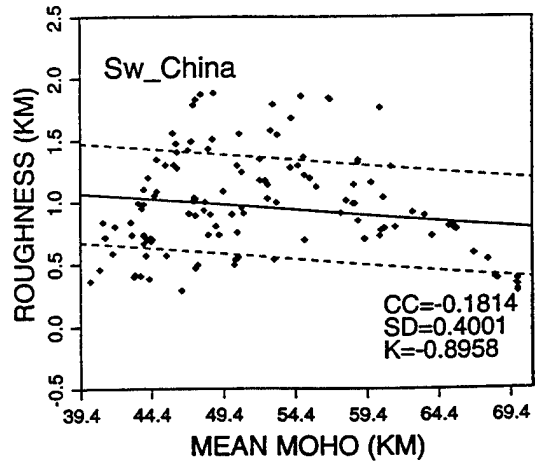
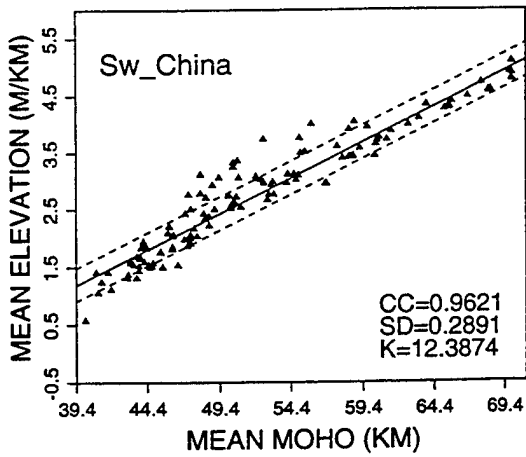
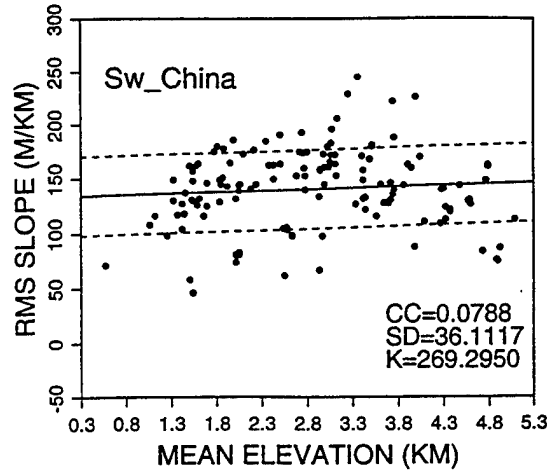
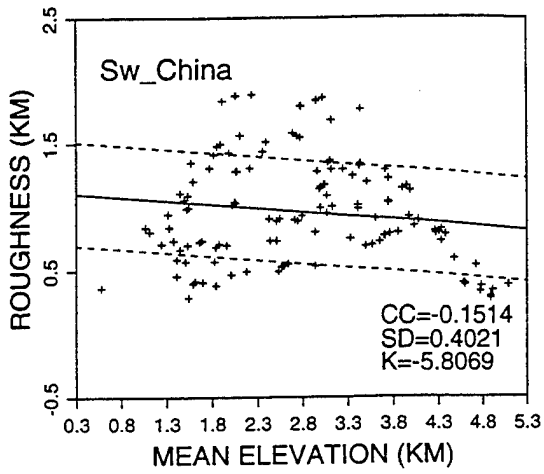


Figure 4. Correlations a) for central Asia; b) for southwest China between rms topographic roughness and rms surface slope with mean path elevation (top) and mean elevation and rms topographic roughness with mean crustal thickness (bottom). CC, linear correlation coefficient; SD, standard deviation of the linear regression; K, slope of the regression line. The dotted lines indicate  $\pm 1$  standard deviation about the regression line.

Figure 4b.



regional combinations, but the modest correlation between waveguide parameters is appealing for our statistical analysis.

The relative amplitudes of regional phases generally experience distance-dependent variations caused by differential attenuation and geometric spreading (Kennett, 1989; McCormack et al., 1995; Zhang et al., 1996). In practice, various relationships are proposed to describe the simplest distance dependence, such as power law, or exponential decay (Serenio, 1991; Baumgardt and Der, 1994; Zhang and Lay, 1994). Using simple empirical distance relationships is defensible as a first order correction for gross characterization of the propagation effects. However, even if the crust were laterally uniform, these simple distance expressions are not strictly correct. We make the simple assumption that logarithmic amplitude ratios are linearly related to path length as well as to other parameters, which effectively invoke power law relationships in each case. This is purely empirical and not based on a particular physical model.

In Figure 5, the  $P_g/L_g$  amplitude ratios for central Asia display significant distance dependence for individual stations and for the combined data set as reflected in correlation coefficients ranging from 0.3 to 0.8 in the three passbands below 6 Hz. The correlations with path length usually decrease with increasing frequency. GAR is an exception, as the correlation with path length is strongest in the 3-6 Hz passband. The frequency dependence of correlation coefficients with distance is stronger in southwest China, where the correlations with distance show negative trends at 3-6 Hz frequencies except for station XAN (see Figure 6). The  $P_g/L_g$  amplitude ratios observed at station LSA have weak correlations ( $\sim 0.32$ ) with distance at low frequencies of 0.75-1.5 Hz, while these amplitude ratios show a strong negative correlation at higher frequencies (3-6 Hz).

Previous analysis of  $L_g$  attenuation indicates that frequency-dependent apparent  $Q$  within the Tibetan Plateau is much lower than observed in typical continental crust, therefore,  $L_g$  should diminish rapidly along propagation paths in Tibet (McNamara et al., 1996). The change in sign of correlation between  $P_g/L_g$  amplitude ratios and propagation

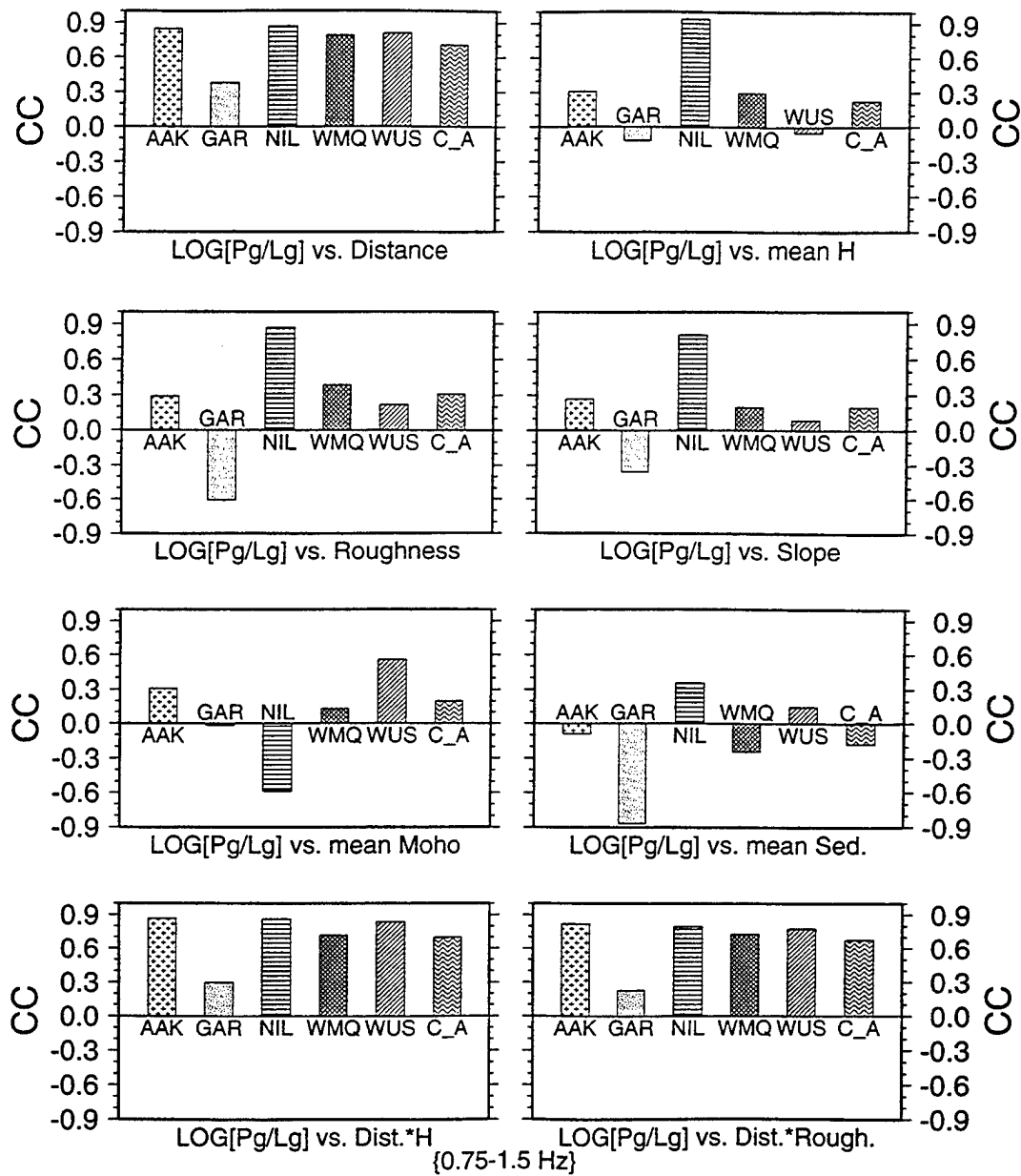


Figure 5. Correlations of  $\text{Log}(P_g/L_g)$  with various waveguide parameters, such as distance, mean path elevation (H), variance of topography (roughness), rms slope (slope), mean crustal thickness (Moho) and mean thickness of sediments (sed) for individual stations and for the combined set of stations (C\_A) in central Asia in three frequency bands (a) 0.75-1.5 Hz, (b) 1.5-3.0 Hz, and (c) 3.0-6.0 Hz. CC, linear correlation coefficients.

Figure 5b.

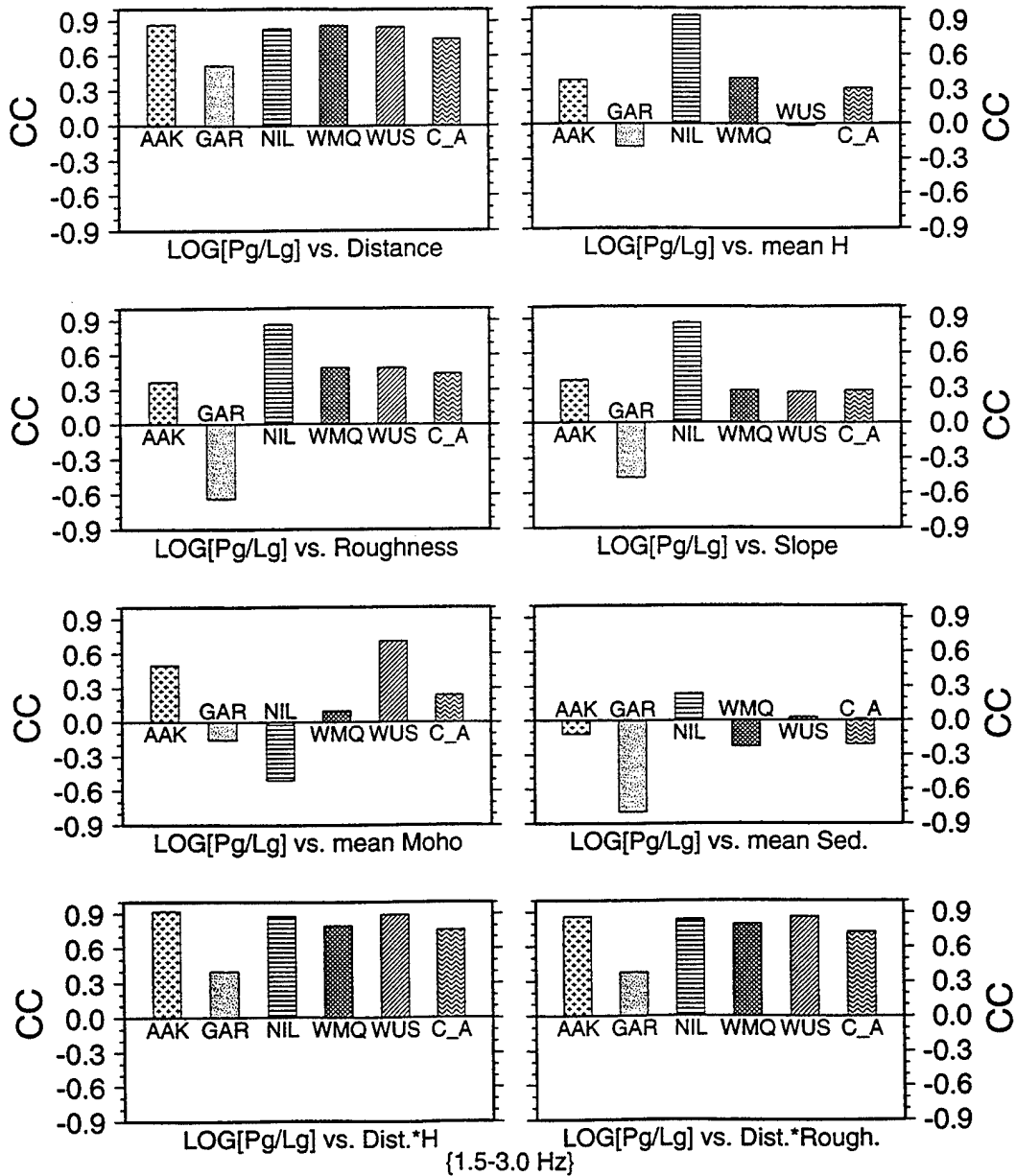
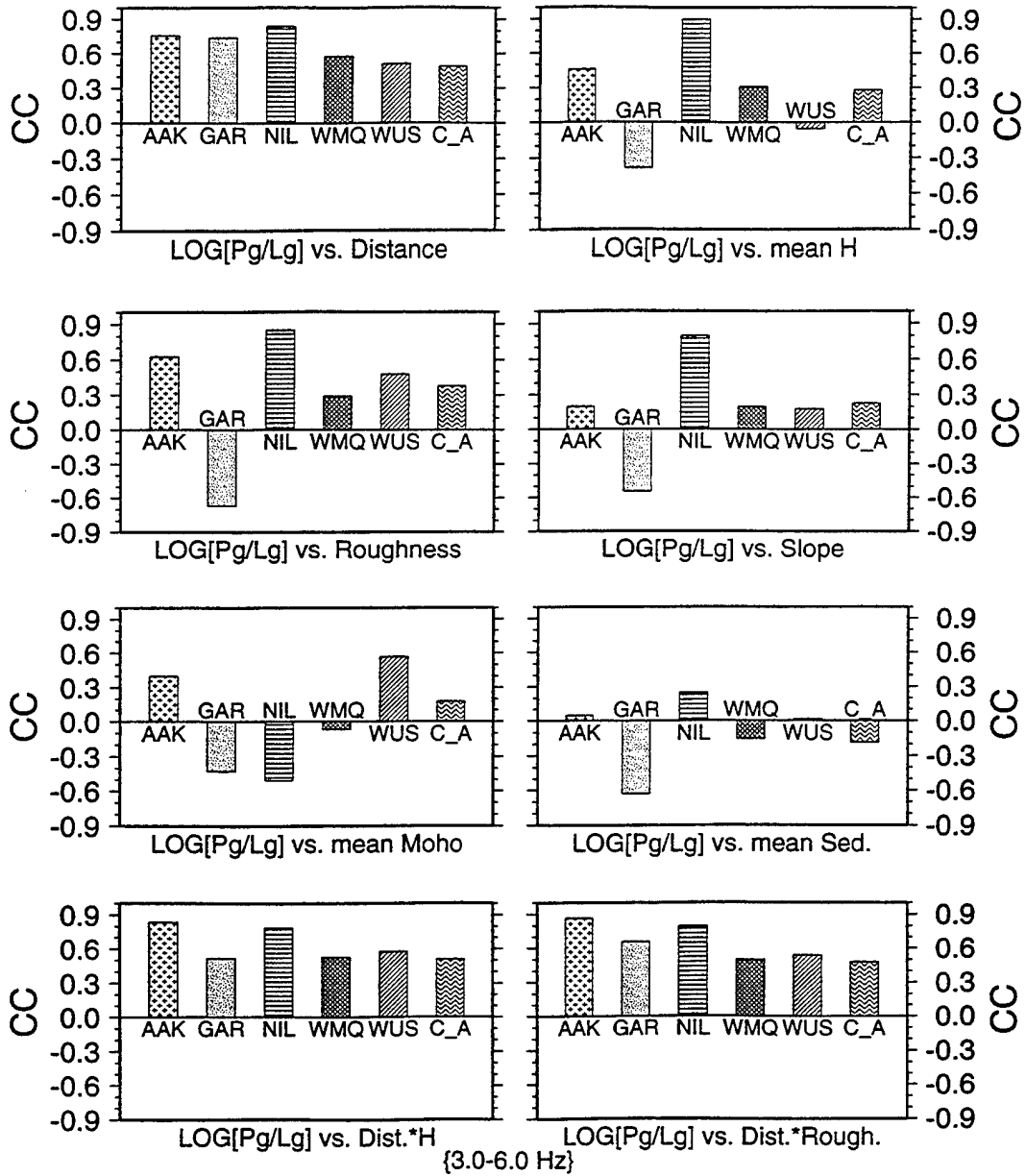


Figure 5c.



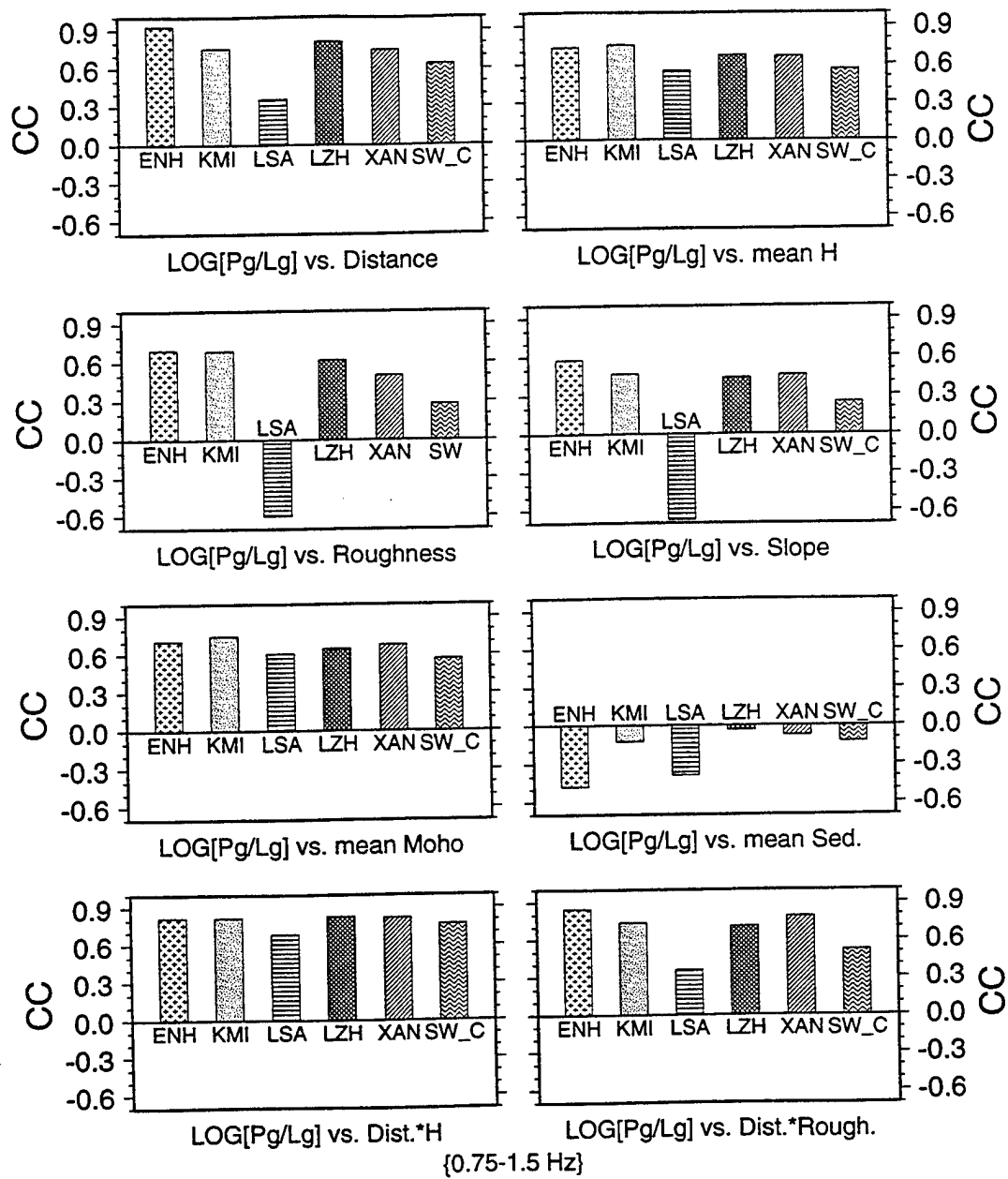


Figure 6. Similar to Figure 5 for stations in southwest China.



Figure 6b.

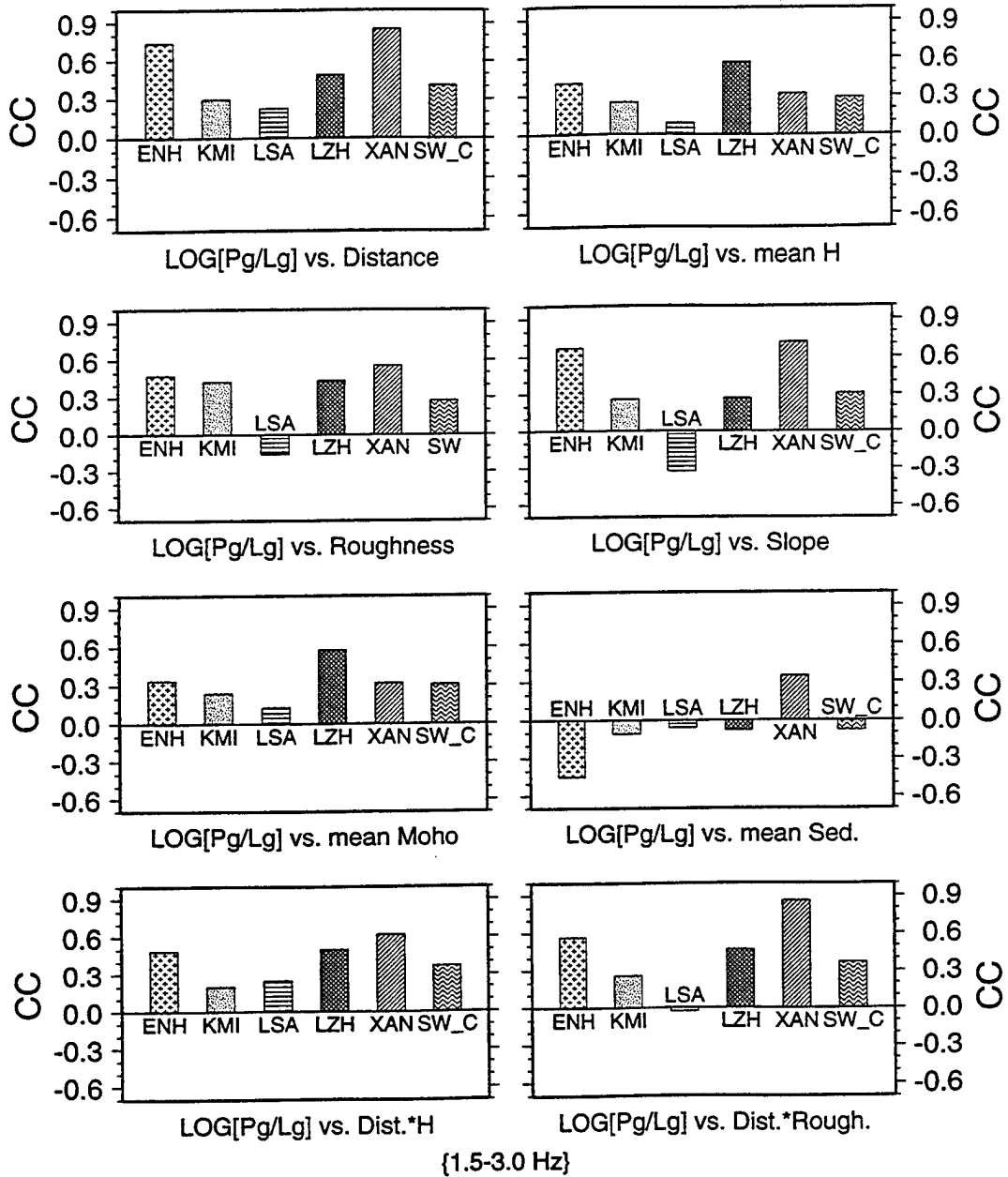
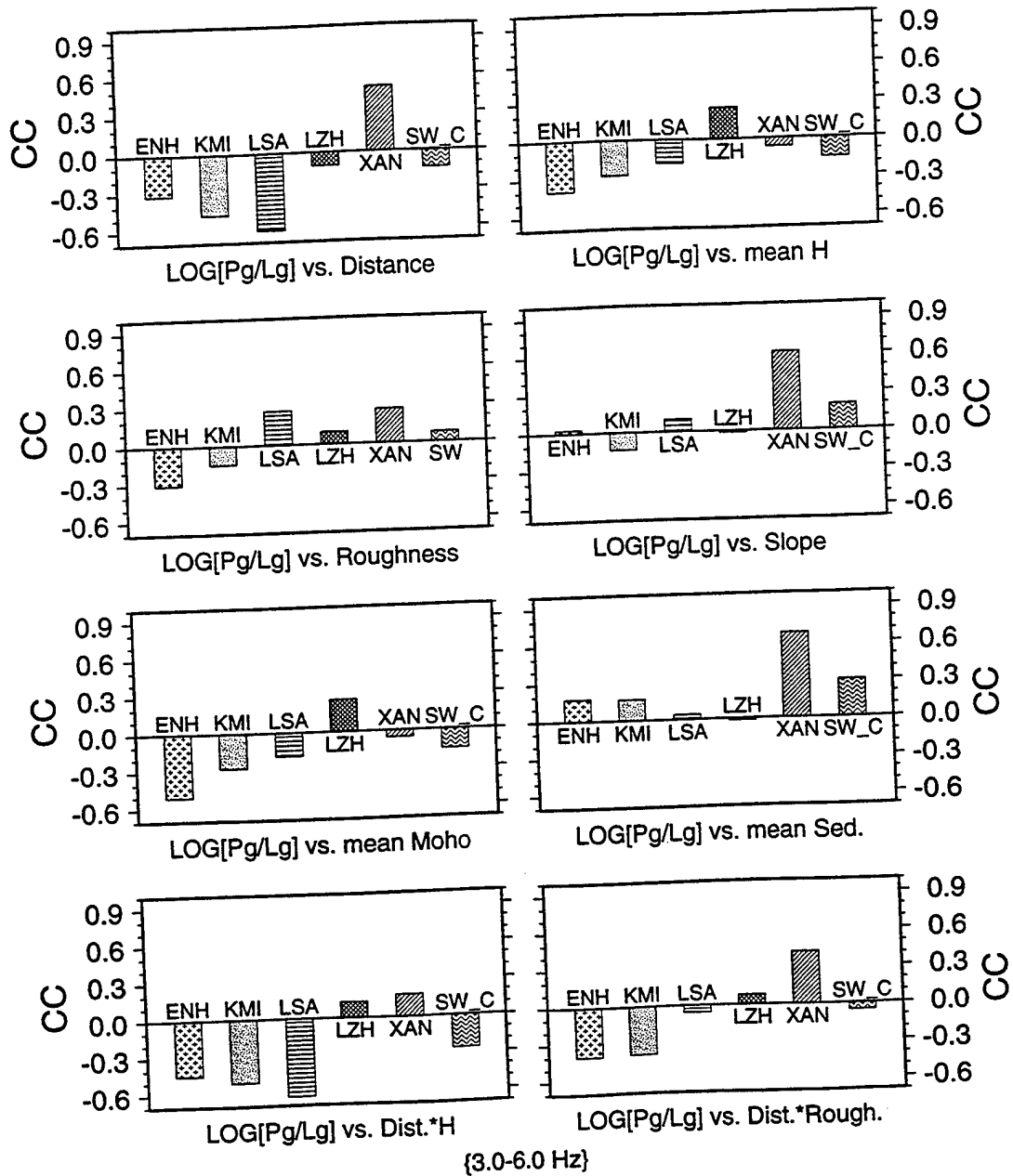


Figure 6c.



path length from positive correlations at lower frequencies (0.75-1.5 Hz) to negative correlations at higher frequencies (3.0-6.0 Hz) is not easily explained. High frequency  $P_g$  energy may attenuate at a faster rate than  $L_g$  energy relative to the lower frequency band, or this may be a manifestation of frequency dependent partial blockage.

While the  $P_g/L_g$  ratios show typically strong correlations with path length, relationships with other waveguide properties vary between stations and regions. In central Asia, linear correlations of the combined data with the various topographic parameters considered are usually weak (Figure 5) and using the product of distance times mean elevation or rms roughness does not give improved correlations relative to those with distance alone. The combined data set appears to average the individual station trends, which are highly variable from station to station. Station NIL shows strong correlations with topographic parameters, and station GAR has strong correlations with sedimentary thickness, but these appear to be very station specific and probably very dependent on data coverage.

In contrast, for southwest China, the  $P_g/L_g$  amplitude ratios are significantly correlated with most of the path-specific parameters, such as mean elevation, rms roughness, and mean crustal thickness, with linear correlation coefficients from 0.3 to 0.8 at low frequencies (0.75-1.5 Hz), except for station LSA (Figure 6a). The correlations between the  $P_g/L_g$  ratios and rms surface slope are moderate with the coefficients varying from 0.3 to 0.6 at each station. The  $P_g/L_g$  amplitude ratios show weak negative correlation trends with mean thickness of sediments. The model of sediment thickness is perhaps of the lowest accuracy; some paths are predicted to have no sediments at all despite the existence of many small grabens and depressions in southwest China (Hu and Gao, 1994). Similar behavior is seen in 1.5-3.0 Hz passband (Figure 6b). At higher frequencies of 3-6 Hz, the linear correlations change sign at many stations and usually have smaller coefficients. Generally speaking, the  $P_g/L_g$  ratios observed at the stations located outside

of the Tibetan Plateau show similar relationship to waveguide parameters to those observed at station WMQ.

### Results of Multivariate Regressions

Following Fan and Lay (1997 a, b), we perform multivariate regressions for the two sub-regions. We are especially interested in establishing an empirical calibration strategy for regional discriminants used in monitoring the CTBT. We want to determine which waveguide parameters can be most effectively utilized for correction of the propagation path effects, and whether this should be done on a station by station or regional average basis. In the western U.S., the strongest single-parameter empirical correlations were found for the product of path length with mean elevation or mean roughness, indicating a cumulative effect on the amplitude ratios (Zhang et al., 1996). At station WMQ, strong correlations with propagation distance as well as with mean crustal thickness and mean elevation are observed (Fan and Lay, 1997a, b). In the Middle East, distance and sedimentary structure are most important (Rodgers et al., 1997c). These results are not conflicting; in any given area, different attributes of the waveguide may prove dominant, depending on the path sampling.

In central Asia, the best models for the entire area generally involve two or more waveguide parameters. Table 3 lists the best combinations of waveguide parameters for various discriminants. Path length and mean elevation are the most important model parameters in regional calibration. Mean crustal thickness, mean sediment thickness and variance of topography are sometimes significant. As rms surface slope is strongly correlated with mean elevation, it does not appear in the final calibration models. This is similar to our previous analysis for WMQ, where rms slope, rms roughness and mean sediment thickness proved to not be as important as path length and mean elevation. In some cases, alternate approaches, such as azimuthal binning (Rodgers et al., 1997b) could

isolate the path effects without needing to involve a waveguide parameterization, but that is a harder procedure to generalize.

The improvement in variance reduction achieved by applying corrections for the best multi-parameter models relative to corrections using only propagation path length is between 4-12% for most of discriminants for the combined data in central Asia (Figure 7). These values are not as large as those achieved at WMQ for which we have a large data set (Fan and Lay, 1997b). For  $\text{Log}(P_g/S_n)$ , the performance of the best model correction is much better than for distance correction, which actually increases the variance. The variance reductions are larger at frequencies below 3 Hz in all cases. As the variance reduces, the discriminant distributions approach normal distributions. The  $P_g/S_n$  ratios show relatively small scatter in uncorrected data, and the corrections give only modest additional variance reductions. The raw  $P_g/L_g$  ratios have moderate variance, which is substantially reduced (50%) by distance correction, and further reduced by 4-8% with correction for the best models. Both the  $P_n/S_n$  and  $P_n/L_g$  ratios have relatively large variance, which correction for path length reduces 43-70%. Correction for the best models reduces the variance by another 4-12%. Standard deviations for  $P_g/L_g$ ,  $P_g/S_n$ , and  $P_n/L_g$  are much lower in the passband of 3.0-6.0 Hz than those in lower frequencies (0.75-1.5 Hz). This was also found for the WMQ data (Fan and Lay, 1997b), and may indicate the lower frequency signals are more sensitive to large-scale waveguide structure variations.

Multivariate regressions on the combined data in southwest China give optimal models with 3 or more parameters (Table 4). Propagation path length and mean crustal thickness are the most important model parameters. There is strong multicollinearity between mean elevation and mean crustal thickness, and these can be interchanged with only minor decrease in model performance (topography is the more reliably measured parameter). Mean sediment thickness and variance of topography are the best additional model parameters. In contrast to central Asia, rms slope has low correlations with other waveguide parameters and emerges as an important factor in southwest China, possibly

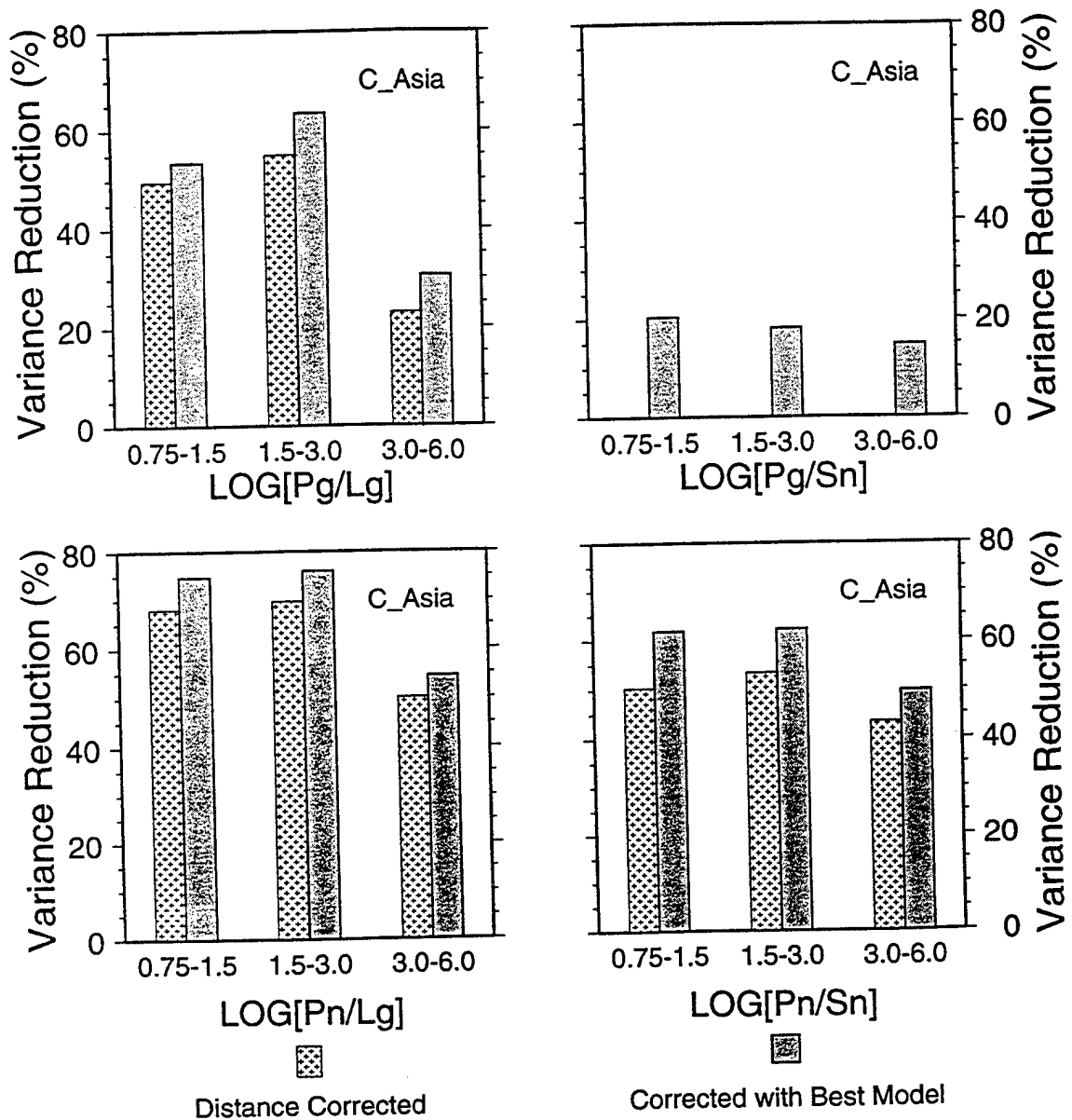


Figure 7. Variance reductions achieved for the  $P_g/L_g$ ,  $P_g/S_n$ ,  $P_n/L_g$ , and  $P_n/S_n$  amplitude ratios in central Asia using all stations together in three frequency bands using only distance corrections or corrections for the optimal set of waveguide parameters.

Table 3. The best parameter combinations for correcting various discriminants observed in central Asia

Discriminants	Frequency Band (Hz)	Distance	Mean Elevation	RMS Roughness	RMS Slope	Mean Crustal Thickness	Mean Sediment Thickness
Log( $P_g/L_g$ )	0.75-1.5	X				X	
	1.5-3.0	X	X			X	
	3.0-6.0	X		X			X
Log( $P_g/S_n$ )	0.75-1.5		X				X
	1.5-3.0		X				X
	3.0-6.0		X	X			
Log( $P_n/L_g$ )	0.75-1.5	X	X			X	X
	1.5-3.0	X	X			X	X
	3.0-6.0	X	X				
Log( $P_n/S_n$ )	0.75-1.5	X	X			X	
	1.5-3.0	X	X				
	3.0-6.0	X	X				

Table 4. The best parameter combinations for correcting various discriminates observed in Southwest China

Discriminants	Frequency Band (Hz)	Distance	Mean Elevation	RMS Roughness	RMS Slope	Mean Crustal Thickness	Mean Sediment Thickness
Log( $P_g/L_g$ )	0.75-1.5	X			X	X	
	1.5-3.0	X			X	X	X
	3.0-6.0	X			X		X
Log( $P_g/S_n$ )	0.75-1.5	X			X		
	1.5-3.0	X			X	X	
	3.0-6.0	X		X	X		
Log( $P_n/L_g$ )	0.75-1.5	X	X	X			X
	1.5-3.0	X		X	X	X	X
	3.0-6.0		X	X	X		X
Log( $P_n/S_n$ )	0.75-1.5	X		X		X	
	1.5-3.0	X		X	X	X	
	3.0-6.0			X	X	X	X

due to the strong gradients in elevation. Measurements at LSA show negative correlations with many waveguide parameters while positive correlations are observed at all other stations outside of the Tibetan Plateau. This perhaps results from the distinct location of LSA. Although ray paths for LSA and seismic stations outside of the Tibetan Plateau sample the same geologic regions, the geometry of the waveguide structure can produce direction-dependent energy partitioning. Previous numerical modeling indicates that crustal thinning and crustal thickening should have different effects on the relative amplitudes of regional phases (Lay, 1996), so LSA will have distinctive behavior relative to the other stations even on common paths. Removing observations from LSA improves the overall variance reduction slightly, and has small effects on the make up of the best models (Table 5).

Figure 8a shows the variance reductions achieved by distance correction in comparison with those for correction by the best models from multivariate regressions for all stations in southwest China combined. Distance correction is most effective for the  $P_n/L_g$  and  $P_n/S_n$  ratios with the variance reduced by about 51-74% at frequencies below 3 Hz. For the  $P_g/L_g$  and  $P_g/S_n$  ratios, variance reduction by distance correction is larger for the frequency band of 0.75-1.5 Hz (about 40% and 21%, respectively), and smaller (about 16% and 8%, respectively) in the frequency band of 1.5-3.0 Hz. At frequencies above 3 Hz the variance is reduced only a few percent by distance correction. When all path parameters are considered, significant improvements in variance reduction are observed. The largest improvement in variance reduction is associated with the  $P_g/L_g$  and  $P_g/S_n$  ratios (from 10% to 25%). For the  $P_n/L_g$  and  $P_n/S_n$  ratios, variance reduction improves by a moderate amount of 8-12% at frequencies below 3 Hz, and by 16-21% at frequencies above 3 Hz.

Omitting station LSA gives slightly better variance reductions for the combined data (Figure 8b). Distance correction reduces the variance by additional 5-10% at frequencies below 3 Hz and by about 3% at frequencies above 3 Hz. Applying the best models reduces



Table 5. The best parameter combinations for correcting various discriminants for 4 seismic stations in Southwest China

Discriminates	Frequency Band (Hz)	Distance	Mean Elevation	RMS Roughness	RMS Slope	Mean Crustal Thickness	Mean Sediment Thickness
Log( $P_g/L_g$ )	0.75-1.5	X			X	X	
	1.5-3.0	X	X		X	X	
	3.0-6.0	X			X		X
Log( $P_g/S_n$ )	0.75-1.5	X			X	X	
	1.5-3.0	X	X		X	X	X
	3.0-6.0	X			X		
Log( $P_n/L_g$ )	0.75-1.5	X			X	X	X
	1.5-3.0	X			X	X	X
	3.0-6.0			X	X		X
Log( $P_n/S_n$ )	0.75-1.5	X	X	X			X
	1.5-3.0	X		X	X	X	X
	3.0-6.0			X			X

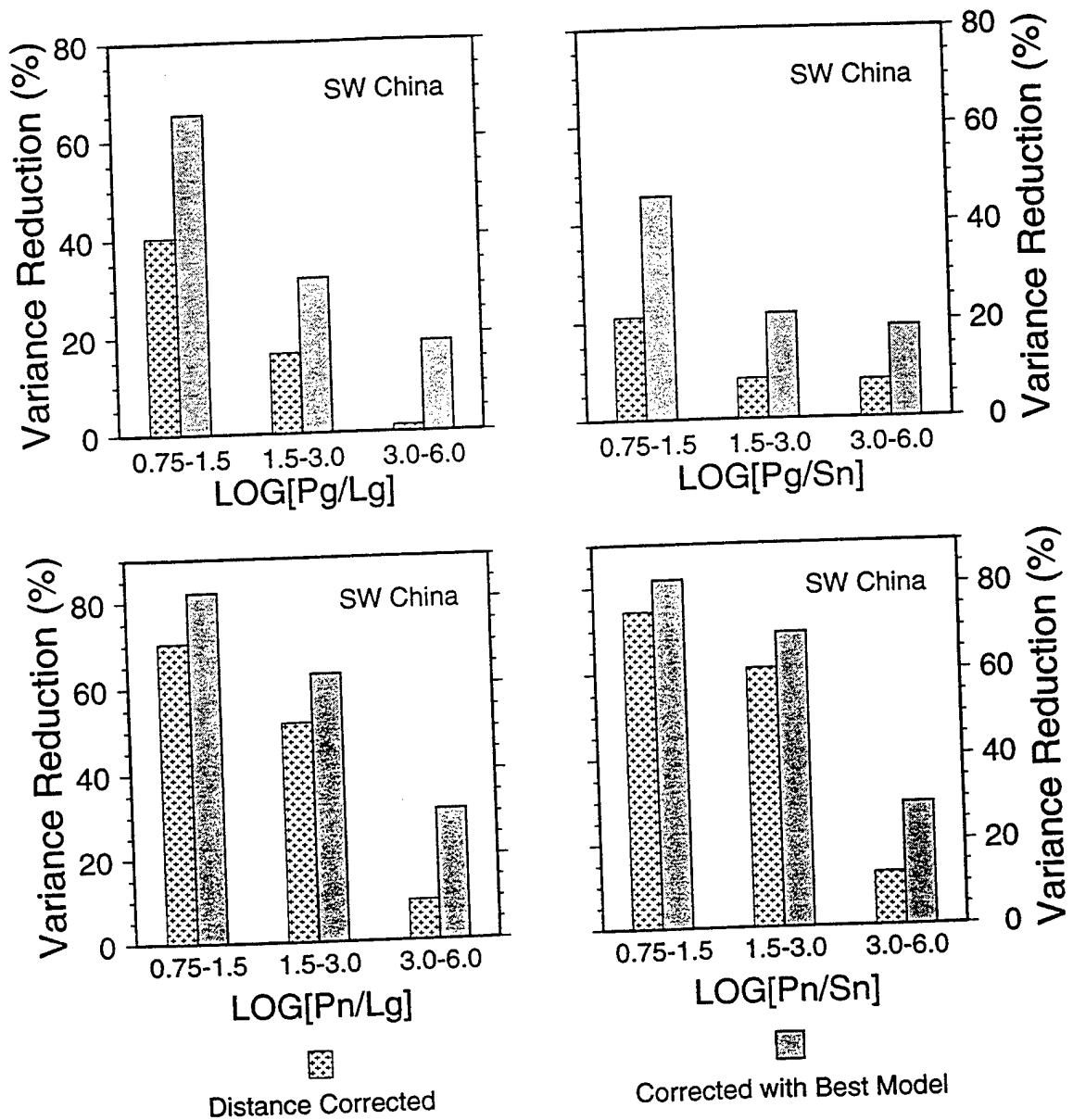
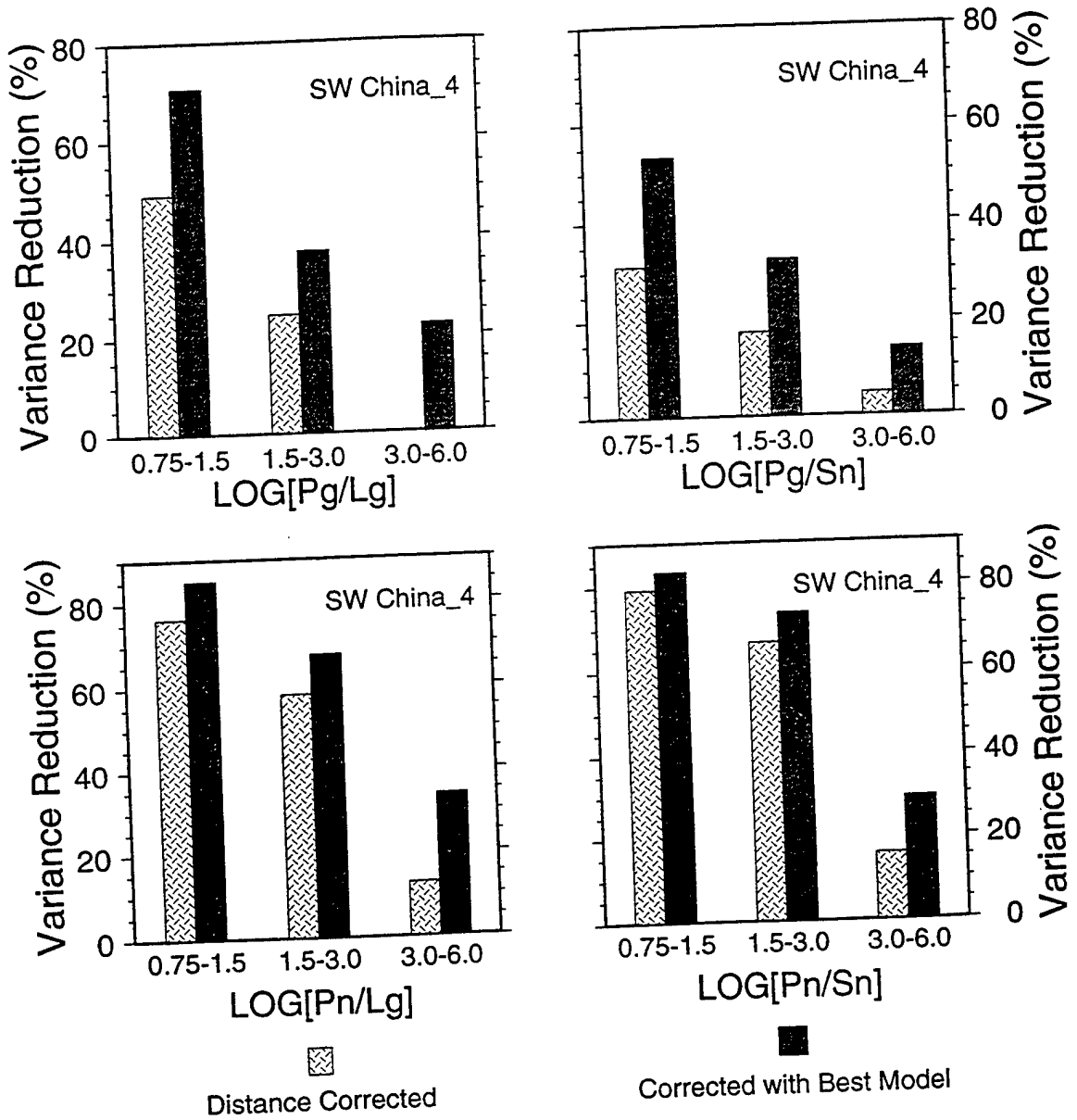


Figure 8. Variance reductions achieved for the  $P_g/L_g$ ,  $P_g/S_n$ ,  $P_n/L_g$ , and  $P_n/S_n$  amplitude ratios in southwest China using all stations together in three frequency bands using only distance corrections or corrections for the optimal set of waveguide parameters. a) including station LSA; b) omitting station LSA.

Figure 8b.



the data scatter by about 3-10% at frequencies below 3 Hz and by 0.5-4% at frequencies above 3 Hz relative to the case with LSA included. The only exception is for the  $P_g/S_n$  ratios, for which no further variance reduction is obtained when corrected for the best models.

We applied separate multivariate regressions to the data from each seismic station. Table 6 shows the best parameter combinations to model the  $P_g/L_g$  amplitude ratios at the four seismic stations outside the Tibetan Plateau in southwest China at frequencies below 3 Hz. Although the linear correlation analysis indicated similar patterns between the  $P_g/L_g$  amplitude ratios and waveguide parameters, the best models from multivariate regressions differ. Figure 9 shows variance reduction achieved by distance correction and by correction for the best model parameters for KMI (Table 7). Variance reductions for the  $P_n/L_g$  and  $P_n/S_n$  ratios decrease as frequency increases, and the improvements from the distance correction to multiple parameter correction are about 4 - 25% over the frequency bands of interest. For the  $P_g/L_g$  and  $P_g/S_n$  ratios there are small variance reductions in the middle frequency band (1.5-3.0 Hz), and larger variance reductions in the high frequency band (3.0-6.0 Hz). The differences in variance reduction between distance correction and correction with the best models are between 9% and 16%. While the overall variance reductions are comparable to those for the combined data in Figure 8, the KMI data are fit significantly better by the individually tuned model. Taking  $P_g/L_g$  amplitude ratios as an example, using parameters derived from the combined data set has resulted in less effective variance reduction for corrections for distance or other path effects relative to using the parameters for individual station. While the decreases in variance reduction are modest in lower frequency band of 0.75-1.5 Hz (1.5% for distance correction and 8% for correction with the best models), the resultant variance reduction changes greatly in higher frequency bands. For distance corrections it decreases by about 10%, and for corrections using the best regional models no variance reduction is observed at all. Given the modest levels of

Table 6. The best parameter combinations for correcting  $P_g/L_g$  ratios observed at 4 seismic stations in southwest China at frequencies below 3 Hz

Seismic Station	Frequency Band (Hz)	Distance	Mean Elevation	RMS Roughness	RMS Slope	Mean Crustal Thickness	Mean Sediment Thickness
ENH	0.75-1.5	X			X		X
	1.5-3.0	X		X	X		X
KMI	0.75-1.5	X				X	X
	1.5-3.0			X			
LZH	0.75-1.5	X	X	X			
	1.5-3.0			X		X	
XAN	0.75-1.5		X	X	X		
	1.5-3.0	X			X		

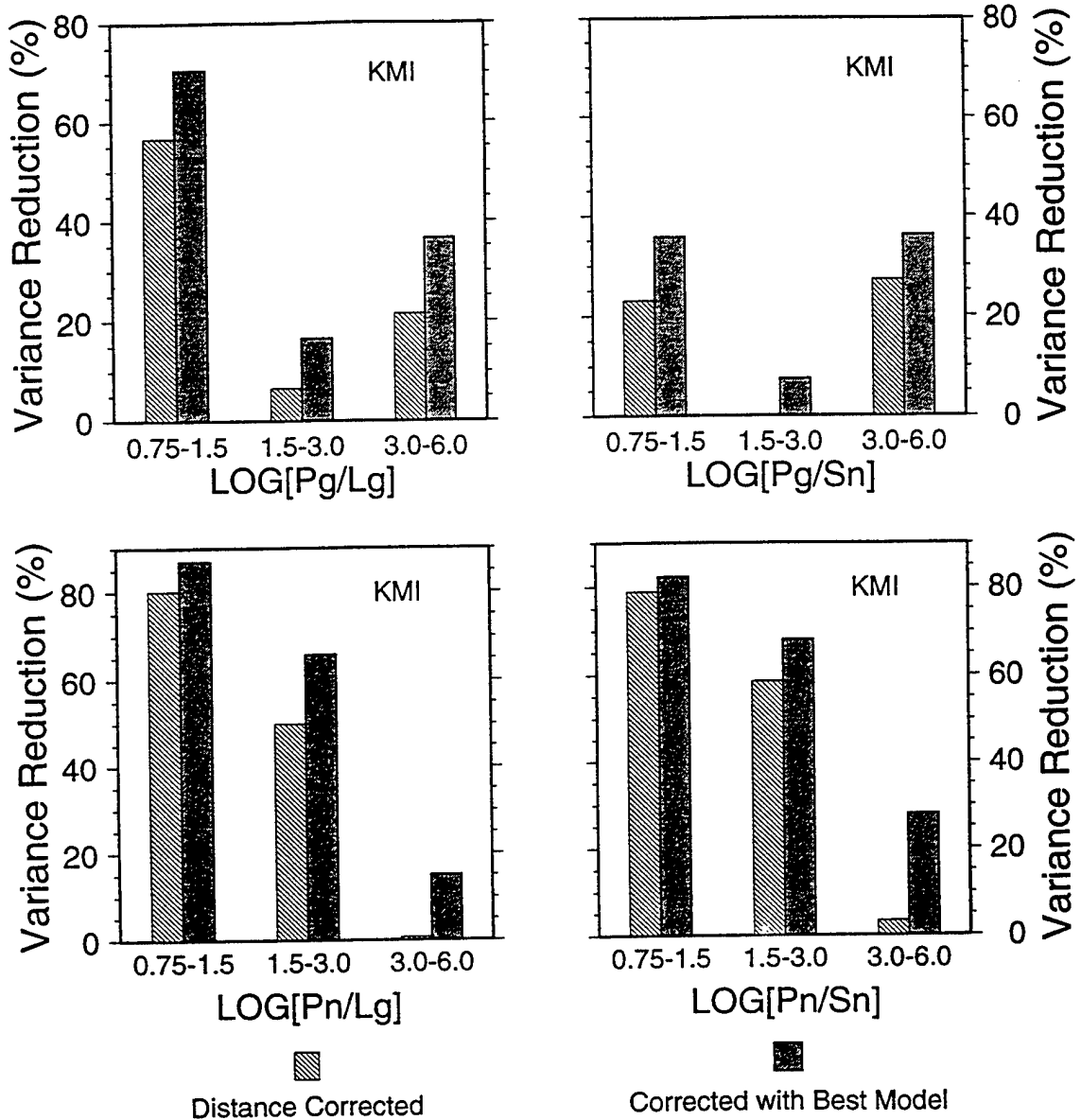


Figure 9. Variance reductions achieved for the  $P_g/L_g$ ,  $P_g/S_n$ ,  $P_n/L_g$ , and  $P_n/S_n$  amplitude ratios at station KMI in three frequency bands using only distance corrections or corrections for the optimal set of waveguide parameters.

Table 7. The best parameter combinations for correcting various discriminants observed at KMI

Discriminants	Frequency Band (Hz)	Distance	Mean Elevation	RMS Roughness	RMS Slope	Mean Crustal Thickness	Mean Sediment Thickness
Log( $P_g/L_g$ )	0.75-1.5	X	X				
	1.5-3.0			X			
	3.0-6.0	X		X			X
Log( $P_g/S_n$ )	0.75-1.5	X					X
	1.5-3.0				X		
	3.0-6.0	X		X			
Log( $P_n/L_g$ )	0.75-1.5	X		X		X	X
	1.5-3.0			X		X	X
	3.0-6.0			X			
Log( $P_n/S_n$ )	0.75-1.5	X			X		
	1.5-3.0	X		X			
	3.0-6.0	X	X	X			X

variance reduction for all path effects this favors separate station analysis.

### Summary and Conclusion

The results of multivariate regression analysis for the two sub-regions in central Asia and southwest China indicate that the waveguide structure indeed plays an important role in regional waveform energy partitioning. The scatter in the P/S amplitude ratios usually can be substantially reduced by applying distance corrections for regional discriminants. Applying corrections for other waveguide parameters can further reduce the scatter of the data from a few percent to more than twenty percent, depending on the type of discriminant and the frequency band under consideration. Complexity of lithospheric and crustal structure in various geographic areas causes the optimal model parameters involved to differ from one region to another. This study has demonstrated that the effects appear to differ from station to station within a given region as well. This is not a problem for empirical calibration, but does motivate station by station treatment. While we did find systematic improvements in variance reduction using waveguide parameters relative to distance correction alone, the resulting model is not transportable and only moderate gains were achieved. This contrasts with the potential improvements for single stations, as demonstrated by the studies for WMQ (Fan and Lay, 1997a, b) and ABKT (Rodgers et al., 1997c). While the single station data sets are much smaller in the present study, it does appear that WMQ and ABKT may be relatively extreme cases of variable waveguide effects.

An interesting observation is that the improvement in variance reduction is usually more significant at lower frequencies ( $< 3$  Hz); in most cases regional discriminants show weak correlations with waveguide features at higher frequencies ( $> 3.0$  Hz). This may be part of the explanation for the poor performance of P/S ratios at low frequencies, although it may also be true that source types are intrinsically not distinctive at low frequencies.



Strong scattering and homogenization of the high frequency wavefield may cause regional waves of higher frequencies to be insensitive to deterministic waveguide structure. Given the lack of single shot explosions with which to calibrate discriminants in most regions of CTBT monitoring concern, it is likely that we will have to rely on outlier analysis to detect clandestine tests. Almost any procedure which objectively and believably reduces scatter caused by propagation effects across the entire frequency band is desirable.

Tectonically complex areas, like our study regions, are likely to have the most pronounced waveguide effects, and also tend to have limited band width in regional signals. Thus, corrections like those explored in this report are most likely to be useful and necessary. Gaining confidence in empirical path corrections that attempt to account for controlling effects on regional phases such as geometric spreading, attenuation, scattering, sedimentary basins, changes in Moho depth, rough surface topography, and internal crustal structure, provides a strong motivation for extensive modeling of realistic (3-dimensional) crustal waveguides with structure at a wide variety of scale lengths.

The systematic relationships found in this study between regional discriminants and parameters of the waveguide structure confirm the notion that regionalized waveguide effects involve a complex continuum of path specific effects. A regional discriminant calibration strategy that invokes multivariate regression analysis of several path parameters such as mean crustal thickness and mean altitude as well as propagation path length provides a means reducing the scatter in regional discriminants beyond standard distance correction. This strategy should be applied on a station-by-station basis rather than on the basis of a geographic region, and the specific results for a given station are unlikely to be transportable. Fortunately, surface topography parameters are usually among the most important ones, and these effects can be reliably estimated. There is a clear need to improve our knowledge of sedimentary basin characteristics.

**Acknowledgments.** We would like to thank the IRIS DMC for providing access to the digital seismic data used in this study. We thank Dr. H. Hartse of Los Alamos National Laboratory and Dr. A. Rodgers of Lawrence Livermore National Laboratory for sending us preprints. Figures were generated using GMT tools developed by P. Wessel and W.H.F. Smith (1991). This research was supported by Phillips Laboratory Contract No. F19628-95-K-0014, and by IGPP-LANL UCRP grant #609. This is contribution #345, the Institute of Tectonics, University of California, Santa Cruz.

#### References

- Baumgardt, D. R. (1990). Investigation of teleseismic Lg blockage and scattering using regional arrays, *Bull. Seism. Soc. Am.*, **80**, 2261-2281.
- Baumgardt, D. R., and Z. Der (1994). Investigation of the transportability of the P/S ratio discriminant to different tectonic regions, *Sci. Report 1, PL-TR-94-2299*, ENSCO, Inc., Springfield, Virginia. ADA292944
- Bostock, M. G., and B. L. N. Kennett (1990). The effects of 3-D structure on Lg propagation pattern, *Geophys. J. Int.*, **101**, 355-365.
- Campillo, M., B. Feignier, M. Bouchon, and N. Bethoux (1993). Attenuation of crustal waves across the Alpine range, *J. Geophys. Res.*, **98**, 1987-1996.
- Fan, G.-W., and T. Lay (1997a). Statistical analysis of irregular waveguide influences on regional seismic discriminants in China, *Bull. Seism. Soc. Am.*, in press.
- Fan, G.-W., and T. Lay (1997b). A multivariate analysis of waveguide effects in Western China, submitted to *Bull. Seism. Soc. Am.*
- Fan, G.-W., J. F. Ni, and T. C. Wallace (1994). Active tectonics of the Pamirs and Karakorum, *J. Geophys. Res.*, **99**, 7131-7160.

- Fielding, E. J., B. L. Isacks, and M. Barazangi (1992). A geological and geophysical information system for Eurasia, *Tech. Report 2, F29601-91-K-DB08*, Philips Lab., Hanscom Air Force Base, Mass.
- Gupta, I. N., W. W. Chan, and R. A. Wagner (1992). A comparison of regional phase from underground nuclear explosions at East Kazakh and Nevada test sites, *Bull. Seism. Soc. Am.*, **82**, 352-382.
- Hartse, H. E., S. R. Taylor, W. S. Phillips, and G. E. Randall (1997a). A preliminary study of regional seismic discrimination in central Asia with emphasis on western China, *Bull. Seism. Soc. Am.*, **87**, 551-568 .
- Hartse, H. E., R. A. Flores, and P. A. Johnson (1997b). Correcting regional seismic discriminants for path effects in western China, submitted to *Bull. Seism. Soc. Am.*
- Hirn, A., A. Nercessian, M. Sapin, G. Jobert, Z. Xu, E. Gao, D. Lu, and J. Teng (1984). Lhasa block and bordering suture--a continuation of a 500-km Moho traverse through Tibet, *Nature*, **307**, 25-27.
- Holt, W. E., and T. C. Wallace (1990). Crustal thickness and upper Mantle velocities in the Tibetan Plateau region from the inversion of regional Pnl waveforms: Evidence for a thick upper Mantle lid beneath southern Tibet, *J. Geophys. Res.*, **95**, 12,499-12,525.
- Holt, W. E., J. F. Ni, T. C. Wallace, and A. J. Haines (1991). The active tectonics of the Eastern Himalayan Syntaxis and surrounding regions, *J. Geophys. Res.*, **96**, 14,595-14,632.
- Hu, H., and S. Gao (1995). Investigation of fine velocity structure of the basement layer of the shallow crust in western Yunnan region, *Earthquake Res. in China*, **9**, 311-319.
- Lay, T. (1996). Calibration of regional wave discriminants in diverse geological environments: Topographic correlations, in *Proceedings of the 18th annual seismic research symposium on monitoring a comprehensive test ban treaty, 4-6 September*

- 1996, J. F. Lewkowicz, J. M. McPhetres, D. T. Reiter editors, 209-218, PL-TR-96-2153, ERP #1195, ADA313692
- Le Dain, A. Y., P. Tapponnier, and P. Molnar (1984). Active faulting and tectonics of Burma and surrounding regions, *J. Geophys. Res.*, **89**, 453-472.
- Kadinsky-Cade, K., M. Barazangi, J. Oliver, and B. Isacks (1981). Lateral variations of high-frequency seismic wave propagation at regional distances across the Turkish and Iranian Plateau, *J. Geophys. Res.*, **86**, 9377-9396.
- Kennett, B. L. N. (1986). L<sub>g</sub> waves and structural boundaries, *Bull. Seism. Soc. Am.*, **76**, 1133-1141.
- Kennett, B. L. N. (1989). On the nature of regional seismic phases - I. Phase representations for P<sub>n</sub>, P<sub>g</sub>, S<sub>n</sub>, L<sub>g</sub>, *Geophys. J.*, **98**, 447-456.
- Kennett, B. L. N. (1993). The distance dependence of regional phase discriminants, *Bull. Seism. Soc. Am.*, **83**, 1155-1166.
- Kvaerna, T., and D. J. Doornbos (1991). Scattering of regional P<sub>n</sub> by Moho topography, *Geophys. Res. Lett.*, **18**, 1273-1276.
- McCormack, D. A., K. F. Priestley, and H. J. Patton (1998). Distance effects on regional discriminants along a seismic profile in northwest Nevada: NPE and nuclear results, *Bull. Seism. Soc. Am.*, in press.
- McNamara, D. E., T. J. Owens, and W. R. Walter (1996). Propagation characteristics of L<sub>g</sub> across the Tibetan plateau, *Bull. Seism. Soc. Am.*, **86**, 457-469.
- Mishra, D. C. (1982). Crustal structure and dynamics under Himalayas and Pamir ranges, *Earth Planet. Sci. Lett.*, **57**, 415-420.
- Ni, J., and M. Barazangi (1983). High-frequency seismic wave propagation beneath the Indian Shield, Himalayan Arc, Tibetan Plateau and surrounding regions: high uppermost mantle velocities and efficient S<sub>n</sub> propagation beneath Tibet, *Geophys. J. R. astr. Soc.*, **72**, 665-689.

- Ni, J., S. M. Guzman, M. Bevis, W. E. Holt, T. C. Wallace, and W. R. Seager, (1989).  
Accretionary tectonics of Burma and three dimensional geometry, *Geology*, **17**, 68-71.
- Press, F., and M. Ewing (1952). Two slow surface waves across North America, *Bull. Seism. Soc. Am.*, **42**, 219-228.
- Rodgers, A. J., J. F. Ni, and T. M. Hearn (1997a). Propagation characteristics of short period  $S_n$  and  $L_g$  in the Middle East, *Bull. Seism. Soc. Am.*, **87**, 396-413.
- Rodgers, A. J., W. R. Walter, and T. Lay (1997b). Calibration of distance and path effects on regional P/S discriminants at station ABKT (Alibek, Turkmenistan): Azimuthal sector regionalization, submitted to *Bull. Seism. Soc. Am.*
- Rodgers, A. J., W. R. Walter, T. Lay, and G. Fan (1997c). Calibration of distance and path effects on regional P/S discriminants at station ABKT (Alibek, Turkmenistan): Statistical analysis of crustal waveguide effects, submitted to *Bull. Seism. Soc. Am.*
- Roecker, S. W., O.V. Soboleva, I. L. Nersesov, A. A. Lukk, D. Hatzfeld, J. L. Chatelain, and P. Molnar (1980). Seismicity and fault plane solutions of intermediate depth earthquakes in the Pamir-Hindu Kush region, *J. Geophys. Res.*, **85**, 1358-1364.
- Ruzaikin, A. I., I. L. Nersesov, V. I. Khalturin, and P. Molnar (1977). Propagation of  $L_g$  and lateral variations in crustal structure in Asia, *J. Geophys. Res.*, **82**, 307-316.
- Sereno, T. J. (1991). Simulation of the detection and location capability of regional seismic networks in the Soviet Union, *Final Report*, SAIC-91/1061, San Diego, California.
- Taylor, S. R. (1996). Analysis of high-frequency  $P_n/L_g$  ratios from NTS explosions and western U.S. earthquakes, *Bull. Seism. Soc. Am.*, **86**, 1042-1053.
- Walter, W. R., K. M. Mayeda, and H. Patton (1995). Phase and spectral ratio discrimination between NTS earthquakes and explosions. Part I: Empirical observations, *Bull. Seism. Soc. Am.*, **85**, 1050-1067.

- Wessel, P., and W.H.F. Smith (1991). Free software helps map and display data, *EOS*, **72**, 441-445.
- Zhang, T.-R., and T. Lay (1994). Analysis of short-period regional phase path effects associated with topography in Eurasia, *Bull. Seism. Soc. Am.*, **84**, 119-132.
- Zhang, T.-R., and T. Lay (1995). Why the L<sub>g</sub> phase does not traverse oceanic crust, *Bull. Seism. Soc. Am.*, **85**, 1665-1678.
- Zhang, T.-R., S. Schwartz, and T. Lay (1994). Multivariate analysis of waveguide effects on short-period regional wave propagation in Eurasia and its application in seismic discrimination, *J. Geophys. Res.*, **99**, 21,929-21,945.
- Zhang, T.-R., T. Lay, S. Schwartz, and W. R. Walter (1996). Variation of regional seismic discriminants with surface topographic roughness in the western United States, *Bull. Seism. Soc. Am.*, **86**, 714-725.

**Calibration of Distance and Path Effects on Regional P/S  
Discriminants at Station ABKT (Alibek, Turkmenistan): Azimuthal  
Sector Regionalization**

Arthur J. Rodgers, William R. Walter  
*Geophysics and Global Security Division,  
Lawrence Livermore National Laboratory,  
Livermore, CA 94551*

and

Thorne Lay  
*Earth Sciences Department,  
University of California, Santa Cruz  
Santa Cruz, CA 95064*

Correspondence: Arthur Rodgers, Lawrence Livermore National Laboratory,

L-206, P.O. Box 808, Livermore, CA 94551

e-mail: [rodgers@s34.es.llnl.gov](mailto:rodgers@s34.es.llnl.gov)

phone: (510)-423-5018; fax: (510)-422-3118

Manuscript submitted to the  
*Bulletin of the Seismological Society of America*

February 25, 1998

## **Abstract**

Regional seismic P/S discriminants for earthquake signals observed at station ABKT (Alibek, Turkmenistan) are analyzed for path effects. ABKT is located on the northern flank of the Kopet Dagh Mountains near the topographic/tectonic boundary separating the Iranian Plateau and the Kazakh Platform. P/S amplitude ratios ( $P_n/L_g$ ,  $P_g/L_g$  and  $P_n/S_n$ ) in four frequency bands between 0.75 and 9.0 Hz show great spatial variability (nearly two orders of magnitude) apparently related to crustal structure and tectonic setting. Events in the Hindu Kush have low P/S, while higher ratios are found for events in the Zagros. This systematic regional variability is not well represented by a single distance correction. The data set is subdivided into four azimuthal sectors and separate distance trends are determined. Each sector has distinct topographic and tectonic characteristics, as well as distinct P/S amplitude ratio behavior. The distance trends for each sector show different slopes and zero-distance intercepts, suggesting regionally dependent attenuation, geometric spreading, scattering and energy partitioning in the regional wavefield. The amplitude ratio scatter is most reduced by distance corrections for frequency bands below 3.0 Hz. In tectonically complex areas, discriminant calibration appears to require azimuthal binning or comparable strategies for accounting for the crustal waveguide variations.

## **Introduction**

Seismic monitoring of the Comprehensive Test Ban Treaty (CTBT) at small magnitudes (body-wave magnitude,  $m_b$ , less than about 4.0) will involve small numbers of observations made at regional distances (less than 2000 km, e.g., Blandford, 1981; Pomeroy et al., 1982). Events larger than about magnitude 4.0 can usually be detected teleseismically (distances greater than 2000 km) can be discriminated by location, depth, radiation pattern and/or  $m_b:M_s$  (body-wave to surface-wave magnitude) ratio. Obtaining



adequate seismic wave signal-to-noise for smaller events requires use of more closely recorded data, with regional signals having complex propagation in the crustal waveguide. Regional P/S discriminants, such as Pn/Lg, Pg/Lg and Pn/Sn amplitude ratios, have been shown to be effective at discriminating earthquakes and explosions at regional distances (Bennett and Murphy, 1986; Taylor et al., 1989; Walter et al., 1995; Taylor, 1996; Hartse et al., 1997a). However, strong heterogeneity in the lithosphere causes the travel times and amplitudes of regional phases to vary greatly and it is essential to develop a strategy for accounting for path effects when using regional phases in CTBT applications. In the Middle East, large variations in Sn and Lg amplitudes for the 0.5-5.0 Hz frequency band have been reported (Nuttli, 1980; Kadinsky-Cade et al., 1981; Rodgers et al., 1997a). These studies found strong attenuation and/or inefficient propagation of Sn for paths across the Turkish-Iranian Plateau and the Dead Sea Rift (Levant Shear Zone). Inefficient Sn propagation is associated with paths crossing high elevations of the Turkish-Iranian Plateau, where there are low Pn velocities (Hearn and Ni, 1994) and recent volcanism. Lg is blocked by remnant oceanic crust (Black and southern Caspian Seas) and weakened by propagation across topographic relief associated with the boundaries of the Turkish-Iranian Plateau (Kadinsky-Cade et al., 1981; Rodgers et al., 1997a). Weak Lg and low Lg Q are associated with the Iranian Plateau (Nuttli, 1980; Mitchell, et al., 1996).

Such observations demonstrate that path effects on regional phases must be accounted for before regional phase amplitude ratios can be reliably used as discriminants. For example, an earthquake observation along a path that blocks Lg could have a high Pg/Lg ratio, similar to an explosion source along a path that does not block Lg (e.g., McNamara et al., 1996). Given only sparse numbers of observations, the path effect may not be identified as such. The behavior of regional phases and discriminants needs to be calibrated for each seismic station that will be used to monitor the CTBT. Various calibration strategies exist and this is currently an active CTBT research topic. Discriminant calibration may involve standard empirical distance corrections, development of explicit

attenuation and propagation models, corrections for parameterized crustal models or corrections based on spatial averaging of observations (e.g., median filtering, contouring, kriging). In regions of homogeneous or smoothly varying discriminant behavior, the particular parameterization used for station calibration may not be very important because data variations can be fully accounted for by different methods. However, in regions of large variations in discriminant measures (usually associated with regions of strong lithospheric heterogeneity) the representation of discriminant behavior may be sensitive to the data used (or not used) and the parameterization of the model. A recent study by Fan and Lay (1997) found that low frequency ( $< 3.0$  Hz) Pg/Lg amplitude ratios for widely distributed earthquakes in western China observed at station WMQ are strongly correlated with parametric representations of path-specific crustal structure. They found that scatter in the Pg/Lg ratios can be reduced by a factor of two or more relative to standard distance corrections when empirical path corrections for mean elevation, topographic roughness, mean sediment thickness and mean crustal thickness are included. This and other studies (e.g., Zhang et al., 1994) developed multiple parameter models that reduce the scatter in P/S discriminants for earthquake populations. These results suggest that some of the variability in regional phase amplitude behavior is controlled by the crustal waveguide (i.e. topography, basin and Moho structure) and will not be accounted for by distance corrections alone. However, correcting for path effects does not guarantee improvement of the separation of earthquake and explosion populations. Hartse et al. (1997b) applied a similar strategy and found little or no improvement in discrimination of smaller, closer and less widely distributed regional events observed at WMQ than those studied by Fan and Lay (1997). Most cases they considered resulted in reduced separation of the earthquake and explosion populations. Differences in the data sets used to calibrate paths effects can play a significant role in determining the performance of various methodologies.

The Middle East is a region of abundant non-uniformly distributed seismicity and complex crustal structure, with few seismic stations for CTBT monitoring. It thus

provides an excellent and challenging test region for developing discriminant calibration strategies. Earthquakes are concentrated in the Hindu Kush and Zagros mountain belts with additional events diffusely distributed throughout the Turkish-Iranian Plateau (Figure 1). Station ABKT (Alibek, Turkmenistan, also shown in Figure 1) is located on the northern flank of the Kopet Dagh Mountains near the Iranian border and is within regional distances of Iran, Afghanistan and several former Soviet Republics. This station lies near the tectonic boundary separating the Iranian Plateau to the south from the Kazakh Platform to the north. ABKT will be the site of a primary station (GEYT) of the International Monitoring System (IMS) for the CTBT, and thus requires complete calibration. The regional seismic signals recorded at ABKT traverse a wide variety of paths, including both high and low elevations and smooth and rough topography. A complex history that included oceanic subduction and continental collision has led to the current tectonic configuration of the region (e.g., Dercourt et al., 1986). High elevations in the Turkish and Iranian Plateaus are associated with recent volcanism (Kazmin et al., 1986) and thickened crust (Snyder and Barazangi, 1986). Thus, there is strong, but poorly constrained crustal heterogeneity that may affect regional signals. We consider discriminant calibration for ABKT involving a regionalization approach. Future papers will consider multivariate path parameter regressions and spatial averaging of the discriminant measurements.

### **Regional Waveform Data at ABKT and P/S Amplitude Ratio Measurements**

Three-component broadband waveform data (20 samples/sec) for regional events recorded at ABKT were requested from the Incorporated Research Institutions for Seismology-Data Management Center (IRIS-DMC). Event parameters were taken from the National Earthquake Information Center-Preliminary Determination of Epicenters (NEIC-PDE) monthly bulletins. Data were requested for earthquakes with reported depths less

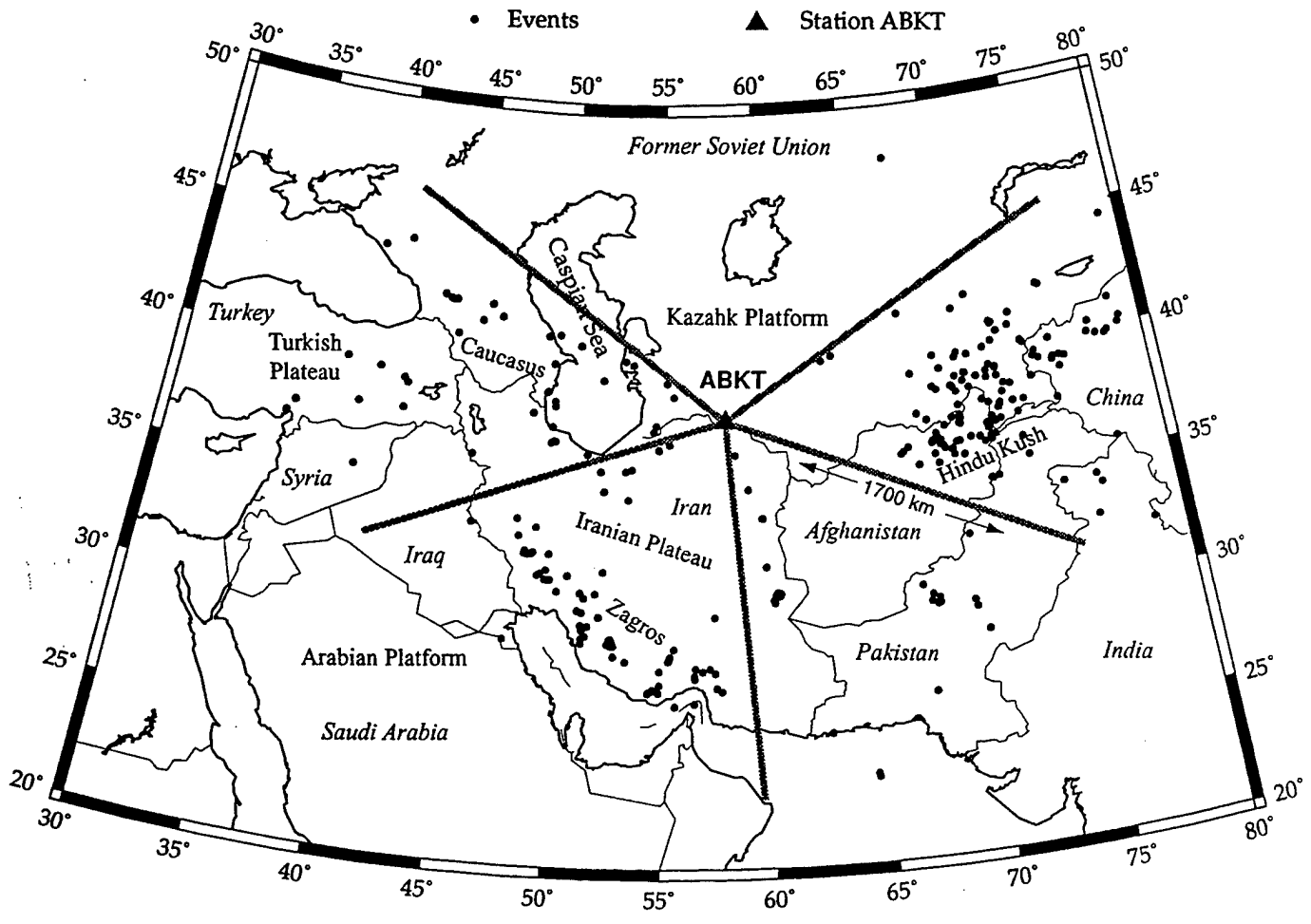


**Figure 1.** Locations of station ABKT, the events studied and the major geographic features of the Middle East. Also shown are the boundaries of the azimuthal sectors used to subdivide the data set.

than 50 km and body-wave magnitudes ( $m_b$ ) greater than or equal to 4.0. All waveforms were previewed and a first-arriving P-wave was picked when possible. Noisy data and data with interfering events were discarded. This screening resulted in over 300 events within 2000 km of ABKT for the years 1993-1995. The location of ABKT, the events used and the major geographic features of the region are shown in Figure 1.

Regional phase amplitude ratios and signal-to-noise ratios were measured on vertical displacement seismograms in four pass bands (0.75-1.5, 1.5-3.0, 3.0-6.0 and 6.0-9.0 Hz). Phases were isolated with the following group velocity windows: Pn 8.0-6.2 km/sec; Pg 6.2-5.0 km/sec; Sn 4.6-4.0 km/sec and Lg 3.6-3.0 km/sec. Noise was estimated using a 35 sec window ending 5 sec before the first-arriving P-wave. The origin time was perturbed so that the Pn phase arrives at 7.9 km/sec. This was done to account for potential origin time, depth or location errors, since it is known that some smaller events ( $m_b < 4.5$ ) have large ( $> 20$  km) mislocations (Sweeney, 1996). If the time shift was greater than 15 sec, the event was removed to eliminate possible gross mislocations.

Amplitude ratios were computed in the frequency domain. Each phase and noise window was de-meant and a 5% cosine taper applied. Then the broadband (0.03-10.0 Hz) spectrum was found for each phase by fast-Fourier transform (FFT). The frequency spectrum was smoothed, re-sampled in evenly spaced log-frequency units and stored. Individual phase amplitudes for a given pass band were estimated from the broadband spectra by computing the  $\log_{10}$  mean spectral amplitude. Amplitude ratios were determined from the  $\log_{10}$  mean spectral amplitudes of two given phases. Recently, Rodgers et al. (1997b) showed that time domain and frequency domain measurements of regional phase amplitude ratios agree very well for frequencies less than 3.0 Hz. However, for frequencies greater than 3.0 Hz, time domain measurements are possibly contaminated by energy from frequencies below the pass band of interest and biased by large amplitude energy in the low end of the pass band. This bias is reduced by log averaging of the spectral amplitude in the frequency domain.

The Pn/Lg, Pg/Lg and Pn/Sn amplitude ratio measurements are plotted with map views in Figures 2, 3 and 4, respectively. For each frequency band only waveforms with pre-Pn/Pn signal-to-noise greater than 2.0 were used. These maps illustrate that the P/S ratios have large spatial variation. In particular for the lowest frequency band, events from the Hindu Kush generally show small P/S ratios ( $P/S < 0.5$ ), while events from the Zagros show larger ratios ( $P/S > 1.0$ ). Also, as the frequency pass band increases few events are retained for the Zagros due to poor signal-to-noise compared to other azimuths. This suggests that attenuation of Pn is stronger for the Iranian Plateau path relative to the Kazahk Platform paths. Note that both the Hindu Kush and Zagros regions are nearly equidistant from ABKT ( $\approx 1100$  km), indicating that the differences in propagation for these two regions are due to path-specific effects and not simply distance effects. Pn travel time tomography shows slower velocities beneath the Iranian Plateau relative to the surrounding regions (Hearn and Ni, 1994). The correspondence of low Pn velocities and inefficient Sn propagation beneath the Iranian Plateau is probably due to partially molten shallow mantle and high attenuation (Rodgers et al., 1997a).

### Distance Corrections and Subdivision of Data into Azimuthal Sectors

Many recent studies on regional discrimination and phase behavior have demonstrated the importance of distance effects (e.g., Taylor, 1996; Hartse et al., 1997a; Fan and Lay, 1997). Generally, researchers have determined the linear dependence of a P/S ratio on distance and removed it from the data before plotting the ratio versus  $m_b$  (the discrimination plot). The instrument corrected amplitude spectrum of a regional phase,  $A(f)$ , is often represented as:

$$A(f) = S(f) R_{\theta\phi} \Delta^{-\kappa} \exp [ - \pi f \Delta / Q(f)U ] ;$$

# ABKT Pn/Lg

Log-Average  
Frequency Domain  
Pn/noise > 2.0

- Pn/Lg < 0.5, Lg efficient
- ◊ 0.5 ≤ Pn/Lg ≤ 1.0, Lg intermediate
- ◻ Pn/Lg > 1.0, Lg weak

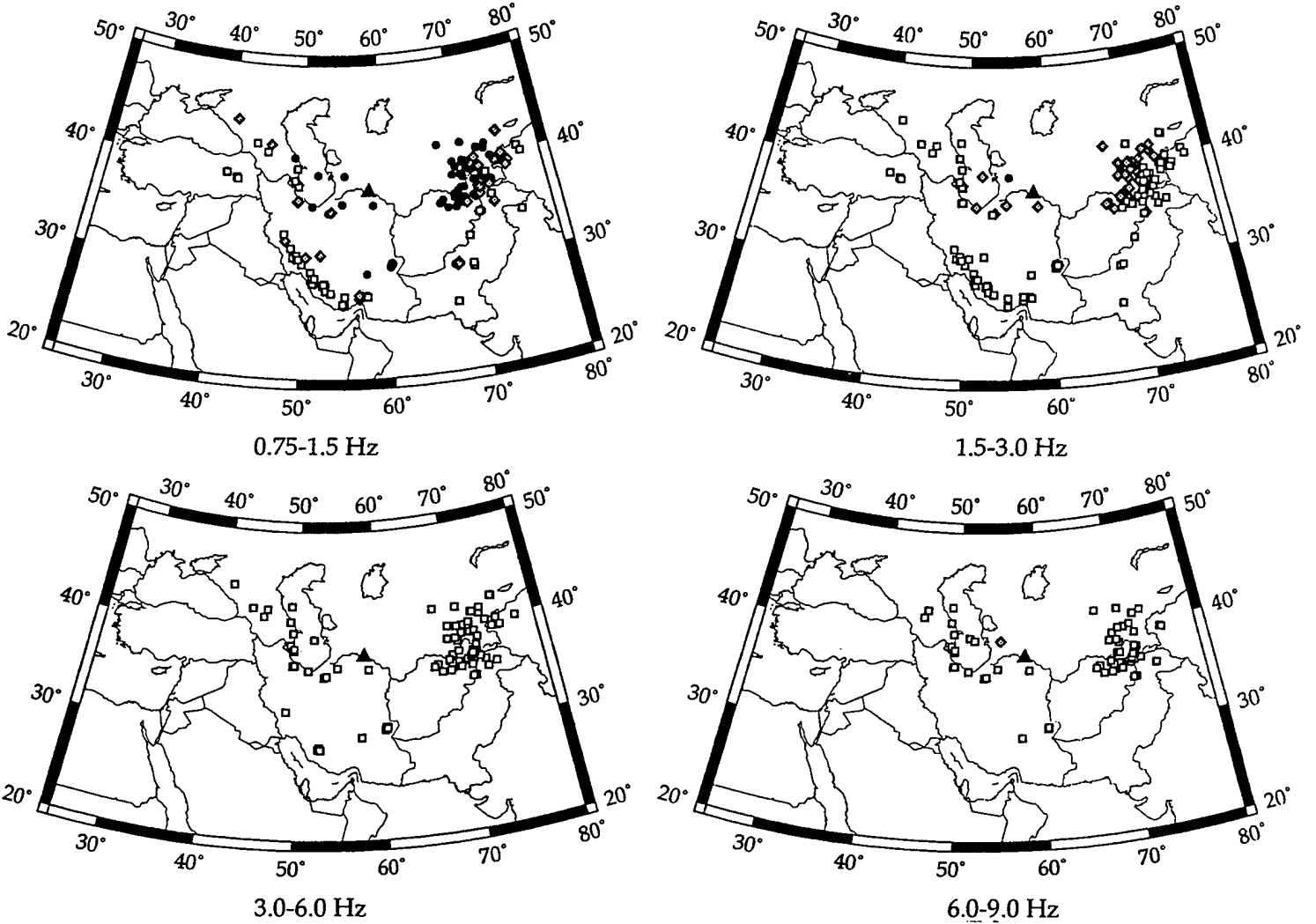
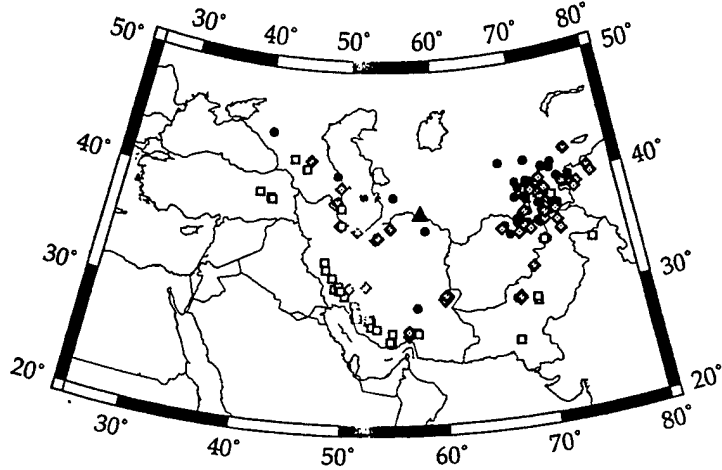


**Figure 2.** Map of  $\log_{10} [Pn/Lg]$  amplitude ratios for the events shown in Figure 1. Panels show the measurements made in the four frequency bands considered. Only data for which the Pn/pre-Pn noise signal-to-noise was greater than 2.0 and the origin time shift was less than  $\pm 15$  sec are plotted.

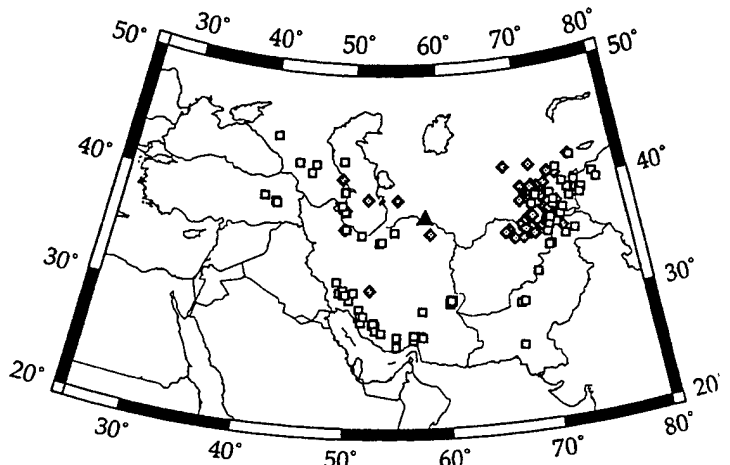
# ABKT Pg/Lg

Log-Average  
Frequency Domain  
Pn/noise > 2.0

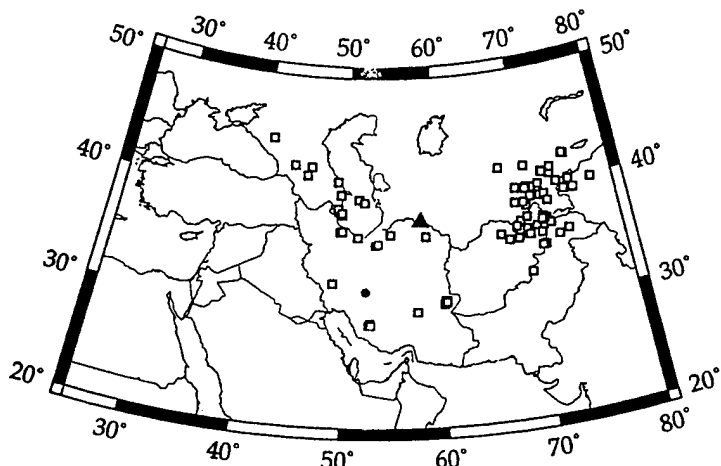
- Pg/Lg < 0.5, Lg efficient
- ◊ 0.5 ≤ Pg/Lg ≤ 1.0, Lg intermediate
- ◻ Pg/Lg > 1.0, Lg weak



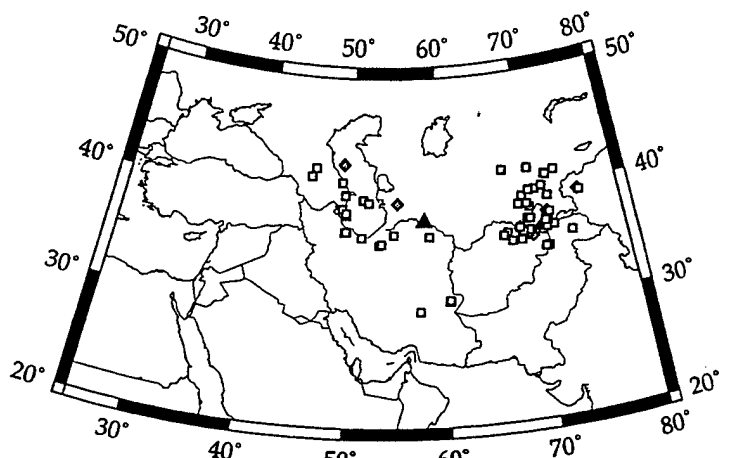
0.75-1.5 Hz



1.5-3.0 Hz



3.0-6.0 Hz



6.0-9.0 Hz

Figure 3. Map of  $\log_{10}$  [Pg/Lg] amplitude ratios, similar to Figure 2.



# ABKT Pn/Sn

Log-Average  
Frequency Domain  
Pn/noise > 2.0

- Pn/Sn < 0.5, Sn efficient
- ◊ 0.5 ≤ Pn/Sn ≤ 1.0, Sn intermediate
- ◻ Pn/Sn > 1.0, Sn weak

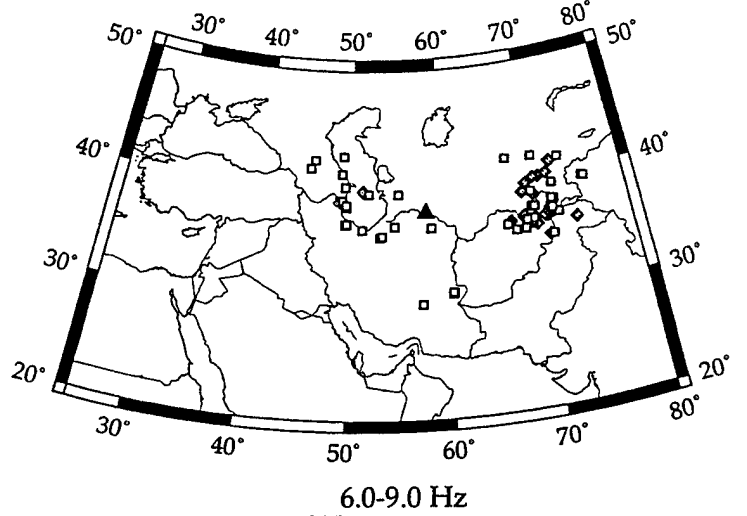
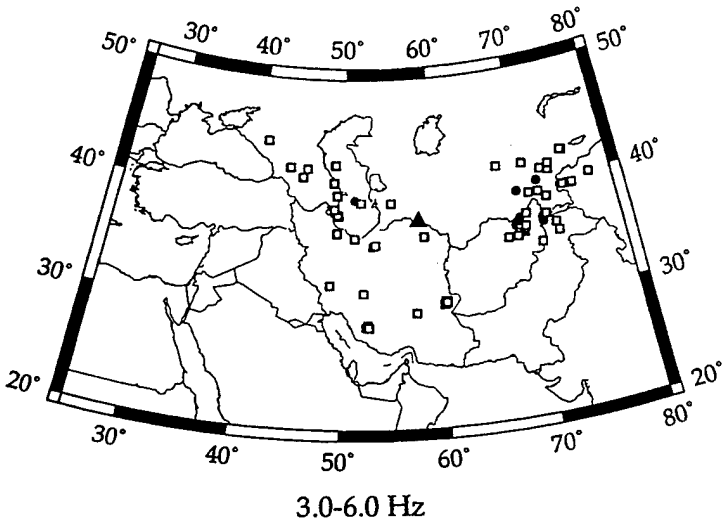
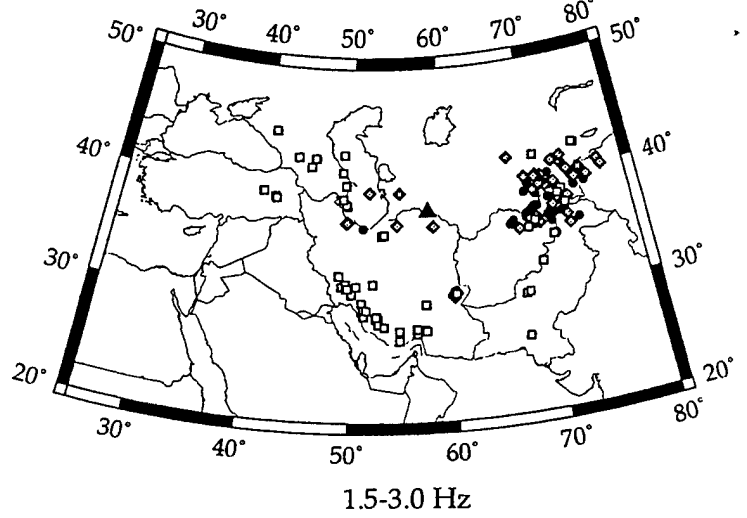
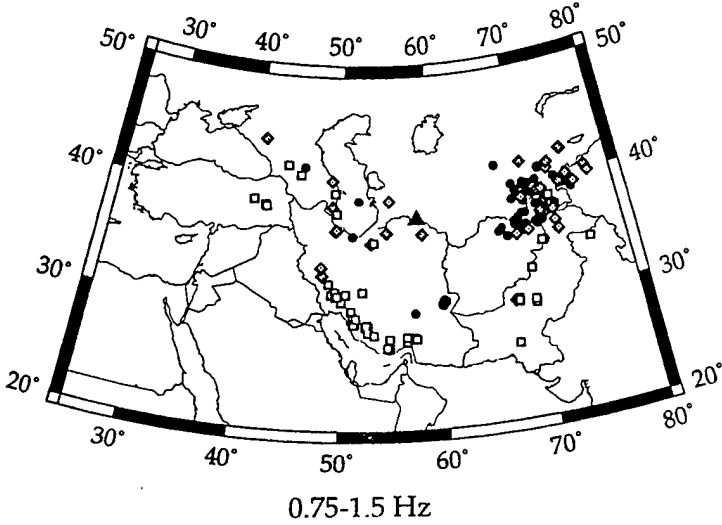


Figure 4. Map of  $\log_{10} [Pn/Sn]$  amplitude ratios, similar to Figure 2.

where:  $f$  is frequency;  $S(f)$  is the source spectrum;  $R_{\theta\phi}$  accounts for the radiation pattern;  $\Delta$  is the epicentral distance;  $-\kappa$  is the exponent of distance that governs geometric spreading;  $Q(f)$  is the frequency dependent attenuation (quality factor, usually specified as  $Q_0 f^n$ ) and  $U$  is the group velocity of the particular phase. Both attenuation and geometric spreading can be viewed as distance effects - geometric spreading depends on distance directly and attenuation can be re-formulated as a distance effect. These effects are difficult to separate in practice. Forming the amplitude ratio of two regional phases in a given frequency band theoretically cancels the source spectrum and results in a form that depends on the differential effects of the radiation pattern, attenuation and geometric spreading:

$$A^P(f) / A^S(f) = R_{\theta\phi}^P / R_{\theta\phi}^S \Delta^{(-\kappa_P + \kappa_S)} \exp [ - \pi f \Delta ( 1/Q^P(f)U^P - 1/Q^S(f)U^S ) ] ;$$

where P and S superscripts denote P- and S-wave variables, respectively. Taking the 10-base logarithm results in:

$$\log_{10} [ A^P(f) / A^S(f) ] = \log_{10} [ R_{\theta\phi}^P / R_{\theta\phi}^S ] + (\kappa_S - \kappa_P) \log_{10} \Delta - \pi f \Delta [ ( 1/Q^P(f) U^P - 1/Q^S(f) U^S ) ] \log_{10} e .$$

The three terms on the right-hand side of the above form are a constant, a log-distance dependence and a linear distance dependence, respectively. The formulation given above does not account for propagation effects related to scattering, focusing and de-focusing by elastic or anelastic heterogeneity. However, if these effects are common to all paths considered, then the representation of the P/S amplitude ratios formulated above should be appropriate. The effects of scattering and heterogeneity are important for the frequencies of concern for regional discrimination; however, accounting for these effects awaits advancement of theoretical methods. In practice, correcting P/S ratios for empirically determined distance effects is a pragmatic approach, although the precise model parameterization to use is unclear. Given the above formulation, fitting the  $\log_{10}[P/S]$  to a linear distance dependence is not unwarranted. Use of a single linear distance-dependence for all data within a given region implicitly assumes uniform propagation effects for all

paths with a given length. As this appears to be problematic for ABKT, we will compare this assumption with a simple regionalization approach.

The observed spatial variation of P/S amplitude ratios seen in Figures 2, 3 and 4 suggests that the data set can be subdivided into azimuthal sectors with distinct amplitude systematics and gross crustal waveguide properties. Four sectors were chosen in an ad hoc fashion to exploit common topographic and tectonic characteristics. These sectors (shown in Figure 1) represent the Hindu Kush (back azimuths  $55^{\circ}$ - $110^{\circ}$ ), Southeast ( $110^{\circ}$ - $175^{\circ}$ , eastern Iran, western Afghanistan and southern Pakistan), Zagros ( $175^{\circ}$ - $255^{\circ}$ ) and Caspian ( $255^{\circ}$ - $310^{\circ}$ ) regions. The paths within each sector have similar along-path topographic profiles, as shown in Figure 5. Profiles were computed by tracing earthquake-station great-circles through the global topography model ETOPO5 using the GMT3.0 software package (Wessel and Smith, 1991). Similarities were also found for the sectorized basement and Moho depth profiles, based on maps developed by the Former Soviet Union, Institute for Physics of the Earth (IPE) (Barazangi et al., 1996). Recent studies of path effects on regional phases have shown that along-path topographic, basement depth and Moho depth statistics (e.g., mean and rms elevation, rms topographic slope, mean basement and crustal thickness) are correlated with regional phase amplitude ratios (e.g., Zhang et al., 1994, 1996; Fan and Lay, 1997). Thus, it is not unreasonable to think that if the crustal waveguide profiles within a sector are similar the sectorized regional discriminants will share common path effects. Our azimuthal regionalization is one approach to correcting for gross waveguide variations. The basic idea is that energy partitioning differs for each waveguide structure, leading to variable amplitude ratios.

We determined the distance trend for the entire data set (all azimuths) in the four frequency bands considered. Figure 6 shows the  $\log_{10}[\text{Pg/Lg}]$  ratios versus distance, the regression fit and standard error about the fit. In this plot, the individual measurements are

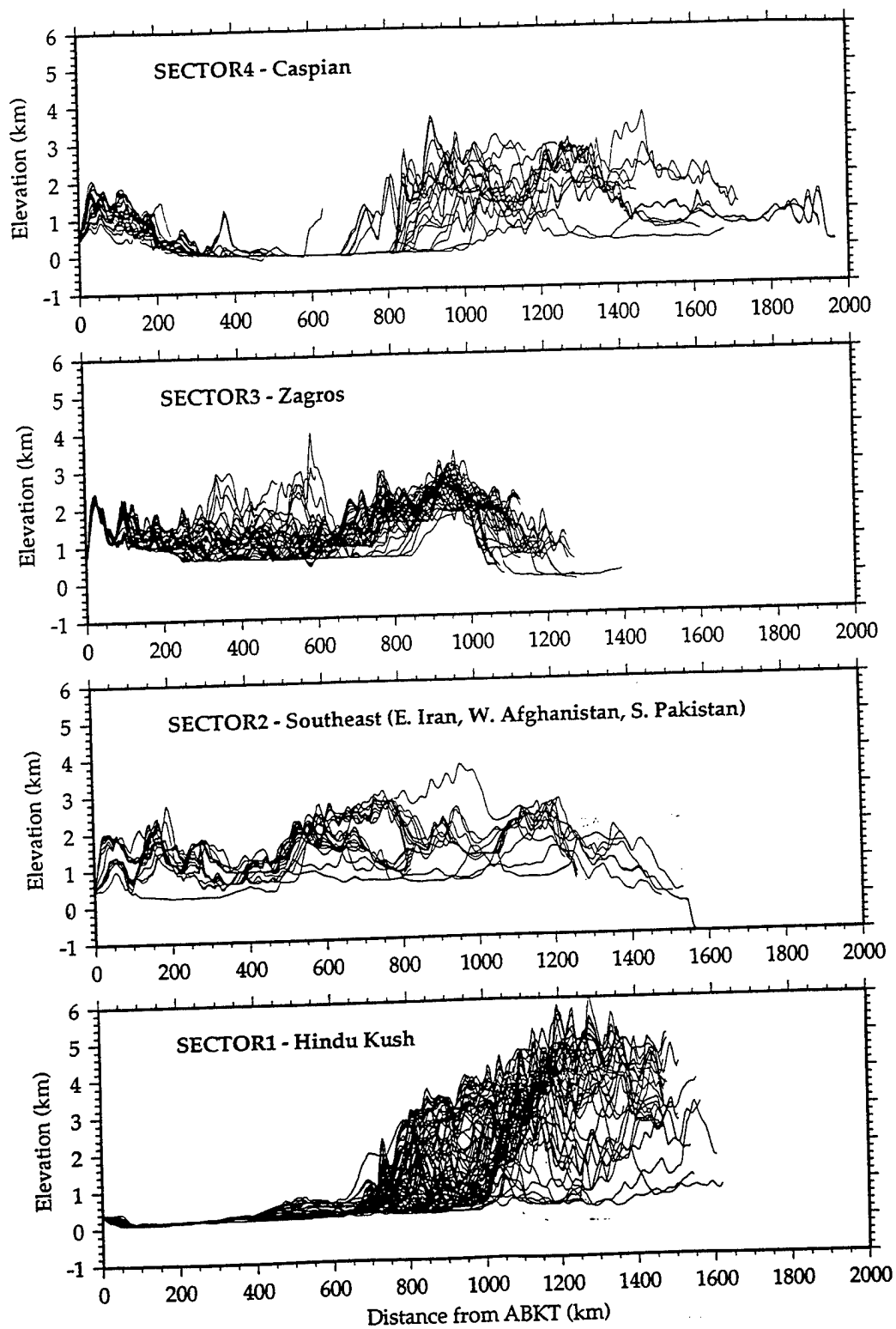


**Figure 5.** Along-path topographic profiles for each sector. Profiles were generated along ABKT-to-earthquake great-circles through the global topography model ETOPO5 using the GMT3.0 software package (Wessel and Smith, 1991).

symbol-coded by sector. The data set for all azimuths shows a weak distance dependence that decreases with frequency (linear correlations less than 0.4). It can be seen for the lower frequency bands (< 3.0 Hz) the data within each sector tend to group together. This is especially apparent for the Hindu Kush (circles) and Zagros (triangles) groups, which are the most numerous and appear to have different  $\log_{10}[\text{Pg/Lg}]$  slopes and zero-distance values.

Next, the distance trends for each azimuthal sector and frequency band were determined separately. Figure 7 shows the  $\log_{10}[\text{Pg/Lg}]$  distance trends for the Hindu Kush sector. Compared to the entire data set (Figure 6), the Pg/Lg amplitude-distance trends for the Hindu Kush sector show much smaller scatter (indicated by the standard error about the regression fit, sd) and stronger linear correlations, especially for the lower frequency bands (< 3.0 Hz). Tables 1, 2 and 3 compile the fit parameters and statistics for the Pn/Lg, Pg/Lg and Pn/Sn data sets, respectively. The linear correlations between the P/S ratios and distance in these tables are generally stronger for the data within the sectors relative to the entire data set. This is especially true for the lower frequency bands (< 3.0 Hz). P/S ratios for the Hindu Kush, Southeast and Zagros sectors consistently show higher linear correlations with distance and smaller scatter relative to the entire data set. However, Pn/Lg and Pg/Lg ratios in the 1.5-3.0 Hz frequency band for the Caspian sector show larger standard error compared to the entire data set. The regression fits reveal significantly different slopes and zero-distance intercepts for each sector. This suggests that each amplitude ratio has a regionally varying attenuation, geometric spreading and propagation behavior.

Removing the distance trends, such as those shown in Figure 7, reduces the scatter of the amplitude ratios, ideally providing enhanced discrimination. Figure 8 shows histograms of the amplitude ratios before and after removal of the distance trends. This is shown for the entire data set (ALL) and for each sector. Statistics of each distribution (number, mean and rms) are given, along with the rms reduction after removal of the

# Pg/Lg vs. Distance

+ Caspian      ○ Hindu Kush  
 △ Zagros      □ Southeast

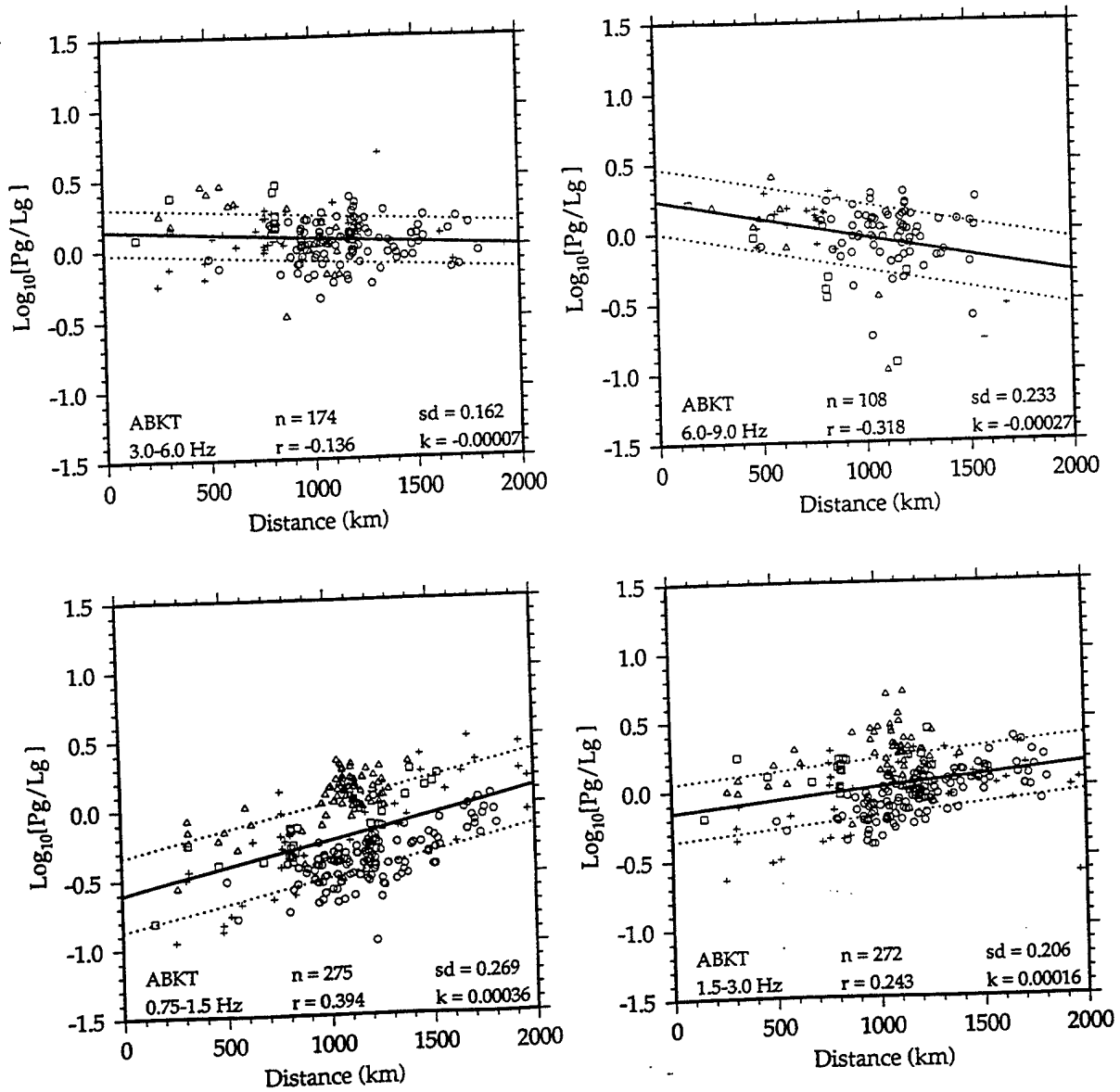


**Figure 6.**  $\text{Log}_{10} [\text{Pg/Lg}]$  amplitude ratios versus distance for the four frequency bands considered. Each measurement is coded by sector (circles Hindu Kush; squares Southeast; triangles Zagros; pluses Caspian). All data were fit to a straight line (solid) by linear regression,  $1-\sigma$  errors are also shown (dotted). The frequency band, number of data,  $n$ , linear correlation,  $r$ , standard error about the fit,  $sd$ , and the slope of the fit,  $k$ , are shown in each panel.

# Pg/Lg vs. Distance Hindu Kush (Sector 1)

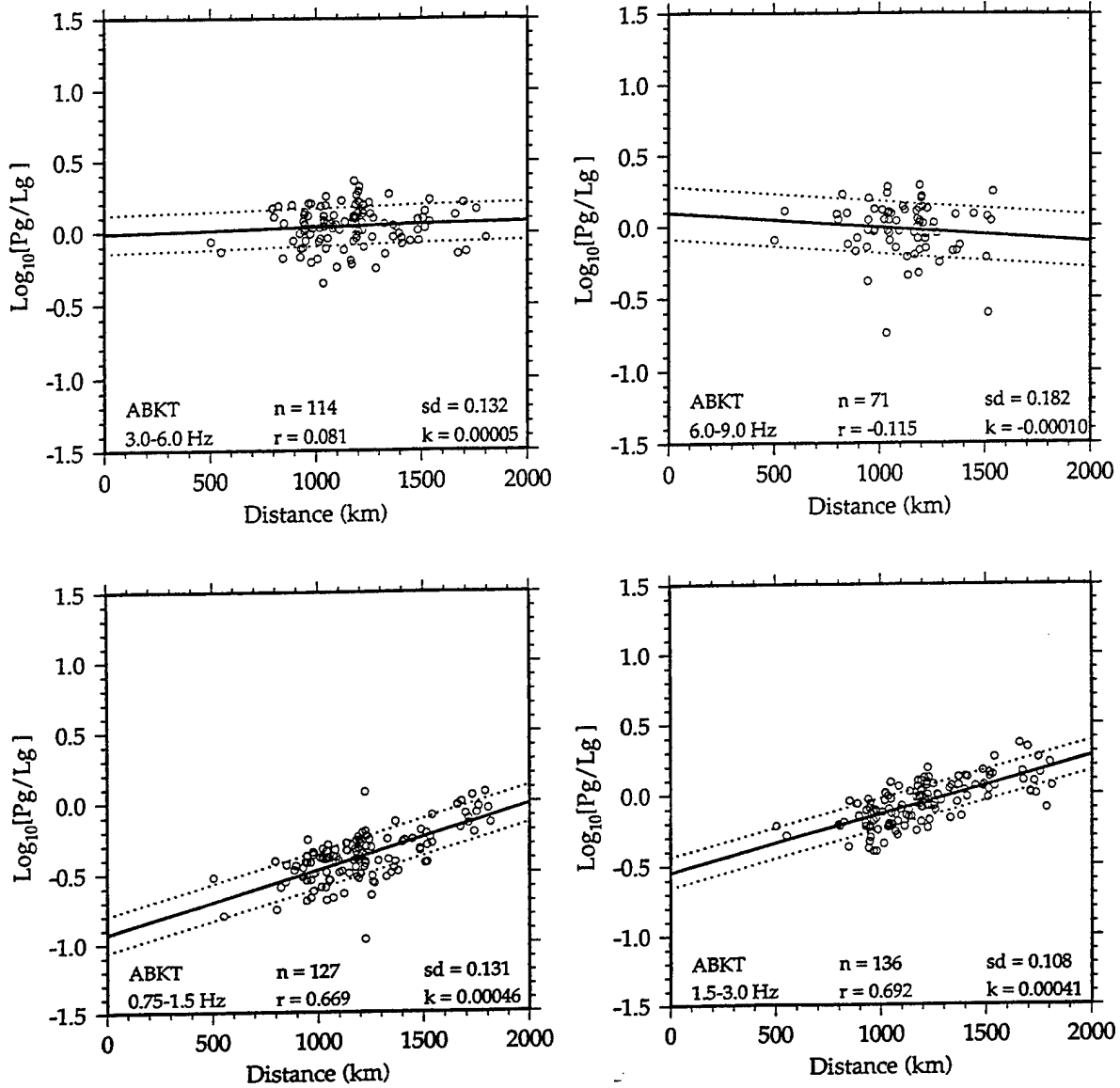


**Figure 7.**  $\text{Log}_{10}[\text{Pg}/\text{Lg}]$  amplitude ratios versus distance for the four frequency bands considered for the Hindu Kush sector considered separately. Statistics and fit parameters are shown, similar to Figure 6.

**Table 1.** Statistics and fit parameters for the  $\log_{10}[\text{Pn/Lg}]$  amplitude ratios versus distance. The standard error is the root-mean square amplitude ratio residual about the linear regression fit. Zero-value is the zero-distance intercept of the regression fit. Slope is given in units of  $\text{km}^{-1}$ . Sectors 1-4 correspond to the Hindu Kush, Southeast, Zagros and Caspian regions.

<b>Pn/Lg 0.75-1.5 Hz</b>	number	linear correlation	standard error	zero-value	slope
All Azimuths	275	0.534	0.393	-1.123	0.00078
Sector 1	127	0.813	0.189	-1.724	0.00102
Sector 2	28	0.881	0.196	-1.379	0.00105
Sector 3	79	0.651	0.239	-0.865	0.00093
Sector 4	41	0.850	0.311	-1.205	0.00099
<b>Pn/Lg 1.5-3.0 Hz</b>	number	linear correlation	standard error	zero-value	slope
All Azimuths	272	0.432	0.288	-0.373	0.00043
Sector 1	136	0.672	0.185	-0.782	0.00066
Sector 2	26	0.760	0.143	-0.370	0.00048
Sector 3	69	0.491	0.248	-0.284	0.00061
Sector 4	41	0.556	0.343	-0.447	0.00047
<b>Pn/Lg 3.0-6.0 Hz</b>	number	linear correlation	standard error	zero-value	slope
All Azimuths	174	0.054	0.227	0.231	0.00004
Sector 1	114	0.062	0.204	0.203	0.00006
Sector 2	10	-0.154	0.174	0.329	-0.00010
Sector 3	21	-0.180	0.229	0.371	-0.00014
Sector 4	29	0.239	0.299	0.143	0.00019
<b>Pn/Lg 6.0-9.0 Hz</b>	number	linear correlation	standard error	zero-value	slope
All Azimuths	108	-0.251	0.324	0.474	-0.00029
Sector 1	71	-0.178	0.209	0.432	-0.00019
Sector 2	7	-0.906	0.143	0.313	-0.00090
Sector 3	8	-0.852	0.280	1.051	-0.00167
Sector 4	22	-0.734	0.234	1.044	-0.00087

**Table 2.** Statistics and fit parameters for the  $\log_{10}[\text{Pg/Lg}]$  amplitude ratios versus distance, similar to Table 1.

<b>Pg/Lg 0.75-1.5 Hz</b>	number	linear correlation	standard error	zero-value	slope
All Azimuths	275	0.394	0.269	-0.604	0.00036
Sector 1	127	0.669	0.131	-0.929	0.00046
Sector 2	28	0.810	0.137	-0.736	0.00054
Sector 3	79	0.611	0.138	-0.433	0.00048
Sector 4	41	0.789	0.225	-0.783	0.00057
<b>Pg/Lg 1.5-3.0 Hz</b>	number	linear correlation	standard error	zero-value	slope
All Azimuths	272	0.243	0.206	-0.152	0.00016
Sector 1	136	0.692	0.108	-0.545	0.00041
Sector 2	26	0.231	0.114	0.050	0.00008
Sector 3	69	0.192	0.174	0.056	0.00015
Sector 4	41	0.426	0.240	-0.298	0.00023
<b>Pg/Lg 3.0-6.0 Hz</b>	number	linear correlation	standard error	zero-value	slope
All Azimuths	174	-0.136	0.162	0.139	-0.00007
Sector 1	114	0.081	0.132	-0.012	0.00005
Sector 2	10	-0.067	0.127	0.248	-0.00003
Sector 3	21	-0.608	0.186	0.480	-0.00047
Sector 4	29	0.242	0.178	-0.004	0.00011
<b>Pg/Lg 6.0-9.0 Hz</b>	number	linear correlation	standard error	zero-value	slope
All Azimuths	108	-0.318	0.233	0.234	-0.00027
Sector 1	71	-0.115	0.182	0.097	-0.00010
Sector 2	7	-0.811	0.193	0.293	-0.00078
Sector 3	8	-0.857	0.213	0.765	-0.00130
Sector 4	22	-0.766	0.156	0.554	-0.00064



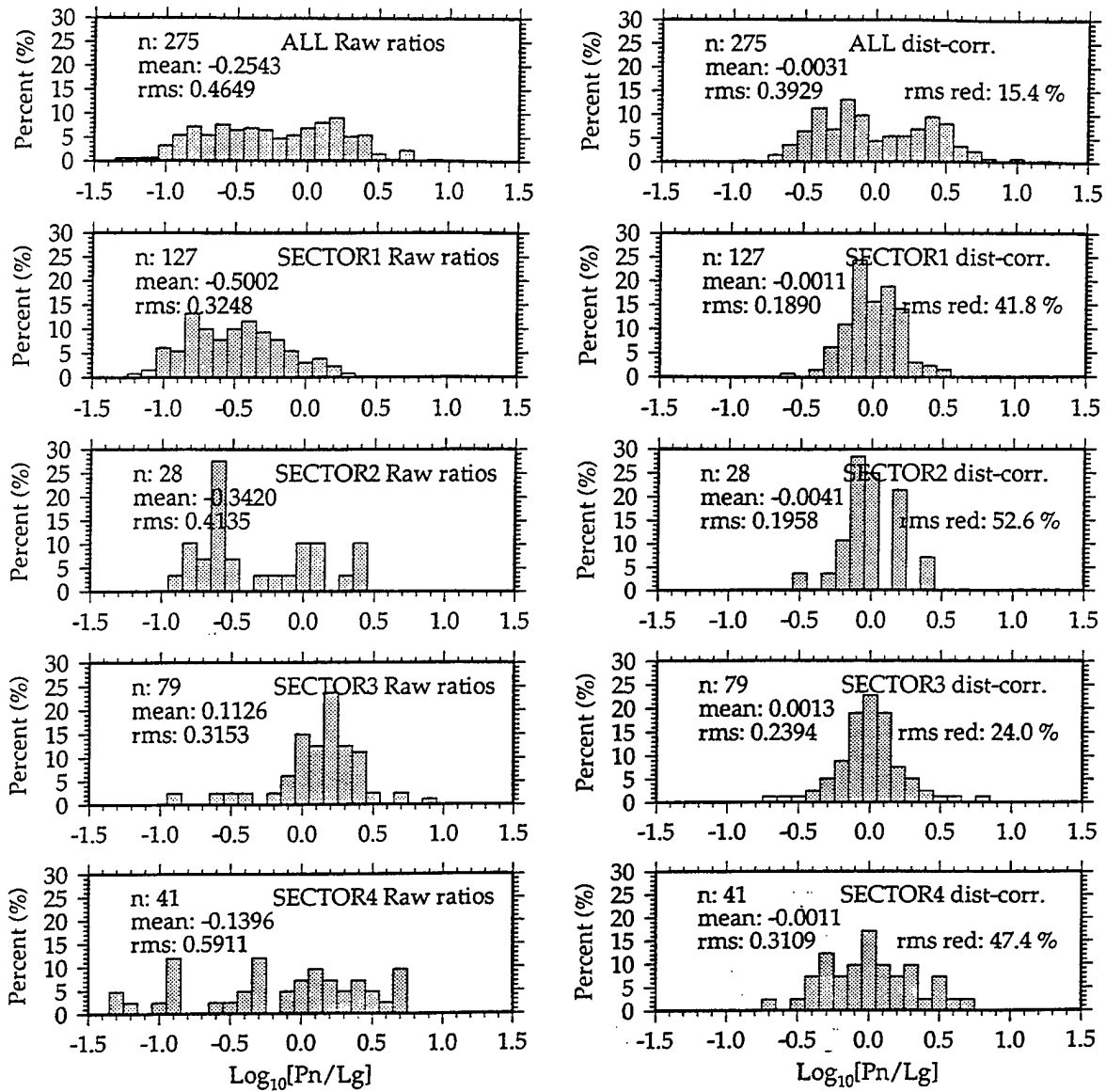
<b>Pn/Sn 0.75-1.5 Hz</b>	number	linear correlation	standard error	zero-value	slope
All Azimuths	275	0.389	0.355	-0.621	0.00047
Sector 1	127	0.611	0.193	-1.032	0.00057
Sector 2	28	0.758	0.214	-0.798	0.00071
Sector 3	79	0.519	0.203	-0.347	0.00056
Sector 4	41	0.861	0.236	-0.834	0.00079
<b>Pn/Sn 1.5-3.0 Hz</b>	number	linear correlation	standard error	zero-value	slope
All Azimuths	272	0.248	0.323	-0.268	0.00026
Sector 1	136	0.482	0.183	-0.662	0.00040
Sector 2	26	0.738	0.150	-0.368	0.00047
Sector 3	69	0.451	0.198	-0.071	0.00043
Sector 4	41	0.785	0.211	-0.500	0.00054
<b>Pn/Sn 3.0-6.0 Hz</b>	number	linear correlation	standard error	zero-value	slope
All Azimuths	174	-0.001	0.229	0.041	0.00000
Sector 1	114	0.445	0.165	-0.459	0.00035
Sector 2	10	-0.535	0.094	0.327	-0.00021
Sector 3	21	0.347	0.166	0.173	0.00020
Sector 4	29	0.423	0.199	-0.075	0.00024
<b>Pn/Sn 6.0-9.0 Hz</b>	number	linear correlation	standard error	zero-value	slope
All Azimuths	108	-0.167	0.155	0.179	-0.00009
Sector 1	71	0.179	0.144	-0.083	0.00013
Sector 2	7	-0.569	0.104	0.188	-0.00021
Sector 3	8	-0.637	0.165	0.495	-0.00050
Sector 4	22	-0.085	0.133	0.199	-0.00004

**Table 3.** Statistics and fit parameters for the  $\log_{10}[\text{Pn/Sn}]$  amplitude ratios versus distance, similar to Table 1.

distance trend. The combined data set shows extreme variations of Pn/Lg (nearly two orders of magnitude). Removing the distance trend reduces the rms by 15.4%; however, the data still show great variability (rms = 0.39 in  $\log_{10}$  [Pn/Lg] units). The sectorized Pn/Lg amplitude ratios show much smaller scatter after removal of the distance trend (rms = 0.19-0.31) and the rms reductions are significant (24.0%-52.6%). The sectorized P/S amplitude ratios for the lower frequencies (< 3.0 Hz) generally show smaller scatter after removal of the distance trends compared to the entire data set. The discriminant distributions tend to look more normal after removing the distance trends and the means are brought closer to zero. The higher frequency P/S ratios show much more variability in the rms reduction after removal of the distance trend, but the scatter for these data is generally reduced to the 0.2 level in  $\log_{10}$  [P/S] units. An exception is the results for the Caspian region. These data often show more scatter than the other sectors. Perhaps data from this region could be sectorized differently to better represent the amplitude ratio behavior.

## Conclusions and Discussion

The regional P/S amplitude ratios we present in this paper show great spatial variability. This variability arises from path effects and is related to tectonic and topographic structure. The ratios for all azimuths show a weak dependence on distance. However, subdivision of the data set into azimuthal sectors (based on tectonic and topographic structure) results in stronger correlations with distance. For each sector, linear regressions on distance result in different slopes and zero-distance intercepts, indicating that attenuation, geometric spreading and propagation effects are different for each azimuthal sector. The variability seen in the P/S ratios at the lower frequencies (< 3.0 Hz) for the Hindu Kush, Southeast and Zagros sectors is consistently reduced by removing the



## ABKT Pn/Lg 0.75-1.5 Hz

**Figure 8.** Histograms of  $\text{Log}_{10}[\text{Pn/Lg}]$  amplitude ratios (0.75-1.5 Hz) for the entire data set ("ALL", all azimuths, top) and the sectorized Pn/Lg ratios. Panels on the left show the raw amplitude ratios ("Raw ratios"). Panels on the right show the ratios after the distance trend of each data set was removed ("dist.-corr."). The number (n), mean and rms of each distribution is shown. For the distance-corrected data the rms reduction (rms red) is given. Sectors 1-4 correspond to the Hindu Kush, Southeast, Zagros and Caspian regions, respectively.

distance trend seen in each sector. Scatter in the higher frequency P/S ratios is sometimes greatly reduced, but not in a consistent fashion. Discriminant scatter for the Caspian region (Sector 4) is not consistently reduced by our sector regionalization. Perhaps the southern boundary of this sector could possibly be chosen differently to reduce discriminant scatter. Paths from the northern Iranian Plateau may have a unique affinity and should not be grouped with paths crossing the southern Caspian Sea. This points out potential problems with azimuthal sector regionalization. If a topographic and/or tectonic boundary is poorly defined or if a region is aseismic it may be difficult to define the sector boundaries. A well defined topographic/tectonic region that can be represented by an azimuthal sector is well suited for the regionalization scheme we present here (e.g., the Hindu Kush and Zagros regions at ABKT). However, if topographic and/or tectonic boundaries are oblique to azimuthal great-circles then another discriminant calibration scheme may be more appropriate. Because of uncertainties in event location (typically less than 30 km), one must be cautious when associating an event with a sector when the event is near a sector boundary. Recent efforts to understand path effects of variable waveguide structure on P/S amplitude ratios has found correlations with along-path topography, basement depth and Moho depth statistics, especially for lower frequencies (e.g., Zhang et al., 1994, 1996; Fan and Lay, 1997). Variable waveguide structure is presumably accounted for to some extent by our sector analysis.

Our efforts to represent the spatial variation of regional P/S discriminants observed at ABKT raise several important issues regarding regional seismological monitoring of the CTBT. For stations located in tectonically active and complex areas, a representation of regional discriminants will be useful for predicting earthquake P/S behavior and identifying possible explosion sources. It is not clear at present how these representations should be parameterized. In regions of dense station coverage, regional P/S behavior could be calibrated jointly for a few stations or for each station separately. However, because monitoring stations are generally separated by more than 2000 km and path effects on the

regional wavefield are direction dependent (e.g., Pn and Sn focusing, Lg blockage) single station calibration is probably more appropriate. Hopefully, two- and three-dimensional wave propagation modeling at higher frequencies can validate some of the empirical observations of regional wavefield energy partitioning. We are currently investigating other calibration strategies for the regional P/S data set observed at ABKT (multivariate path parameter regression and spatial averaging) and hope to be able to settle on a recommendation for single station calibration. In the absence of explosion data, it remains to be determined if corrections for path effects on regional P/S ratios will improve discrimination of earthquake and explosion sources. The fact that lower frequency (< 3.0 Hz) P/S ratios show stronger distance and path dependence relative to higher frequency P/S ratios (e.g., Zhang et al., 1996; Fan and Lay, 1997) is a potentially problematic issue. Typically, higher frequencies discriminate better than lower frequencies. If distance and path corrections for higher frequency P/S ratios have little or no effect on discriminant scatter, but separation of earthquake and explosion sources is acceptable then path effects on higher frequency P/S ratios need not be pursued. However, attenuation and poor signal-to-noise at high frequencies and 1000-km distances always will be problematic for most broadband seismic stations and this motivates the need to understand low frequency P/S ratios. If lower frequency P/S ratios show large scatter and reduced separation of earthquakes and explosions after correction for path effects (as suggested by Hartse, et al., 1997b), then improved strategies for discrimination at frequencies less than 3.0 Hz need to be sought. Nonetheless, sector regionalization appears to be a simple, easily performed calibration strategy for reducing scatter in seismic discriminants and characterizing the earthquake population, yet it does raise issues of how to define sectors and how to interpolate between them.

## **Acknowledgments**

Waveform data were obtained from the Incorporated Research Institutions for Seismology-Data Management Center (IRIS-DMC). Data were processed using Datascope3.0, developed by the University of Colorado, IRIS-JSPC and SAC2000 developed by the Lawrence Livermore National Laboratory. Figures were made using the GMT3.0 software package (Wessel and Smith, 1991). We are grateful to Dogan Seeber and Muawia Barazangi of Cornell University for providing the Former Soviet Union Institute of Physics of the Earth (IPE) basement and Moho depth maps. The initial phase of this research was supported by Phillips Laboratory Contract Number F19628-95-K-0014. Contribution number 340 University of California, Santa Cruz Institute of Tectonics. Research was performed under the auspices of the U.S. Department of Energy by the Lawrence Livermore National Laboratory under contract W-7405-ENG-48. This is LLNL journal contribution UCRL-JC-128318.

## References

- Barazangi, M., E. Fielding, B. Isacks and D. Seeber (1996). Geophysical and geological databases and CTBT monitoring: A case study of the Middle East, in *Monitoring a Comprehensive Test Ban Treaty*, E. Husebye and A. Dainty (Editors), Academic Publishers, Dordrecht, 197-224.
- Bennett, T. and J. Murphy (1986). Analysis of seismic discrimination capabilities using regional data from western United States events, *Bull. Seism. Soc. Am.*, **76**, 1069-1086.
- Blandford, R. (1981). Seismic discrimination problems at regional distances, in *Identification of Seismic Sources-Earthquake or Explosion*, E. Husebye and S. Mykkeltveit (Editors), Reidel, Boston, 695-740.
- Dercourt, J. et al. (1986). Geological evolution of the Tethys belt from the Atlantic to the Pamirs since the Lias, *Tectonophysics*, **123**, 241-315.

- Fan, G. and T. Lay (1997). Statistical analysis of irregular waveguide influences on regional seismic discriminants in China, submitted to *Bull. Seism. Soc. Am.*
- Hartse, H., S. Taylor, S. Phillips and G. Randall (1997a). A preliminary study of regional seismic discrimination in Central Asia with emphasis on western China, *Bull. Seism. Soc. Am.*, **87**, 551-568.
- Hartse, H., R. Flores and Johnson (1997b). Correcting regional seismic discriminants for path effects in western China, submitted to *Bull. Seism. Soc. Am.*
- Hearn, T. and J. Ni (1994). Pn velocities beneath continental collision zones: the Turkish-Iranian Plateau, *Geophys. J. Int.*, **117**, 273-283.
- Kadinsky-Cade, K., M. Barazangi, J. Oliver and B. Isacks (1981). Lateral variations of high frequency seismic wave propagation at regional distances across the Turkish and Iranian Plateaus, *J. Geophys. Res.*, **86**, 9377-9396.
- Kazmin, V., I. Sbornshikov, L. Ricou, L. Zonenshain, J. Boulin and A. Knipper (1986). Volcanic belts as markers of the Mesozoic-Cenozoic active margins of Eurasia, *Tectonophysics*, **123**, 123-152.
- McNamara, D., T. Owens and W. Walter (1996). Propagation characteristics of Lg across the Tibetan Plateau, *Bull. Seism. Soc. Am.*, **86**, 457-469.
- Mitchell, B., J. Xie and Y. Pan (1996). Attenuation and blockage of Lg in Eurasia, in *Monitoring a Comprehensive Test Ban Treaty*, E. Husebye and A. Dainty (Editors), Academic Publishers, Dordrecht, 645-654.
- Nuttli, O. (1980). The excitation and attenuation of seismic crustal phases in Iran, *Bull. Seism. Soc. Am.*, **70**, 469-485.
- Pomeroy, P., W. Best and T. McEvelly (1982). Test ban treaty verification with regional data - a review. *Bull. Seism. Soc. Am.*, **72B**, S89-S129.
- Rodgers, A., J. Ni and T. Hearn (1997a). Propagation characteristics of short-period Sn and Lg in the Middle East, *Bull. Seism. Soc. Am.*, **87**, 396-413.

- Rodgers, A., T. Lay, W. Walter and K. Mayeda (1997b). Comparison of regional phase amplitude ratio measurement techniques, in press *Bull. Seism. Soc. Am.*
- Snyder, D. and M. Barazangi (1986). Deep crustal structure and flexure of the Arabian Plate beneath the Zagros collisional mountain belt as inferred from gravity observations, *Tectonics*, **5**, 361- 373.
- Sweeney, J. (1996). Accuracy of teleseismic event locations in the Middle East and North Africa, Lawrence Livermore National Laboratory report, UCRL-ID-125868, Livermore, CA.
- Taylor, S., M. Denny, E. Vergino and R. Glasner (1989). Regional discrimination between NTS explosions and western U.S. earthquakes, *Bull. Seism. Soc. Am.*, **79**, 1142-1176.
- Taylor, S. (1996). Analysis of high-frequency Pg/Lg ratios from NTS explosions and western U.S. earthquakes, *Bull. Seism. Soc. Am.*, **86**, 1042-1053.
- Walter, W., K. Mayeda and H. Patton (1995). Phase and spectral ratio discrimination between NTS earthquakes and explosions. Part I: empirical observations, *Bull. Seism. Soc. Am.*, **85**, 1050-1067.
- Wessel, P. and W. Smith (1991). Free software helps map and display data, *EOS*, **72**, 441, 445-446.
- Zhang, T.-R., S. Schwartz and T. Lay (1994). Multivariate analysis of waveguide effects on short-period regional wave propagation in Eurasia and its application in seismic discrimination, *J. Geophys. Res.*, **99**, 21,929-21,945.
- Zhang, T.-R., T. Lay, S. Schwartz and W. Walter (1996). Variation of regional seismic discriminants with surface topographic roughness in the western United States, *Bull. Seism. Soc. Am.*, **86**, 714-725.

**Affiliations:**



Geophysics and Global Security Division, Lawrence Livermore National Laboratory, L-206, P.O. Box 808, Livermore, CA 94551 (A.J.R., W.R.W.)

Earth Sciences Department, University of California, Santa Cruz, Santa Cruz, CA 95064 (T.L.).

**Calibration of Distance and Path Effects on Regional P/S  
Discriminants at Station ABKT (Alibek, Turkmenistan):  
Statistical Analysis of Crustal Waveguide Effects**

Arthur J. Rodgers <sup>1</sup>, Thorne Lay <sup>2</sup>, Guangwei Fan <sup>2</sup>, William R. Walter <sup>1</sup>

*<sup>1</sup>Geophysics and Global Security Division,  
Lawrence Livermore National Laboratory, Livermore, CA 94551*

*<sup>2</sup>University of California, Santa Cruz,  
Institute of Tectonics and Earth Sciences Department,  
Santa Cruz, CA 95064*

Correspondence: Arthur Rodgers, Lawrence Livermore National Laboratory,

L-205, P.O. Box 808, Livermore, CA 94551

e-mail: [rodders@s34.es.llnl.gov](mailto:rodders@s34.es.llnl.gov)

phone: (510)-423-5018; fax: (510)-423-4077

Manuscript submitted to the  
*Bulletin of the Seismological Society of America*  
February 25, 1998

## Abstract

Short-period regional seismic wave amplitudes for earthquake signals observed at ABKT (Alibek, Turkmenistan) are analyzed for crustal waveguide effects. Paths to ABKT sample diverse tectonic regions and crustal structures. P/S amplitude ratios ( $P_n/L_g$ ,  $P_g/L_g$ ,  $P_n/S_n$  and  $P_g/S_n$ ) for nearly 300 earthquakes in four frequency bands between 0.75 and 9.0 Hz show great spatial variability caused in part by wave propagation effects. For these data to be useful for seismic source discrimination associated with monitoring the Comprehensive Test Ban Treaty (CTBT), techniques need to be developed to reduce contributions from propagation. Empirical correlations are established between the P/S ratios and various parameters which characterize the path specific crustal waveguide. Univariate regressions indicate that the most important individual crustal waveguide parameters influencing regional P/S ratios are distance, mean elevation, rms slope of elevation, mean sediment thickness and minimum Moho depth. Correlations with waveguide shape properties are sometimes stronger than correlations with distance. The successful univariate regressions typically reduce the variance of the P/S ratios by 20-40%. Multivariate regressions provide optimal combinations of crustal waveguide parameters that reduce the scatter in P/S amplitude ratios. Strongest correlations and variance reductions are found for frequencies below 3.0 Hz. Multivariate regression models with three, four or five parameters reduce the data variance by as much as 50-60%, although most of the variance reduction can be achieved with just two parameters. Distance and mean sediment thickness are the most important joint crustal waveguide parameters influencing the low frequency  $P_n/L_g$ ,  $P_g/L_g$  and  $P_n/S_n$  ratios, while mean crustal thickness and mean sediment thickness are the most important joint factors influencing the low frequency  $P_g/S_n$  ratios. It is hoped that large reductions in the scatter of low frequency P/S amplitude ratios should enhance discrimination, however lacking explosion data for the region prevents an assessment of discriminant performance.

## Introduction

Short-period regional seismic phases will play an important role in monitoring the Comprehensive Test Ban Treaty (CTBT) for events with body-wave magnitudes ( $m_b$ ) less than about 4.0. Because signal-to-noise is generally small for low magnitude events at teleseismic distances (distances greater than about 2000 km), discrimination strategies based on  $M_s:m_b$ , radiation pattern and/or source depth may not provide sufficiently reliable source characterization (e.g. Blandford, 1981; Pomeroy et al., 1982; National Research Council, 1997). Short-period regional P/S discriminants, e.g. Pn/Lg, Pg/Lg and Pn/Sn amplitude ratios, have been shown to be effective at discriminating earthquakes and explosions (Bennett and Murphy, 1986; Taylor et al., 1989; Walter et al., 1995; Taylor, 1996; Hartse et al., 1997a). However, the travel times and amplitudes of regional phases vary greatly due to acute sensitivity to highly heterogeneous lithospheric structure. An understanding of earthquake generated regional seismic phase behavior is necessary before regional P/S ratios can be used reliably as discriminants. Efforts to quantify regional P/S ratio behavior are being pursued in support of CTBT monitoring goals.

For many years, observations of short-period Sn and Lg amplitudes have been qualitatively characterized in terms of spatially varying propagation efficiency. For example, studies by Kadinsky-Cade et al. (1981) and Rodgers et al. (1997a) report regional variations in short-period (frequencies 0.5-5.0 Hz) Sn and Lg amplitude behavior in the Middle East. These studies report strong attenuation or inefficient propagation of Sn for the Turkish-Iranian Plateau and blockage of Lg by oceanic crust. Inefficient propagation of Sn is associated with high elevations of the Turkish-Iranian Plateau, low Pn velocities (Hearn and Ni, 1994), and recent volcanism. Seismic source discrimination and monitoring of the CTBT requires quantitative representation of P/S amplitude ratio behavior. Recent investigations have sought to understand the quantitative behavior of

short-period regional P/S amplitude ratios in terms of crustal waveguide structure. These studies establish empirical correlations between P/S amplitude behavior and along-path topographic, bathymetric, sediment and crustal structures (Baumgardt, 1990; Zhang and Lay, 1994a, 1994b; Zhang et al., 1996; Baumgardt, 1996; Baumgardt and Schneider, 1997). Studies by Zhang et al. (1994) and Fan and Lay (1997a, 1997b) investigate crustal waveguide effects using multivariate regression analysis. Multivariate regressions find linear combinations of propagation path parameters that best describe the observed amplitude ratio data. Fan and Lay (1997a) found that the most important crustal waveguide parameters controlling low frequency ( $< 3.0$  Hz) Pg/Lg behavior in western China are distance, mean elevation, mean crustal thickness and mean sediment thickness. These results show that the scatter in regional P/S discriminants can be significantly reduced with simple empirical models (variance reductions of 75% have been obtained). Baumgardt and Schneider (1997) showed that average basement depth is an important factor influencing Pn/Lg amplitude ratios in Iran. They used short-period waveform data recorded at the Iran Long-Period Array (ILPA) for paths propagating primarily within the Iranian Plateau. Studies of crustal waveguide effects on regional amplitude ratios will hopefully lead to a physical basis for understanding short-period P/S behavior and can be used to guide theoretical modeling of short-period regional seismic wave propagation.

This article explores the effects of along-path crustal waveguide structures on short-period regional P/S amplitude ratio measurements at station ABKT (Alibek, Turkmenistan) using both univariate and multivariate regression methods. The data are the same used in previous regionalization studies (Rodgers et al., 1997a, 1997c). Station ABKT is located on the northern flank of the Kopet Dagh Mountains near the major tectonic boundary separating the Iranian Plateau to the south from the Kazakh Platform to the north and ABKT is within regional distances of Iran, Afghanistan and many former Soviet Republics. The P/S amplitude ratios observed at ABKT show strong spatial variability

(Rodgers et al., 1997c), presumably related to topographic, geologic, tectonic and crustal waveguide structure. ABKT is near the site of a planned primary station (GEYT) of the International Monitoring System (IMS). GEYT data will be used for event location and screening by the International Data Center (IDC) and thus will require complete calibration of regional discriminants.

### **Regional Waveform Data at ABKT and P/S Amplitude Ratio Measurements**

We use the data set of Rodgers et al. (1997c). Broadband waveform data (20 samples/sec) recorded at station ABKT were requested from the Incorporated Research Institutions for Seismology-Data Management Center (IRIS-DMC). Event parameters were taken from the National Earthquake Information Center-Preliminary Determination of Epicenters (NEIC-PDE). Data were requested for earthquakes with depths less than 50 km and body-wave magnitudes,  $m_b$ , greater than or equal to 4.0. All waveforms were previewed and a first-arriving P-wave was picked when possible. We considered only vertical component data and distances were limited to 2000 km. Noisy data and data with interfering events were immediately discarded. Previewing resulted in nearly 300 regional events recorded at ABKT for the years 1993-1995. These events are plotted in Figure 1.

Regional phase amplitude ratios and signal-to-noise ratios were measured for these data in four pass bands (0.75-1.5, 1.5-3.0, 3.0-6.0 and 6.0-9.0 Hz). Phases were isolated with the following group velocities: Pn 8.0-6.2 km/sec; Pg 6.2-5.0 km/sec; Sn 4.6-4.0 km/sec and Lg 3.6-3.0 km/sec. Noise measurements were taken for a 35 sec window ending 5 sec before the first-arriving P-wave. To account for possible location and/or origin time errors, the origin time was shifted such that the Pn arrival came in at 7.9 km/sec. A Pn tomography study by Hearn and Ni (1994) reports that 7.9 km/sec is an appropriate average value for the region. If this time shift was greater than 15 seconds the

waveform was discarded. This was done to avoid gross location and/or origin time errors and their effects on windowing the regional phases. Investigations of these origin time shifts show that they are typically smaller than 10 seconds. Given the uncertainties in event location, depth and origin time, these shifts window the first arriving P-wave in a consistent fashion. To the extent that our group velocity windows are appropriate, the later arriving phases should be windowed better after applying these time shifts. Strictly speaking, the first arriving P-wave for distances beyond about 1600 km is not the regional head-wave (Pn) and arrives with a velocity greater than the regional Pn velocity. However, we have determined that the P-wave first arrival times are well fit by a velocity of 7.9 km/s without an intercept time correction.

Amplitude ratios (Pn/Lg, Pg/Lg, Pn/Sn and Pg/Sn) were measured in each frequency band by computing the log-10 mean spectral amplitude of each phase from the smoothed broadband instrument-deconvolved spectrum. Pn/pre-Pn signal-to-noise ratios were computed for each event and frequency band. Only data for which the signal-to-noise ratio was greater than 2.0 were used in the analysis. Signal-to-noise is not measured for later arriving phases, thus we could be including cases where Sn and/or Lg are very weak or blocked. Rodgers et al. (1997b) showed that time domain and frequency domain measurements of regional phase amplitude ratios are similar for frequencies less than 3.0 Hz. However, for frequencies greater than 3.0 Hz, time domain measurements are possibly contaminated by energy from outside the pass band of interest. Complete control of the frequencies contributing to each measurement is possible in the frequency domain. Furthermore, time domain measurements are biased towards the large amplitude energy at the low end of the pass band considered. This bias is reduced by log averaging of the spectral amplitude in the frequency domain. Maps of the Pn/Lg, Pg/Lg and Pn/Sn amplitude ratio measurements are plotted in Figures 2, 3 and 4 of Rodgers et al. (1997b). These maps show that the P/S ratios from the Hindu Kush region are often low ( $< 0.5$ ,

indicating strong S-wave energy) and the P/S ratios from the Zagros region are typically high ( $>1.0$ , indicating weak S-wave energy).

### **Crustal Waveguide Profiles**

Information about the crustal waveguide profile for each event-ABKT path was used to define path specific waveguide parameters. Surface topography was taken from the global topography model GTOPO30. This model represents continental surface elevation above sea-level on a 30-second by 30-second (0.93 km) grid and is shown in decimated form in Figure 1. Topography for the region of interest spans elevations below sea level in the Caspian Basin to high peaks of the Hindu Kush (over 6000 m). The basement depth (sediment thickness, shown in Figure 2) and Moho depth (crustal thickness, shown in Figure 3) were taken from models compiled by Cornell University (Barazangi et al., 1996). These models were digitized from maps produced at the Former Soviet Union Institute of Physics of the Earth (IPE) by Kunin and Sheykh-Zade (1983) and Kunin (1987) based on deep seismic sounding (DSS) profiles and gridded on a 10 km by 10 km grid (Fielding et al., 1992). Extremely thick sediments are reported for the southern Caspian sea ( $> 30$  km). Deep sedimentary cover ( $> 5$  km) is found in the Mesopotamian foredeep, the Black and Mediterranean Seas and in various basins in and around Iran. Crustal thickness reaches extremes of greater than 60 km beneath the Hindu Kush and values greater than 50 km beneath the Zagros Mountains. Generally, the Moho depth is near 45 km for most of the region. Without a doubt, these models of basement and Moho depth are poorly resolved. Nonetheless, they provide the only models of sediment and crustal thickness for the entire region spanned by the events considered and probably are adequate to represent the first-order path-averaged properties to sufficient accuracy for the purpose of this investigation. Point-wise properties and gradients are probably very poorly resolved in these models. Profiles of crustal waveguide structure along each event-ABKT paths were traced through



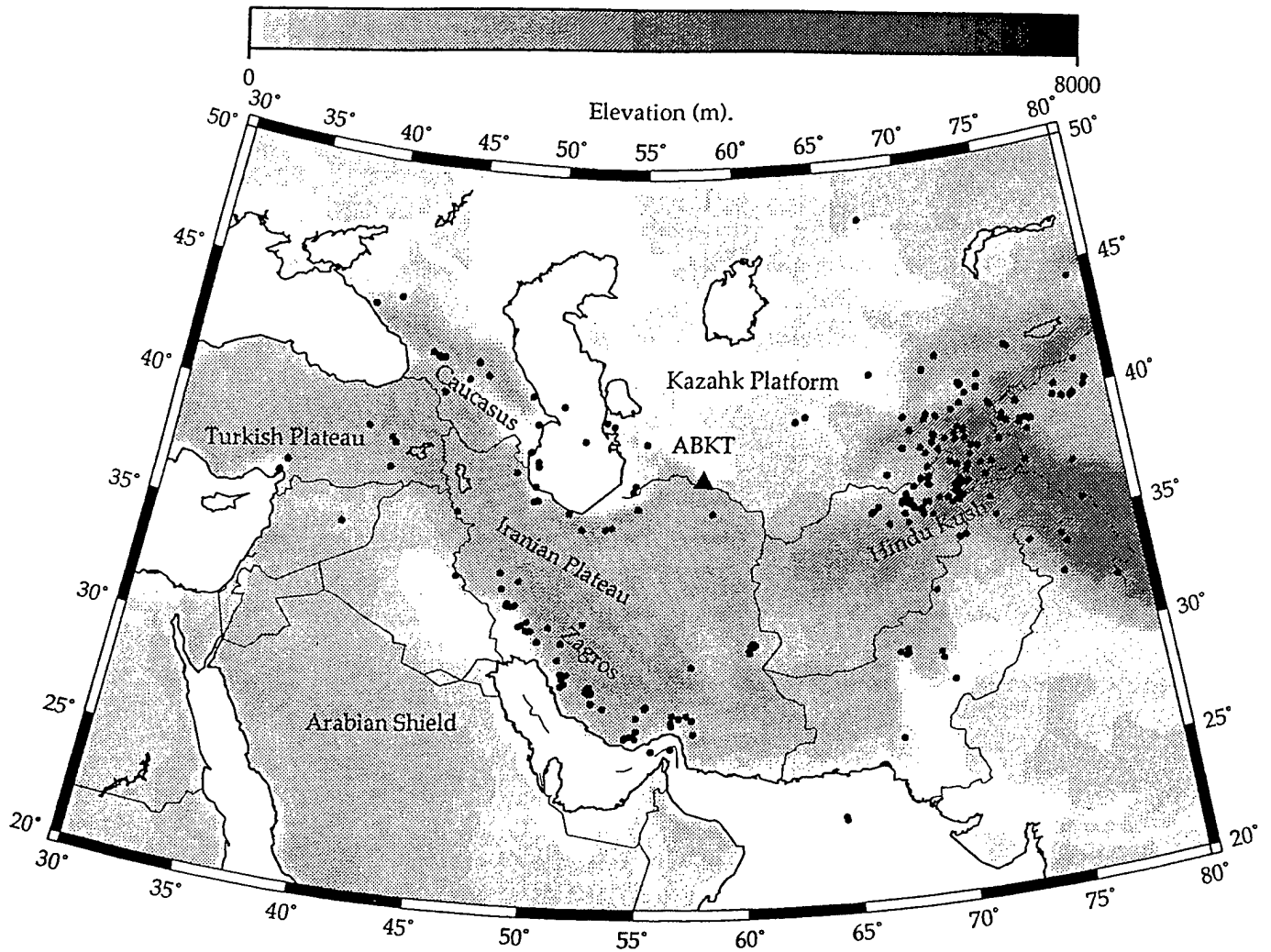


**Figure 1.** Map of the study region with the locations of station ABKT (triangle) and the events (circles) considered. Tectonic features and topography of the region, taken from GTOPO30 but plotted at lower resolution, are also shown.

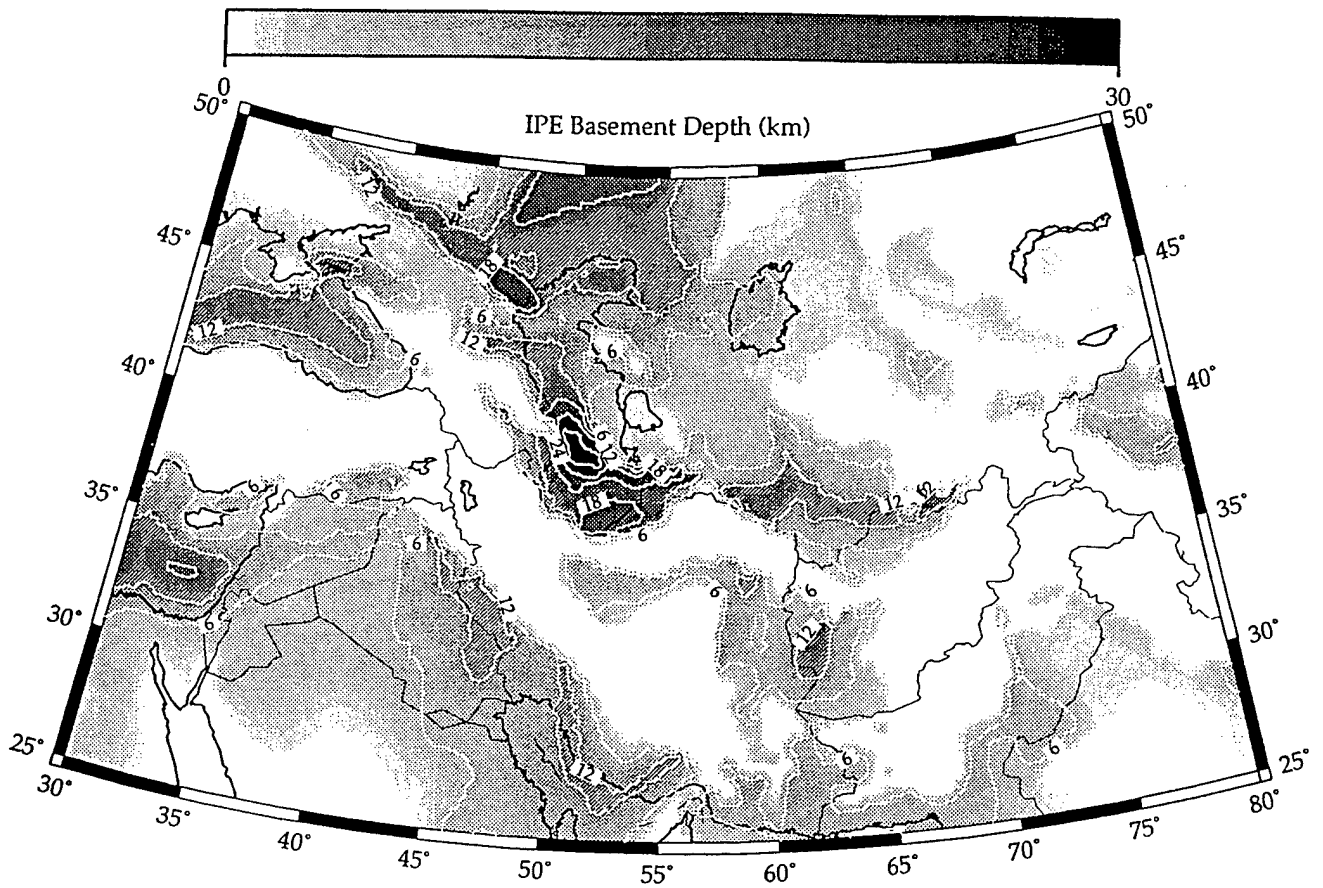


**Figure 2.** Basement depth (sediment thickness) of the region studied, taken from the Institute of Physics of the Earth and compiled by Cornell University (Barazangi, et al., 1996). Contour interval is 6 km.

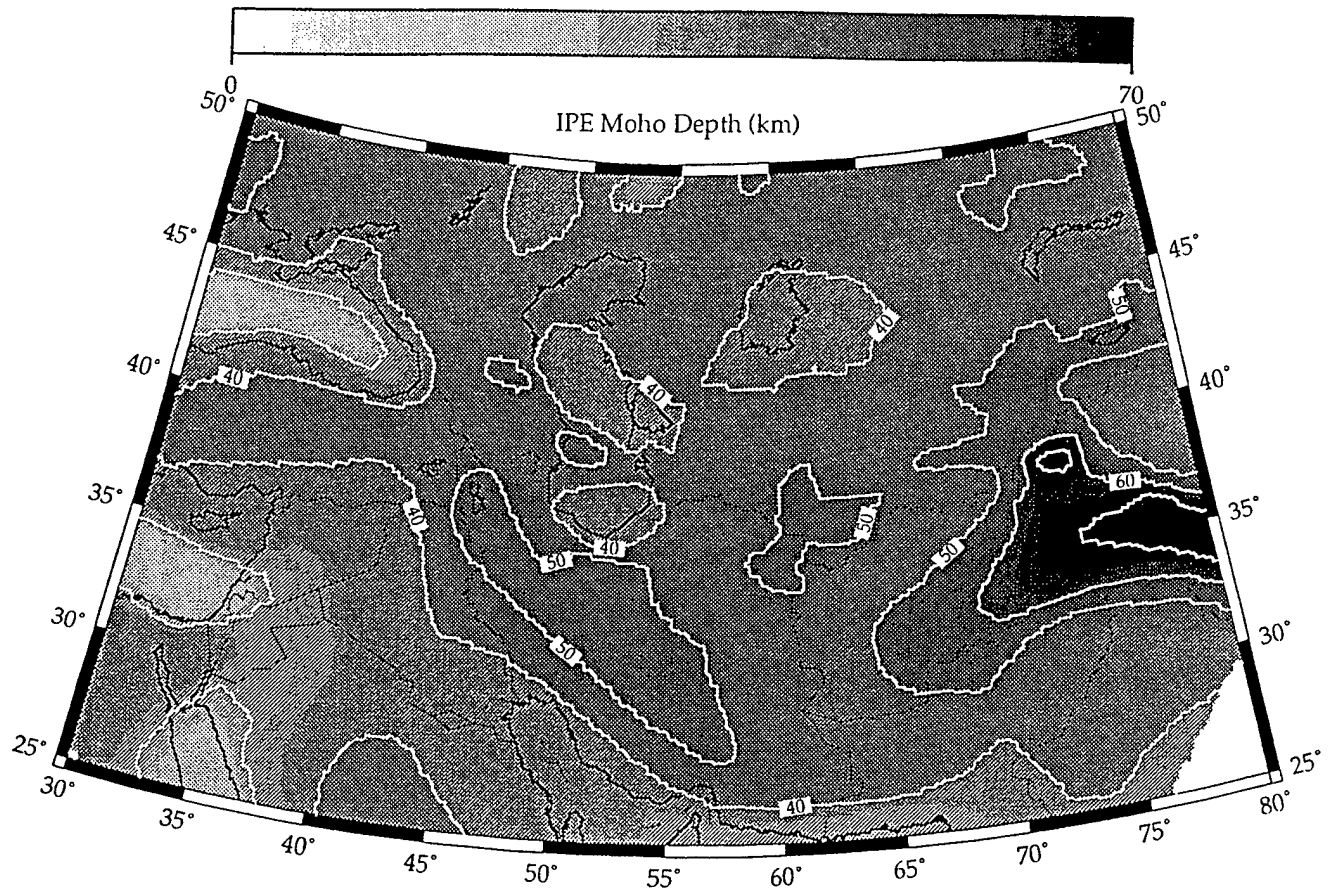
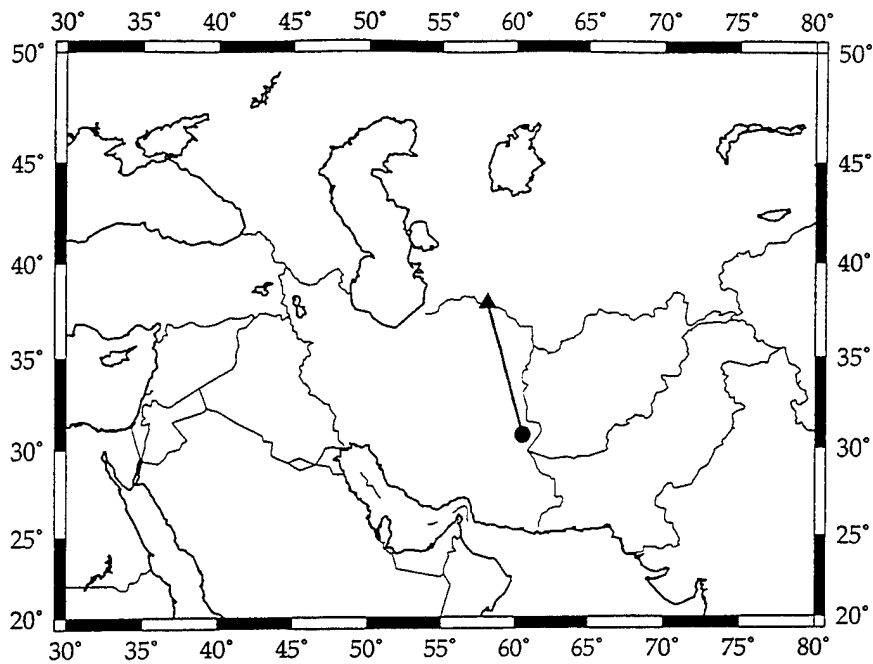


**Figure 3.** Moho depth (crustal thickness) of the region studied, taken from the Institute of the Physics of the Earth and compiled by Cornell University (Barazangi, et al., 1996). Contour interval is 10 km.

these topography, basement and Moho depth models. Figure 4 shows an example of such a crustal waveguide profile for a path crossing the eastern Iranian Plateau. Because the topographic profiles are most well resolved, we considered the mean, rms, rms slope, skewness, maximum, minimum and the difference between the maximum and minimum. The parameters considered for the crustal thickness profiles were mean, maximum, minimum and the difference between the maximum and minimum. For the sediment thickness profiles we considered only the mean and maximum, because the minimum thickness was almost always zero. A potential shortcoming of these path specific parameters is that they are all independent of the propagation direction.

### **Univariate Regressions of P/S Ratios On Crustal Waveguide Parameters**

P/S amplitude ratios for the four frequency bands considered were correlated with and regressed on various crustal waveguide parameters in order to identify the most important single influences on the regional wavefield. The path parameters considered were: distance; mean elevation; rms elevation; rms slope of elevation; skewness of elevation; maximum elevation; minimum elevation; difference of maximum and minimum elevation; mean basement depth; maximum basement depth; mean Moho depth; maximum Moho depth; minimum Moho depth; difference of maximum and minimum Moho depth. Regressions on body-wave magnitude ( $m_b$ ) were also performed. Similar to the univariate regressions presented in Zhang and Lay (1994a, 1994b), Zhang et al. (1994, 1996), Fan and Lay (1997a) and Rodgers et al. (1997c), we regressed the individual P/S ratios within each frequency band on each path parameter, computed the slope and zero-value intercept, the standard error about the regression fit and the linear correlation. Each regression seeks to represent the linear relationship between a given P/S ratio,  $y_i$ , with path parameter,  $x_i$ , as:  $y_i = a + b x_i$ , where  $a$  is the zero-value intercept and  $b$  is the slope.



TOPOGRAPHY	mean: 1.49 km	rms: 0.48 km
BASEMENT	mean: -4.9 km	rms: 3.9 km
MOHO	mean: -44.4 km	rms: 3.5 km

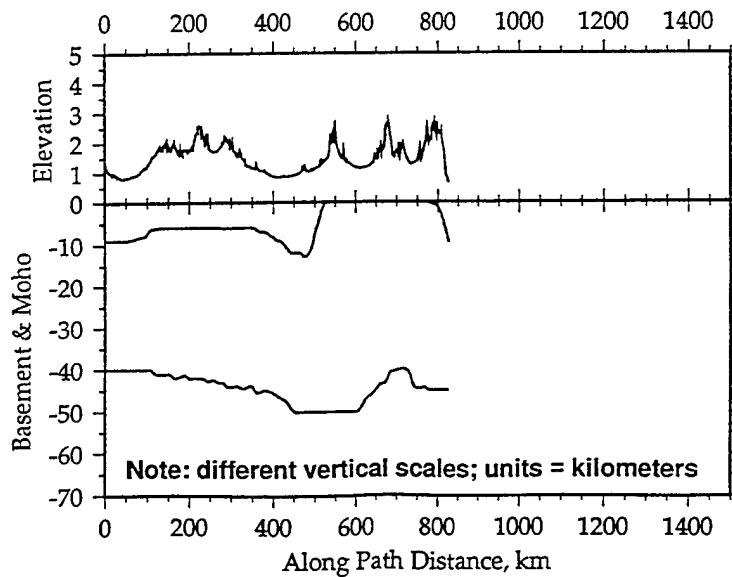


**Figure 4.** Example of a crustal waveguide profile. (top) A map view of the profile location. (bottom) A crustal waveguide profile taken from the models of surface elevation, basement and Moho depths shown in Figures 1-3, respectively. The mean and rms values of topography, basement depth and Moho depth are given.

Results of the univariate regressions are compiled in Tables 1, 2, 3 and 4 for Pn/Lg, Pg/Lg, Pn/Sn and Pg/Sn, respectively. We discuss only the results for the frequencies below 3.0 Hz, as correlations are weak at higher frequencies. Also, as discussed in Rodgers et al. (1997c) the P/S data from the Zagros region at frequencies above 3.0 Hz are preferentially lost due to poor signal-to-noise. Consistent, although modest correlations (linear correlations  $> 0.3$ ), are found between the P/S ratios and distance, mean elevation, rms slope of elevation, maximum and mean sediment thickness and minimum crustal thickness. The strongest correlations for each ratio are found for either distance, mean elevation or mean sediment thickness. These correlations indicate that on one crustal waveguide parameter controls the P/S amplitude ratio behavior. Correlations may result purely from covariance between path parameters, rather than direct physical controls on the wavefield. Correlations between many of the path parameters for the events considered are compiled in Table 5. Many of these are rather strong ( $> 0.5$ ). For example, mean elevation and rms slope of elevation are strongly correlated with each other (linear correlation of 0.710) and both of these path parameters are well correlated with the low frequency ( $< 3.0$  Hz) P/S amplitude ratios. Similarly, mean and maximum basement depth are strongly correlated with each other (linear correlation of 0.758). However, in this case the low frequency P/S ratios are consistently more strongly correlated with the mean basement depth. This suggests that the maximum basement depth (a point-wise path property) is not a strong predictor of P/S ratios.

To illustrate the univariate regression results we present plots of the Pg/Lg ratios versus distance, mean elevation, rms elevation, mean crustal thickness and mean sediment thickness in Figures 5, 6, 7, 8 and 9, respectively. Only paths for which the Pn/pre-Pn signal-to-noise was greater than 2.0 are considered. These path parameters are shown because they are the parameters for which we perform the multivariate regression analysis, presented in the next section. Univariate regressions show that distance, mean elevation

Table 1.

**Pn/Lg 0.75-1.5 Hz ABKT - Univariate Regression Statistics**

Path Parameter	linear correlation	zero-value	slope	standard error
Distance	0.532	-1.120	0.00077	0.393
mb	0.144	-1.014	0.16274	0.460
Mean Elevation	0.453	-0.694	0.43731	0.414
Rms Elevation	0.239	-0.441	0.25060	0.451
Rms Slope Elevation	0.360	-0.493	0.00242	0.433
Skewness Elevation	-0.008	-0.252	-0.00025	0.464
Maximum Elevation	0.296	-0.644	0.11381	0.444
Minimum Elevation	-0.111	-0.253	-0.03897	0.462
Max-Min Elevation	0.283	-0.502	0.07373	0.445
Mean Moho	0.022	-0.424	0.00365	0.464
Maximum Moho	0.026	-0.368	0.00214	0.464
Minimum Moho	-0.335	2.389	-0.06615	0.438
Max-Min Moho	0.179	-0.459	0.01608	0.457
Mean Basement	-0.461	0.092	-0.05766	0.412
Maximum Basement	-0.205	0.082	-0.02171	0.455

**Pn/Lg 1.5-3.0 Hz ABKT - Univariate Regression Statistics**

Path Parameter	linear correlation	zero-value	slope	standard error
Distance	0.432	-0.373	0.00043	0.288
mb	0.135	-0.380	0.10466	0.316
Mean Elevation	0.428	-0.169	0.28327	0.288
Rms Elevation	0.250	-0.026	0.17808	0.309
Rms Slope Elevation	0.327	-0.053	0.00169	0.302
Skewness Elevation	0.017	0.102	0.00040	0.319
Maximum Elevation	0.368	-0.214	0.09351	0.297
Minimum Elevation	-0.025	0.108	-0.00687	0.319
Max-Min Elevation	0.287	-0.071	0.05344	0.306
Mean Moho	0.151	-0.700	0.01745	0.316
Maximum Moho	0.168	-0.383	0.00928	0.315
Minimum Moho	-0.168	1.016	-0.02266	0.315
Max-Min Moho	0.256	-0.087	0.01524	0.309
Mean Basement	-0.354	0.303	-0.03063	0.299
Maximum Basement	-0.220	0.363	-0.01622	0.311

Table 2.

**Pg/Lg 0.75-1.5 Hz ABKT - Univariate Regression Statistics**

Path Parameter	linear correlation	zero-value	slope	standard error
Distance	0.390	-0.602	0.00036	0.270
mb	0.183	-0.812	0.13100	0.288
Mean Elevation	0.498	-0.506	0.30371	0.254
Rms Elevation	0.136	-0.268	0.08999	0.290
Rms Slope Elevation	0.364	-0.352	0.00154	0.273
Skewness Elevation	0.156	-0.250	0.00328	0.289
Maximum Elevation	0.195	-0.362	0.04716	0.287
Minimum Elevation	-0.094	-0.200	-0.02075	0.292
Max-Min Elevation	0.201	-0.312	0.03308	0.287
Mean Moho	-0.027	-0.070	-0.00285	0.293
Maximum Moho	-0.089	0.045	-0.00469	0.292
Minimum Moho	-0.335	1.468	-0.04177	0.276
Max-Min Moho	0.056	-0.241	0.00315	0.292
Mean Basement	-0.537	0.054	-0.04235	0.247
Maximum Basement	-0.335	0.146	-0.02236	0.276

**Pg/Lg 1.5-3.0 Hz ABKT - Univariate Regression Statistics**

Path Parameter	linear correlation	zero-value	slope	standard error
Distance	0.243	-0.152	0.00016	0.206
mb	0.246	-0.564	0.12710	0.206
Mean Elevation	0.555	-0.211	0.24456	0.177
Rms Elevation	0.151	-0.026	0.07172	0.210
Rms Slope Elevation	0.346	-0.085	0.00119	0.199
Skewness Elevation	0.260	-0.028	0.00398	0.205
Maximum Elevation	0.260	-0.124	0.04404	0.205
Minimum Elevation	0.032	0.027	0.00592	0.212
Max-Min Elevation	0.169	-0.042	0.02092	0.210
Mean Moho	0.100	-0.328	0.00770	0.212
Maximum Moho	0.036	-0.042	0.00132	0.212
Minimum Moho	-0.070	0.280	-0.00630	0.212
Max-Min Moho	0.070	-0.008	0.00277	0.212
Mean Basement	-0.546	0.229	-0.03150	0.178
Maximum Basement	-0.385	0.325	-0.01888	0.196



Table 3.

**Pn/Sn 0.75-1.5 Hz ABKT - Univariate Regression Statistics**

Path Parameter	linear correlation	zero-value	slope	standard error
Distance	0.387	-0.620	0.00047	0.355
mb	0.202	-0.984	0.19003	0.377
Mean Elevation	0.456	-0.464	0.36516	0.342
Rms Elevation	0.085	-0.152	0.07365	0.383
Rms Slope Elevation	0.308	-0.266	0.00171	0.366
Skewness Elevation	0.131	-0.151	0.00359	0.381
Maximum Elevation	0.109	-0.216	0.03454	0.382
Minimum Elevation	-0.092	-0.096	-0.02674	0.383
Max-Min Elevation	0.142	-0.200	0.03058	0.381
Mean Moho	-0.082	0.437	-0.01156	0.383
Maximum Moho	-0.162	0.489	-0.01115	0.380
Minimum Moho	-0.335	2.093	-0.05481	0.363
Max-Min Moho	-0.022	-0.077	-0.00166	0.385
Mean Basement	-0.554	0.249	-0.05745	0.320
Maximum Basement	-0.277	0.280	-0.02431	0.370

**Pn/Sn 1.5-3.0 Hz ABKT - Univariate Regression Statistics**

Path Parameter	linear correlation	zero-value	slope	standard error
Distance	0.248	-0.268	0.00026	0.323
mb	0.239	-0.881	0.19368	0.324
Mean Elevation	0.472	-0.298	0.32638	0.294
Rms Elevation	0.016	0.011	0.01209	0.334
Rms Slope Elevation	0.297	-0.132	0.00161	0.319
Skewness Elevation	0.219	-0.054	0.00528	0.326
Maximum Elevation	0.064	-0.038	0.01690	0.333
Minimum Elevation	-0.031	0.021	-0.00876	0.334
Max-Min Elevation	0.068	-0.024	0.01315	0.333
Mean Moho	-0.125	0.720	-0.01512	0.331
Maximum Moho	-0.217	0.684	-0.01256	0.326
Minimum Moho	-0.305	1.743	-0.04298	0.318
Max-Min Moho	-0.099	0.099	-0.00620	0.332
Mean Basement	-0.586	0.358	-0.05301	0.271
Maximum Basement	-0.352	0.448	-0.02713	0.312

Table 4.

**Pg/Sn 0.75-1.5 Hz ABKT - Univariate Regression Statistics**

Path Parameter	linear correlation	zero-value	slope	standard error
Distance	0.064	-0.101	0.00005	0.257
mb	0.252	-0.782	0.15838	0.249
Mean Elevation	0.432	-0.276	0.23161	0.232
Rms Elevation	-0.150	0.020	-0.08695	0.255
Rms Slope Elevation	0.224	-0.125	0.00083	0.251
Skewness Elevation	0.386	-0.149	0.00711	0.237
Maximum Elevation	-0.151	0.066	-0.03209	0.255
Minimum Elevation	-0.044	-0.043	-0.00849	0.257
Max-Min Elevation	-0.070	-0.010	-0.01007	0.257
Mean Moho	-0.192	0.792	-0.01807	0.253
Maximum Moho	-0.389	0.902	-0.01797	0.237
Minimum Moho	-0.278	1.173	-0.03044	0.247
Max-Min Moho	-0.294	0.141	-0.01459	0.246
Mean Basement	-0.607	0.210	-0.04214	0.205
Maximum Basement	-0.425	0.344	-0.02495	0.233

**Pg/Sn 1.5-3.0 Hz ABKT - Univariate Regression Statistics**

Path Parameter	linear correlation	zero-value	slope	standard error
Distance	-0.012	-0.047	-0.00001	0.281
mb	0.317	-1.065	0.21612	0.266
Mean Elevation	0.495	-0.340	0.28780	0.244
Rms Elevation	-0.151	0.011	-0.09420	0.277
Rms Slope Elevation	0.243	-0.164	0.00111	0.272
Skewness Elevation	0.437	-0.184	0.00886	0.252
Maximum Elevation	-0.146	0.053	-0.03255	0.278
Minimum Elevation	0.017	-0.060	0.00401	0.281
Max-Min Elevation	-0.118	0.006	-0.01935	0.279
Mean Moho	-0.244	1.092	-0.02487	0.272
Maximum Moho	-0.422	1.024	-0.02051	0.254
Minimum Moho	-0.225	1.007	-0.02661	0.273
Max-Min Moho	-0.356	0.179	-0.01867	0.262
Mean Basement	-0.708	0.284	-0.05389	0.198
Maximum Basement	-0.460	0.411	-0.02980	0.249

Table 5.

**ABKT Path Parameter Cross-Correlations**

Path Parameter Pair	linear correlation
dist-mb	0.024
dist-meanelev	0.221
dist-minelev	-0.136
dist-maxelev	0.541
dist-rmselev	0.561
dist-rmsslopeelev	0.250
dist-meanmoho	0.458
dist-meanbas	-0.083
meanelev-maxelev	0.495
meanelev-minelev	0.158
meanelev-diffelev	0.230
meanelev-rmselev	0.340
meanelev-rmsslopeelev	0.406
meanelev-skewelev	0.449
meanelev-meanmoho	0.349
meanelev-minmoho	0.243
meanelev-maxmoho	0.219
meanelev-diffmoho	0.128
meanmoho-maxmoho	0.771
meanmoho-minmoho	0.656
meanelev-meanbas	-0.790
meanelev-maxbas	-0.573
meanelev-minbas	-0.164
meanbas-maxbas	0.758

# ABKT Pg/Lg vs. Distance

Log<sub>10</sub>-mean spectral amplitude ratio, Pn/pre-Pn noise > 2.0

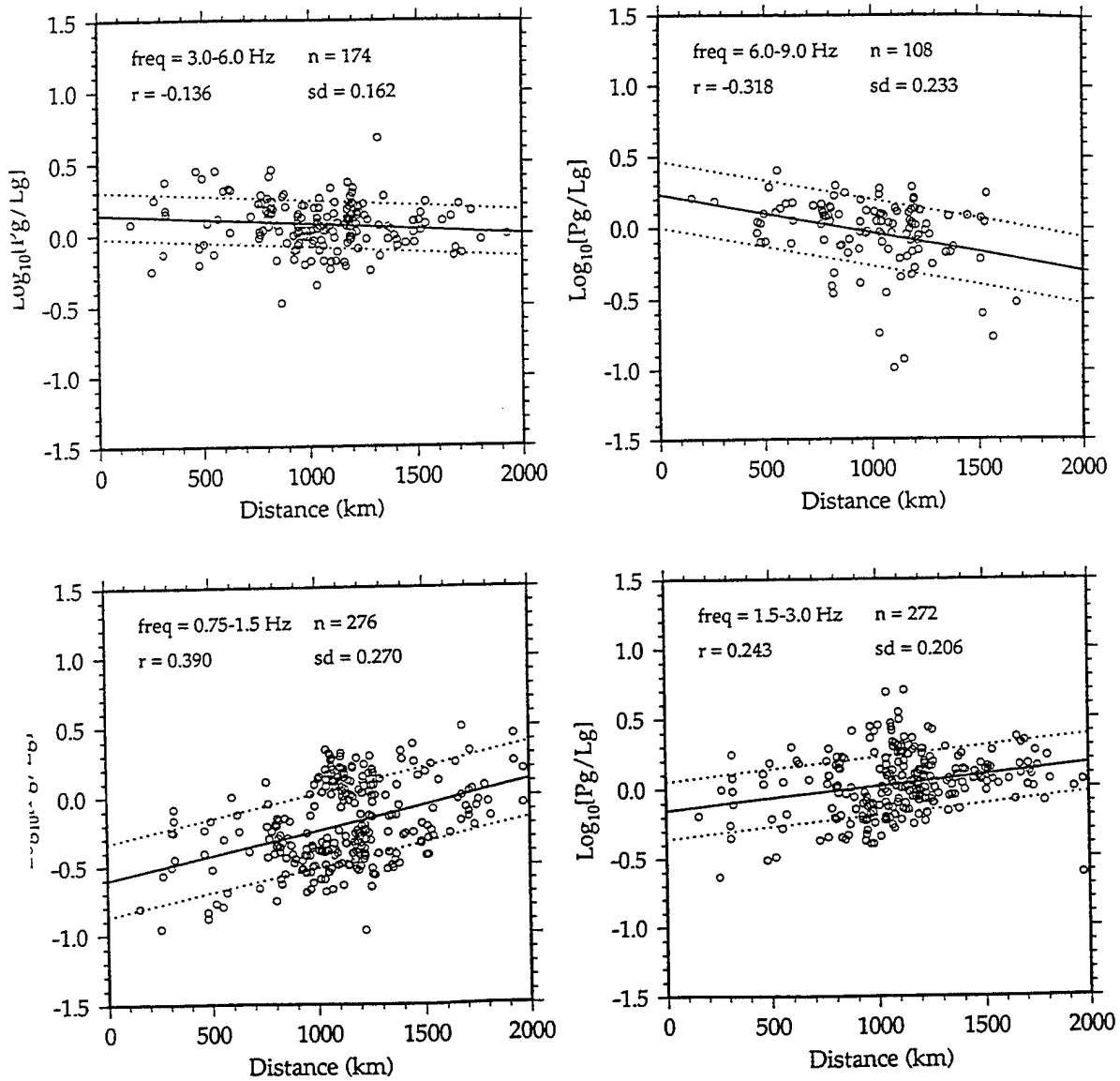


**Figure 5.** Univariate regression of the Pg/Lg ratios (all four frequency bands) on distance. Fit statistics shown in each panel are: n number of data; r linear correlation, sd standard error about regression. The solid and dashed lines are the regression fit and standard error about the fit, respectively.

# ABKT Pg/Lg vs. Mean Elevation

Log<sub>10</sub>-mean spectral amplitude ratio, Pn/pre-Pn noise > 2.0

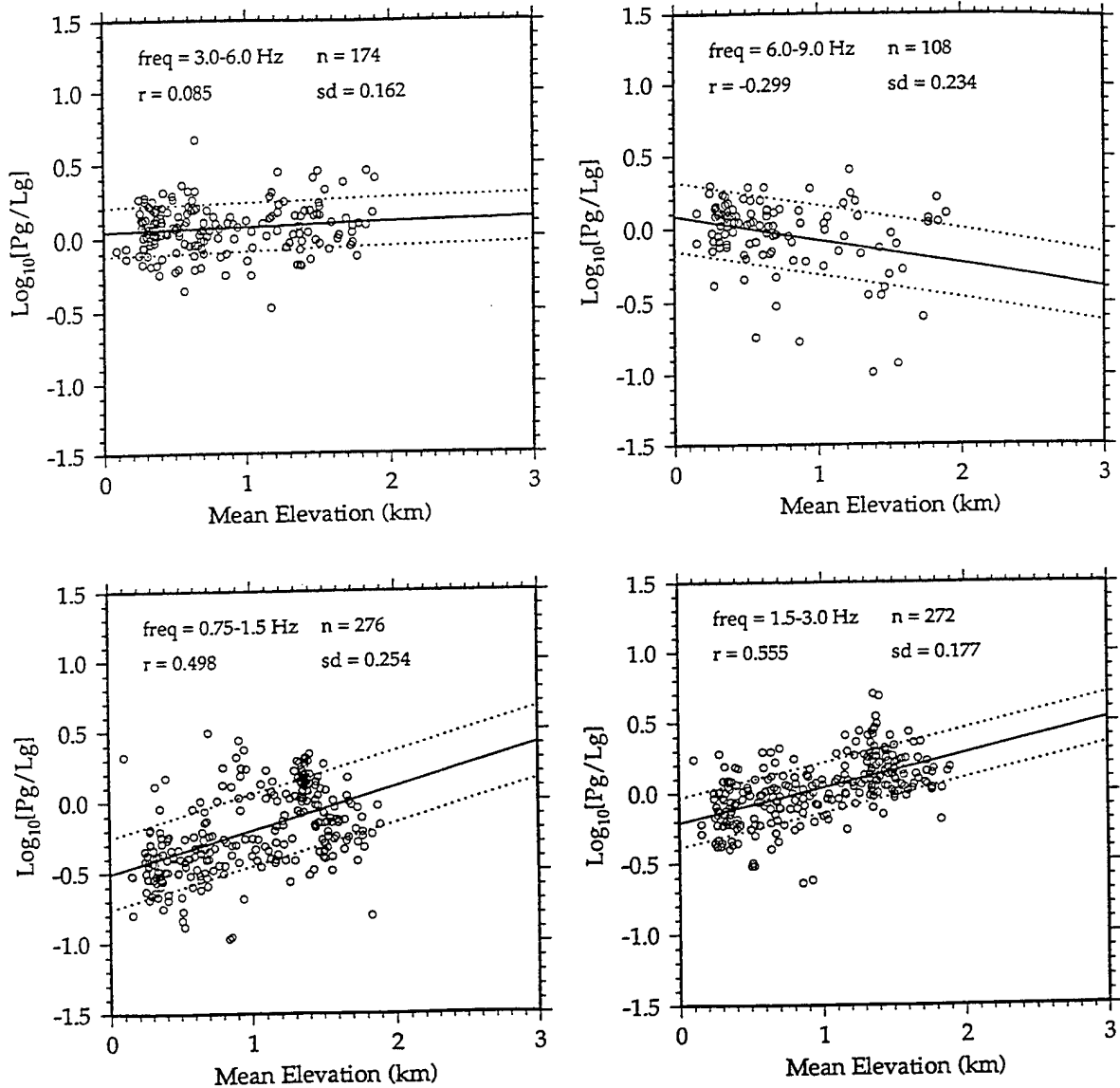


**Figure 6.** Univariate regression of the Pg/Lg ratios (all four frequency bands) on mean elevation, similar to Figure 5.

# ABKT Pg/Lg vs. Rms Elevation

$\text{Log}_{10}$ -mean spectral amplitude ratio, Pn/pre-Pn noise > 2.0

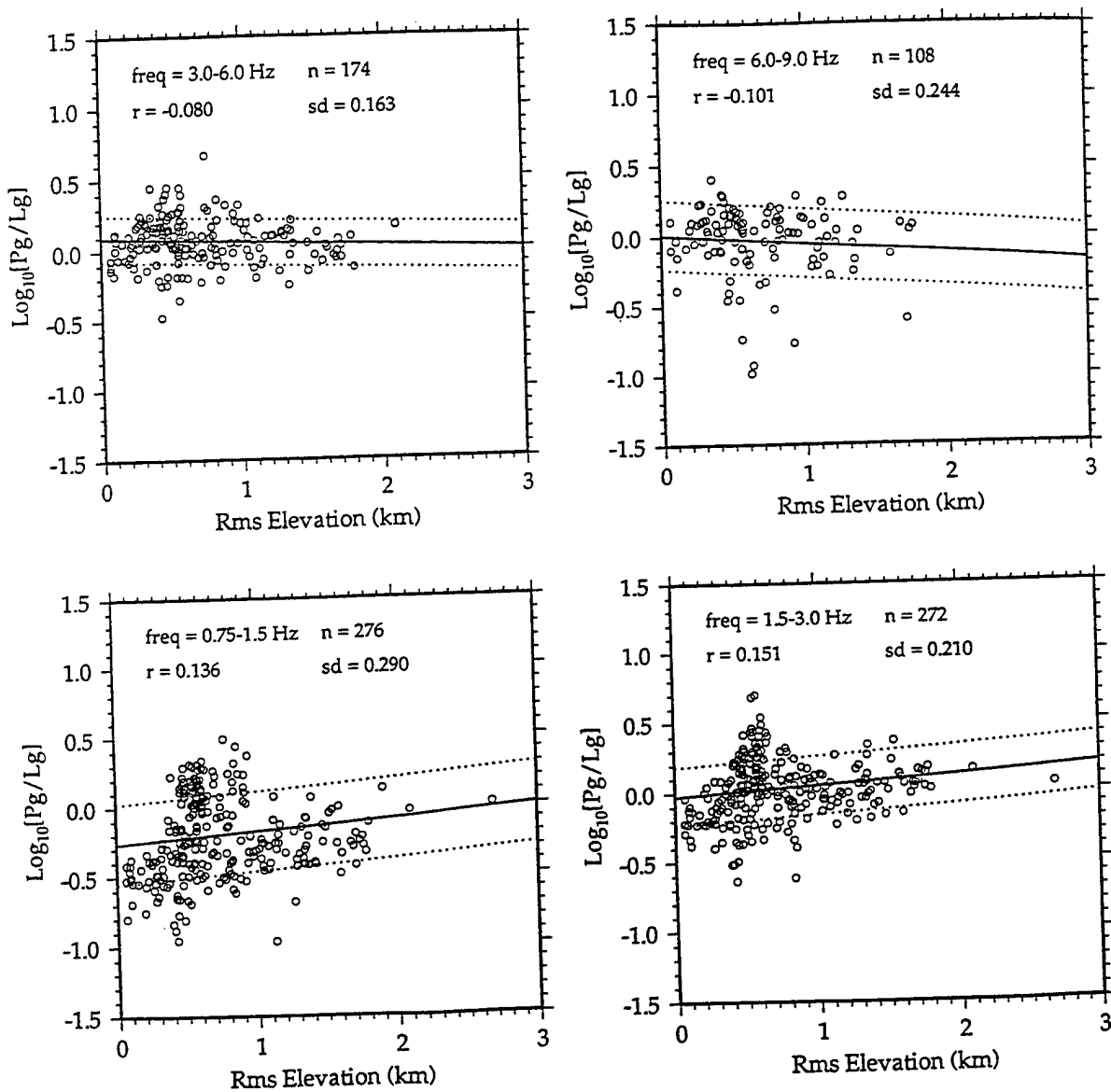


Figure 7. Univariate regression of the Pg/Lg ratios on rms elevation, similar to Figure 5.

# ABKT Pg/Lg vs. Mean Moho

Log<sub>10</sub>-mean spectral amplitude ratio, Pn/pre-Pn noise > 2.0

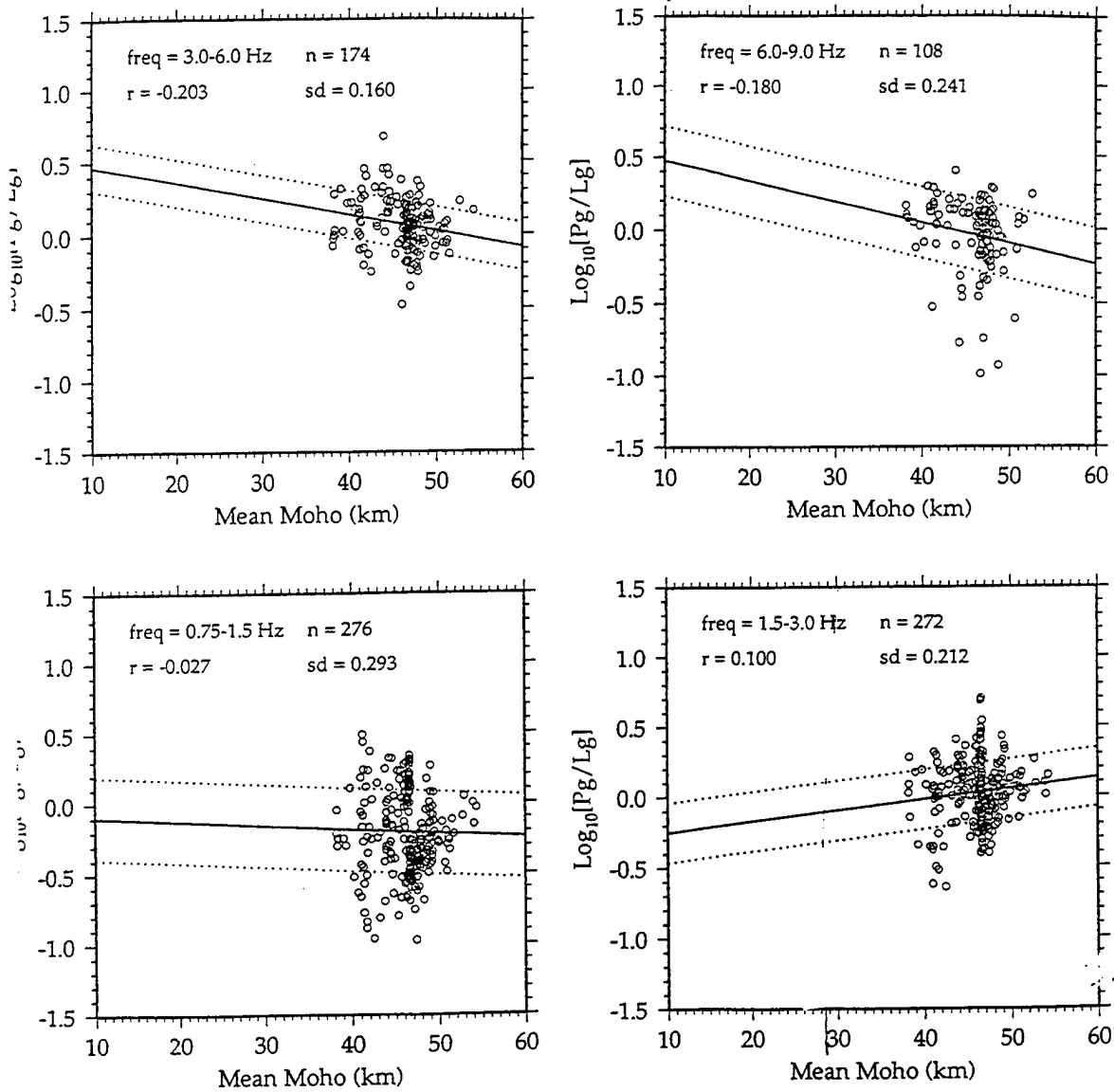


Figure 8. Univariate regression of the Pg/Lg ratios on mean crustal thickness, similar to Figure 5.

# ABKT Pg/Lg vs. Mean Basement

$\text{Log}_{10}$ -mean spectral amplitude ratio, Pn/pre-Pn noise > 2.0

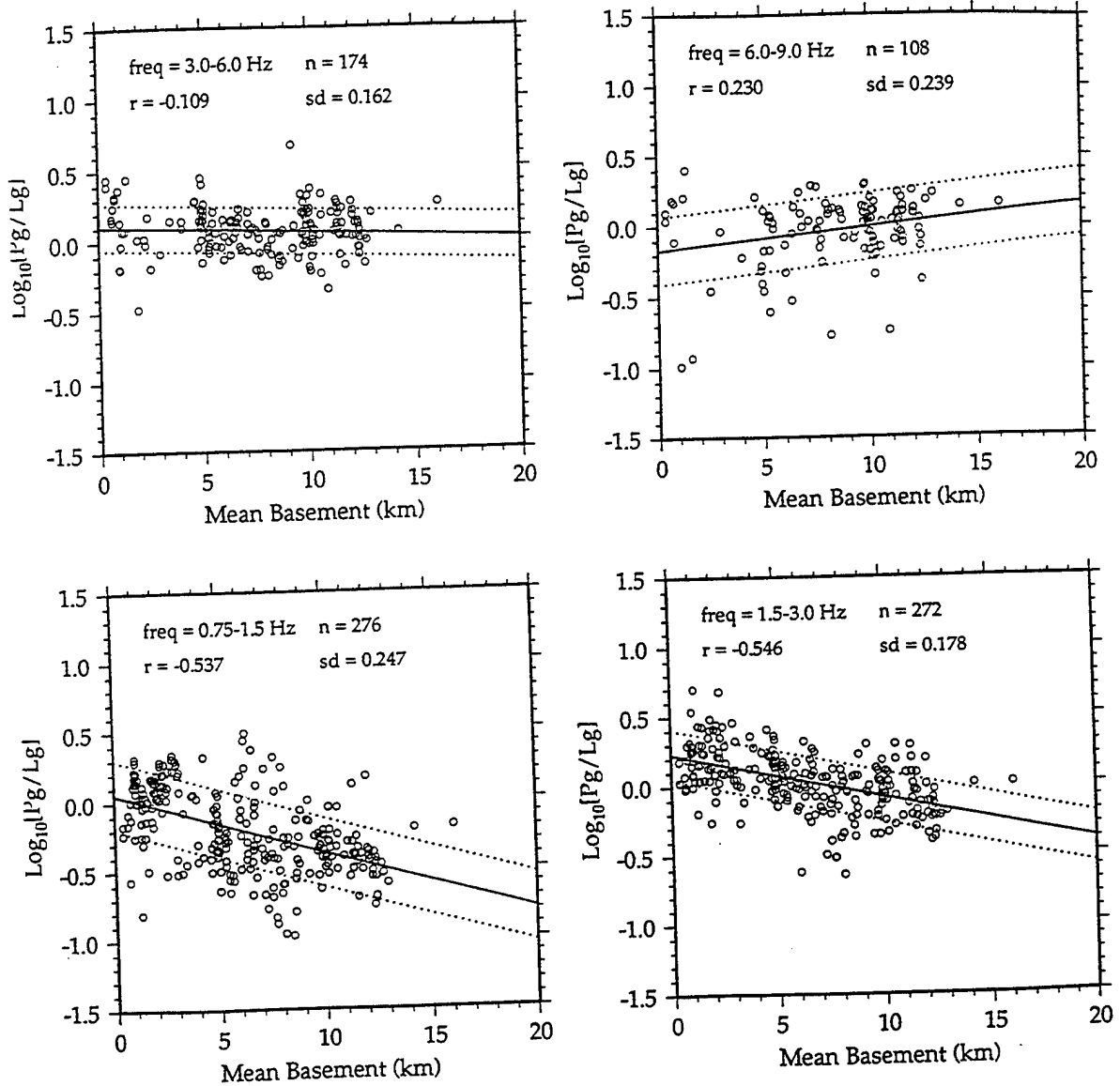


Figure 9. Univariate regression of the Pg/Lg ratios on mean sediment thickness, similar to Figure 5.



and mean basement depth are most strongly correlated with the low frequency Pg/Lg ratios. It is interesting to note that mean elevation and mean basement depth are better predictors of the low frequency Pg/Lg ratios than distance. Similar behavior was observed for Pn/Lg, Pn/Sn and Pg/Sn. These figures show that the earthquake-ABKT paths sample wide ranges of distance (Figure 5), mean elevation (Figure 6), rms elevation (Figure 7) and mean basement depth (Figure 9), but sample relatively narrow range of mean crustal thickness (Figure 8).

### **Multivariate Regressions of P/S Ratios On Crustal Waveguide Parameters**

In order to develop models that further reduce the scatter in the regional P/S amplitude ratios, we computed multivariate regressions of P/S amplitude ratios on crustal waveguide parameters, similar to Zhang et al. (1996) and Fan and Lay (1997a, 1997b). This approach seeks to find the linear relationship between the observed data (the P/S ratios in a given frequency band) and a set of crustal waveguide parameters. We chose the set of parameters based largely on the univariate analysis presented above. Cases where path parameters are strongly correlated with each other (as shown in Table 5) suggest that there exists redundancy in crustal waveguide information, as parameterized by our measures. For example, mean elevation and rms slope of elevation should not be included together in the multivariate analysis as their strong covariance destabilizes the multiple regression. Similarly, we exclude maximum basement depth and maximum Moho depth due to correlations with respective mean values. Maximum and minimum values are also point-wise properties that may not be well constrained by our crustal databases.

Similar to Fan and Lay (1997a, 1997b) we used the following set of predictor variables for the multivariate path parameter analysis:  $x_1$ , distance (Dist);  $x_2$ , mean elevation

(mH);  $x_3$  rms elevation (rmsH);  $x_4$  mean crustal thickness (mM);  $x_5$  mean sediment thickness (mS). Each individual P/S ratio,  $y_i$ , is represented by the form:

$$y_i = b_1 x_{i1} + b_2 x_{i2} + b_3 x_{i3} + b_4 x_{i4} + b_5 x_{i5} + b_6 + e_i \quad i = 1, 2, 3, \dots, n ;$$

where the  $b_j$  are the regression coefficients and  $e_i$  is the random error associated with the  $i$ <sup>th</sup> data. A constant term,  $b_6$ , is included in each regression model. The coefficients,  $b_j$ , are found by setting up the  $n$  equations of condition for the entire data set (all  $\log_{10}[\text{P/S}]$  measurements in a given frequency band) and solving the system by generalized inverse. Regression coefficients and formal uncertainties are found for each combination of the five path parameters (including all pairs, triplets, quadruplets and quintuplets) and the goodness-of-fit is determined. Predicted P/S ratios ( $Y_i$ ) are found by applying the regression results to each set of path parameters ( $x_{ij}$ ) with the above equation. By computing the regression coefficients for every possible model we could investigate the statistics of each solution and assess each model relative to other models.

Multivariate regression statistics for each model were computed and compiled. The data variance,  $s$ , was computed before and after the regression coefficients were estimated and the model predictions were removed. The coefficient of determination,  $R^2$ , was tabulated for each regression model.  $R^2$  measures the proportion of the data variance which is explained by the regression predictions and is simply the fractional variance reduction,  $Ds/\sigma$ . If  $R^2 = 1.0$ , then this indicates that the data variance is completely explained by the regression coefficients. The sum of the squared errors ( $SSE$ ) is computed as the sum of the squares of the  $n$  data values ( $y_i$ , the P/S ratios) minus the predictions from the regression results ( $Y_i$ ):

$$SSE = \sum_i (y_i - Y_i)^2 .$$

This was used to compute the mean squared error ( $MSE$ ):

$$MSE = SSE / (n - p) ;$$

where  $n$  is the number of data and  $p$  is the number of parameters used in a particular regression including the constant term. Finally, Mallows's  $C_p$  statistic was computed:

$$C_p = [ SSE_p / MSE_k ] - (n - 2p) ;$$

where  $SSE_p$  is the sum of the squared errors for the  $p$  predictor variables (including the constant term);  $MSE_k$  is the mean squared error for the complete set of  $k$  predictor variables ( $k=6$  in this case). Regression models for which  $C_p$  is close to  $p$  (i.e. low values) are most desirable. For the case when all path parameters are included ( $p=6$ )  $C_p$  is identically equal to  $p$ . Partial F-tests were performed on all model coefficients to investigate the null hypothesis that one of the coefficients is zero,  $b_j = 0.0$ . For the cases where  $F(b_j = 0.0) > F(0.95, 1, n-p)$ , the null hypothesis can be rejected at the 95% confidence level and the parameter is important to include in the model.

### Multivariate Regression Results

Multivariate regression coefficients and formal uncertainties for all 32 models of the Pg/Lg ratios in the 0.75-1.5 Hz frequency band are compiled in Table 6. Goodness-of-fit statistics for these models are compiled in Table 7. The best two-parameter model involves distance and mean sediment thickness, as measured by the largest variance reduction,  $R^2$ , minimum SSE and minimum  $C_p$  in Table 7. Both parameters have relatively small formal uncertainties (Table 6) and pass the partial F-test at or higher than the 99% confidence interval. Including both distance and mean sediment thickness reduces the variance of the Pg/Lg ratios in the 0.75-1.5 Hz band by 41.4%, much more than for distance or sediment thickness alone (15.2% and 28.9%, respectively). This two-predictor variable model

Table 6.

**Pg/Lg 0.75-1.5 Hz ABKT - Multivariate Regression Parameters**

number of data: 276

$b_1$ Dist	$b_2$ mH	$b_3$ rmsH	$b_4$ mM	$b_5$ mS	$b_6$ const.
- (-)	- (-)	- (-)	- (-)	- (-)	-0.2014 (0.0602)
0.0004 (0.0002)	- (-)	- (-)	- (-)	- (-)	-0.6018 (0.2192)
- (-)	0.3037 (0.1252)	- (-)	- (-)	- (-)	-0.5059 (0.1392)
- (-)	- (-)	0.0900 (0.1358)	- (-)	- (-)	-0.2679 (0.1170)
- (-)	- (-)	- (-)	-0.0028 (0.0220)	- (-)	-0.0697 (1.0185)
- (-)	- (-)	- (-)	- (-)	-0.0424 (0.0162)	0.0541 (0.1149)
0.0003 (0.0002)	0.2651 (0.1282)	- (-)	- (-)	- (-)	-0.7725 (0.2342)
0.0004 (0.0002)	- (-)	-0.0767 (0.1632)	- (-)	- (-)	-0.6112 (0.2201)
0.0005 (0.0002)	- (-)	- (-)	-0.0271 (0.0246)	- (-)	0.5344 (1.0552)
0.0003 (0.0002)	- (-)	- (-)	- (-)	-0.0404 (0.0163)	-0.3218 (0.2464)
- (-)	0.3095 (0.1324)	-0.0192 (0.1436)	- (-)	- (-)	-0.4974 (0.1528)
- (-)	0.3497 (0.1332)	- (-)	-0.0237 (0.0234)	- (-)	0.5461 (1.0452)
- (-)	0.1206 (0.2044)	- (-)	- (-)	-0.0300 (0.0265)	-0.1413 (0.3506)
- (-)	- (-)	0.1234 (0.1524)	-0.0119 (0.0247)	- (-)	0.2582 (1.0961)
- (-)	- (-)	0.0621 (0.1362)	- (-)	-0.0418 (0.0163)	0.0047 (0.1580)
- (-)	- (-)	- (-)	-0.0055 (0.0220)	-0.0425 (0.0162)	0.3102 (1.0288)
0.0004 (0.0002)	0.3000 (0.1325)	-0.1741 (0.1688)	- (-)	- (-)	-0.8162 (0.2380)
0.0004 (0.0002)	0.3306 (0.1335)	- (-)	-0.0449 (0.0256)	- (-)	1.0676 (1.0769)
0.0003 (0.0002)	0.0312 (0.2117)	- (-)	- (-)	-0.0373 (0.0269)	-0.3637 (0.3763)
0.0005 (0.0002)	- (-)	-0.0296 (0.1698)	-0.0259 (0.0256)	- (-)	0.4794 (1.1014)
0.0004 (0.0002)	- (-)	- (-)	-0.0282 (0.0246)	-0.0408 (0.0163)	0.8612 (1.0632)
0.0004 (0.0002)	- (-)	-0.0974 (0.1634)	- (-)	-0.0409 (0.0163)	-0.3303 (0.2469)
- (-)	0.3420 (0.1360)	0.0435 (0.1557)	-0.0265 (0.0253)	- (-)	0.6480 (1.1070)
- (-)	0.0988 (0.2264)	0.0338 (0.1509)	- (-)	-0.0319 (0.0278)	-0.1329 (0.3526)
- (-)	0.1938 (0.2355)	- (-)	-0.0159 (0.0254)	-0.0230 (0.0287)	0.4774 (1.0487)
- (-)	- (-)	0.0974 (0.1527)	-0.0126 (0.0247)	-0.0419 (0.0163)	0.5630 (1.1025)
0.0005 (0.0002)	0.3480 (0.1361)	-0.1149 (0.1730)	-0.0411 (0.0263)	- (-)	0.8819 (1.1126)
0.0004 (0.0002)	0.0870 (0.2265)	-0.1213 (0.1749)	- (-)	-0.0322 (0.0278)	-0.4494 (0.3961)
0.0004 (0.0002)	0.1709 (0.2358)	- (-)	-0.0369 (0.0274)	-0.0236 (0.0287)	0.9993 (1.0801)
0.0005 (0.0002)	- (-)	-0.0498 (0.1700)	-0.0261 (0.0256)	-0.0410 (0.0163)	0.7704 (1.1075)
- (-)	0.1657 (0.2443)	0.0689 (0.1584)	-0.0194 (0.0266)	-0.0254 (0.0292)	0.6320 (1.1072)
0.0005 (0.0002)	0.2049 (0.2450)	-0.0900 (0.1766)	-0.0349 (0.0277)	-0.0206 (0.0293)	0.8626 (1.1130)

Table 7.

## Pg/Lg 0.75-1.5 Hz ABKT. - Multivariate Regression Statistics

number of data: 276

Predictor Variables						Regression Statistics			
$b_1$ Dist	$b_2$ mH	$b_3$ rmsH	$b_4$ mM	$b_5$ mS	$b_6$ const.	$\sigma$	$R^2$	SSE	$C_p$
0	0	0	0	0	1	0.0861	0.0000	23.68	268.05
1	0	0	0	0	1	0.0730	0.1524	20.07	187.46
0	1	0	0	0	1	0.0647	0.2484	17.80	135.39
0	0	1	0	0	1	0.0845	0.0185	23.24	260.00
0	0	0	1	0	1	0.0860	0.0007	23.66	269.66
0	0	0	0	1	1	0.0613	0.2879	16.86	113.99
1	1	0	0	0	1	0.0574	0.3330	15.79	91.53
1	0	1	0	0	1	0.0722	0.1617	19.85	184.40
1	0	0	1	0	1	0.0686	0.2035	18.86	161.72
1	0	0	0	1	1	0.0505	0.4135	13.89	47.92
0	1	1	0	0	1	0.0647	0.2492	17.78	136.98
0	1	0	1	0	1	0.0610	0.2920	16.77	113.79
0	1	0	0	1	1	0.0600	0.3026	16.51	108.02
0	0	1	1	0	1	0.0837	0.0284	23.01	256.66
0	0	1	0	1	1	0.0606	0.2967	16.65	111.23
0	0	0	1	1	1	0.0611	0.2906	16.80	114.55
1	1	1	0	0	1	0.0536	0.3780	14.73	69.17
1	1	0	1	0	1	0.0463	0.4624	12.73	23.38
1	1	0	0	1	1	0.0504	0.4144	13.87	49.43
1	0	1	1	0	1	0.0685	0.2048	18.83	163.03
1	0	0	1	1	1	0.0457	0.4687	12.58	19.97
1	0	1	0	1	1	0.0492	0.4285	13.53	41.80
0	1	1	1	0	1	0.0607	0.2953	16.69	114.00
0	1	1	0	1	1	0.0599	0.3047	16.46	108.87
0	1	0	1	1	1	0.0586	0.3192	16.12	101.04
0	0	1	1	1	1	0.0596	0.3077	16.39	107.24
1	1	1	1	0	1	0.0447	0.4811	12.29	15.29
1	1	1	0	1	1	0.0487	0.4347	13.39	40.42
1	1	0	1	1	1	0.0438	0.4909	12.05	9.94
1	0	1	1	1	1	0.0454	0.4724	12.49	20.01
0	1	1	1	1	1	0.0579	0.3272	15.93	98.71
1	1	1	1	1	1	0.0429	0.5019	11.79	6.00

(distance, mean sediment depth and a constant) performed the best for the Pn/Lg, Pg/Lg and Pn/Sn ratios in the 0.75-1.5 Hz pass bands and the Pg/Lg and Pn/Sn ratios in the 1.5-3.0 Hz band, as measured by variance reduction,  $R^2$ ,  $C_p$  and SSE for models whose regression coefficients pass the partial F-test at or greater than the 95% confidence level. When three parameters are considered, the best-fitting model involves: distance, mean Moho depth and mean basement depth, and the variance reduction increases to 46.9%. The best-fitting four parameter model adds mean elevation to the previous parameter set, but only increases the variance reduction by a few percent (to 49.1%). When rms elevation is added to this set (all five predictor variables included in the model) the variance reduction is increased by slightly more than 1% (to 50.2%). All five predictor variables pass the partial F-test when included, but rms elevation is the least significant parameter. This is consistent with the large formal uncertainties for rms elevation ( $b_3$ , rmsH in Table 6).

Best-fitting multivariate models (path parameter combinations) along with each associated variance reduction are compiled for the low frequency P/S ratios in Table 8. Only models for which each regression coefficient,  $b_i$ , passes the partial F-test at greater than or equal to the 95% confidence interval are included. Formal uncertainties for each regression coefficient are typically smaller for the best-fitting models which pass the partial F-tests relative to those models which do not perform as well or fail the partial F-test. Distance and mean sediment thickness are usually the best predictors of the low frequency Pn/Lg, Pg/Lg and Pn/Sn amplitude ratios. These two path parameters can account for 34-47% of the total uncorrected data variance of the Pn/Lg, Pg/Lg and Pn/Sn ratios. Mean elevation and mean Moho depth appear to be only moderately successful at predicting Pn/Lg, Pg/Lg and Pn/Sn behavior. Pg/Sn ratios are strongly correlated with mean sediment depth. This parameter alone accounts for 36.9% and 50.2% of the variance for the 0.75-1.5 Hz and 1.5-3.0 Hz ratios, respectively. Perhaps this correlation is due to the fact that many Zagros paths to ABKT have little or no Sn energy (Rodgers et al., 1997). If

Table 8.

**ABKT Best-Fitting Multivariate Regression Models**

These models pass the partial F-test ( $F(b_j=0)$ ) for each parameter at greater than or equal to the 95% confidence level. Freq= frequency band; m= number of predictor variables in each model.

Data & Model Ratio Freq m	Predictor Variables					$\Delta\sigma(\%)$
	$b_1$ Dist	$b_2$ mH	$b_3$ rmsH	$b_4$ mM	$b_5$ mS	
Pn/Lg 0.75-1.5 Hz m=1	x	-	-	-	-	28.3
Pn/Lg 0.75-1.5 Hz m=2	x	-	-	-	x	46.3
Pn/Lg 0.75-1.5 Hz m=3	x	x	-	x	-	52.9
Pn/Lg 0.75-1.5 Hz m=4	x	x	-	x	x	54.6
Pn/Lg 1.5-3.0 Hz m=1	x	-	-	-	-	18.7
Pn/Lg 1.5-3.0 Hz m=2	x	x	-	-	-	30.2
Pn/Lg 1.5-3.0 Hz m=3	x	x	-	x	-	32.9
Pn/Lg 1.5-3.0 Hz m=4	x	x	x	-	x	33.3
Pg/Lg 0.75-1.5 Hz m=1	-	-	-	-	x	28.8
Pg/Lg 0.75-1.5 Hz m=2	x	-	-	-	x	41.4
Pg/Lg 0.75-1.5 Hz m=3	x	-	-	x	x	46.9
Pg/Lg 0.75-1.5 Hz m=4	x	x	-	x	x	49.1
Pg/Lg 1.5-3.0 Hz m=1	-	x	-	-	-	30.8
Pg/Lg 1.5-3.0 Hz m=2	x	-	-	-	x	33.8
Pg/Lg 1.5-3.0 Hz m=3	x	x	-	-	x	36.3
Pg/Lg 1.5-3.0 Hz m=4	x	x	-	x	x	37.2
Pn/Sn 0.75-1.5 Hz m=1	-	-	-	-	x	30.7
Pn/Sn 0.75-1.5 Hz m=2	x	-	-	-	x	43.0
Pn/Sn 0.75-1.5 Hz m=3	x	-	-	x	x	51.7
Pn/Sn 0.75-1.5 Hz m=4	x	-	x	x	x	52.9
Pn/Sn 1.5-3.0 Hz m=1	-	-	-	-	x	34.3
Pn/Sn 1.5-3.0 Hz m=2	x	-	-	-	x	38.7
Pn/Sn 1.5-3.0 Hz m=3	x	-	-	x	x	47.1
Pn/Sn 1.5-3.0 Hz m=4	x	-	x	x	x	48.9
Pg/Sn 0.75-1.5 Hz m=1	-	-	-	-	x	36.9
Pg/Sn 0.75-1.5 Hz m=2	-	-	-	x	x	41.7
Pg/Sn 0.75-1.5 Hz m=3	x	-	-	x	x	43.6
Pg/Sn 0.75-1.5 Hz m=4	x	-	x	x	x	47.2
Pg/Sn 1.5-3.0 Hz m=1	-	-	-	-	x	50.2
Pg/Sn 1.5-3.0 Hz m=2	-	-	-	x	x	57.7
Pg/Sn 1.5-3.0 Hz m=3	x	-	-	x	x	58.4
Pg/Sn 1.5-3.0 Hz m=4	x	-	x	x	x	61.3

no Sn energy is present, then the Pg/Sn ratio is measuring Pg/Pg-coda, which should be related to crustal attenuation and scattering. The Pg/Sn amplitude ratios are well represented by a univariate model with mean sediment thickness and a two predictor variable model of mean Moho and mean sediment thickness. Distance is not a particularly important factor influencing the Pg/Sn ratios. Rms elevation is a very poor predictor of P/S amplitude ratio behavior - it only enters into models with four or more predictor variables. This was also observed in some cases by Fan and Lay (1997a).

## Discussion and Conclusions

Short-period regional P/S amplitude ratios will be valuable for monitoring the Comprehensive Test Ban Treaty at low magnitudes. However, the scatter in P/S ratios due to propagation effects must be accounted for before P/S ratios can be used to characterize events of unknown source. The exact form by which P/S ratio behavior is represented is not clear. In this report, we present a technique for representing regional earthquake P/S behavior. A large part (30-60%) of the scatter in regional P/S amplitude ratios below 3.0 Hz can be reduced using simple linear models of parameterized along-path crustal waveguide structure. The best-fitting univariate regression models identify distance and mean sediment thickness as the most important properties influencing the P/S ratios. The best-fitting two parameter models feature distance and mean sediment thickness for Pn/Lg, Pg/Lg and Pn/Sn and mean sediment thickness and mean crustal thickness for Pg/Sn. The fact that similar results for Pn/Lg were found by Baumgardt and Schneider (1997) using different data and slightly different techniques is encouraging. This may indicate that, at least for the Iranian Plateau, distance and mean sediment thickness are the main factors influencing the regional wavefield. Models involving more parameters do not significantly increase the variance reduction beyond what can be achieved with a one or two predictor variable model. It is odd that mean sediment thickness should play a role in controlling the



Pn/Sn amplitude ratio behavior, as these phases propagate for the most part in the shallow mantle. It is easy to imagine that shallow waveguide structure (e.g. topography and basin structure) could influence the Pg and Lg amplitudes through Rg scattering and P-S conversion. Perhaps shallow crustal and basement structure affects the Pn and Sn phases near the source and station, similar to a site effect. The remaining scatter in P/S ratios after propagation effects are removed could be due in part to source depth and/or radiation pattern effects. These effects are impossible to assess with our data set because focal depths and mechanisms are either poorly constrained or completely unconstrained.

Our results differ slightly from those of Fan and Lay (1997a) in that mean crustal thickness is not a major controlling factor on the P/S ratios observed at ABKT. However, as we pointed out earlier, the paths we consider do not sample a wide range of mean Moho depths (40-50 km, Figure 8), whereas the paths Fan and Lay (1997a) considered for WMQ in western China sampled a larger range of crustal thickness (45-60 km). Conversely, the data observed at ABKT sample a wide range of sediment thicknesses (0-15 km, Figure 9), whereas the data analyzed by Fan and Lay (1997a) sample a smaller range (0-8 km). These considerations suggest that each region must be characterized separately and there may be no transportability of regional path corrections. Ideally, we would like to find the most important crustal waveguide parameters that represent the P/S ratios in one region and then apply them to another, somewhat similar region. Scatter in low frequency regional P/S amplitude ratios can clearly be reduced by empirical regressions, although the procedure may have to be applied to each monitoring station separately. The fact that results for western China (Fan and Lay, 1997a, 1997b) differ from the results presented here may indicate that the path specific parameterization is not identifying the factors which truly control the P/S ratios. The reductions in P/S scatter may result because the path specific parameters are surrogates for the true controlling factors. For example, the path parameters we employ are independent of propagation direction. Numerous studies have shown that a

thinning of the crust (necking) strongly weakens short-period Lg amplitudes (e.g. Kennett, 1986; Zhang and Lay, 1995). Path parameters such as mean crustal thickness cannot characterize Moho topography and the current models of the crustal waveguide do not likely represent crustal waveguide roughness to sufficient accuracy to yield meaningful results.

The fact that certain waveguide properties are better predictors of P/S behavior than distance alone supports the azimuthal sector regionalization strategy presented in Rodgers et al. (1997c). That study reports that P/S amplitude behavior is much better characterized by azimuth-dependent distance corrections (data are subdivided into azimuthal sectors based on tectonic character) rather than by a single azimuth-independent distance correction. The paths coming into ABKT from different azimuths sample different topographic, sediment and crustal structures causing variations in the P/S ratios that are greater than what can be accounted for by an azimuth-independent distance effect. The use of a single distance correction for a region implicitly assumes that the propagation effects are common for all paths in the region. Azimuthal sectorization forms a discrete spatial parameterization of the data set. However, the choice of sector boundaries is not unambiguous. The sector representation may lead to complications when an event is located near a sector boundary. An advantage of the path specific parameterization given here is that it is a continuous representation, to the extent that models of the crustal waveguide are accurate. Yet another approach to represent the behavior of regional amplitudes is to spatially average the observed P/S ratios projected to their source location. Median filtering (e.g. Phillips et al., 1997) and kriging (e.g. Schultz et al., 1997) are possible strategies to generate regional phase amplitude correction surfaces. In this approach, observed amplitudes are spatially averaged and/or smoothed on some appropriate scale length to form a correction surface from which corrections for new events are generated. Spatial averaging does not necessarily require a choice of sector or region boundaries and can be broadly considered

as a continuous parameterization like the crustal waveguide path parameterization presented in this article. Important decisions such as the extent of spatial smoothing must be made for surface fitting strategies. We are currently investigating spatial averaging approaches with the ABKT data set.

The path correction strategies presented here consistently reduce the scatter in the low frequency ( $< 3.0$  Hz) P/S amplitude ratios, while not significantly reducing the scatter in the higher frequencies in a consistent fashion. Similar results were reported by Fan and Lay (1997a, 1997b) and Rodgers et al. (1997c). Many studies have reported that higher frequency P/S ratios discriminate better than lower frequency P/S ratios (e.g. Walter et al., 1995; Taylor, 1996). However, strong lithospheric attenuation can significantly reduce the signal-to-noise in the higher frequency bands for the smaller events ( $m_b < 4.5$ ) at distances of 500 km or more that are of particular concern to the CTBT monitoring effort. It is possible that for such events there will not be sufficient signal-to-noise to measure P/S ratios at frequencies above 3.0 Hz. Thus, if the strategies presented here can reduce the scatter in the low frequency P/S ratios they may enhance discrimination capabilities. Unfortunately, we cannot ensure that reducing the scatter in low frequency P/S ratios will improve discrimination. We have included all paths for which the Pn signal-to-noise is greater than 2.0. It is certainly possible that we have included paths for which Sn or Lg are weak or blocked, given previous studies of regional phase behavior (Kadinsky-Cade, et al., 1981; Rodgers et al., 1997a). The P/S ratios show a continuous distribution, suggesting that blockage cannot be easily identified by a maximum P/S ratio. However, if blockage and/or attenuation is complete, blocked paths cannot be used for source discrimination. The wide variation in P/S ratios probably make it easier to establish linear correlations with crustal waveguide parameters. If paths with weak or absent S-wave energy were discarded, then the variability would be reduced and the linear correlations with path parameters might not be as strong. The representations presented here certainly

describe the expected earthquake P/S behavior, including paths for which Sn or Lg is blocked. So at the very least, the analysis presented here helps us understand the regional phase propagation and predict the behavior of future earthquake P/S ratios recorded at ABKT.

Hartse et al. (1997b) found that univariate regression results improved discrimination of earthquakes and explosions when corrections for topographic roughness times distance and rms basement depth gradient times distance were applied to Pg/Lg ratios at WMQ. They did not find corrections that consistently improved discrimination at both stations AAK and WMQ, though the scatter was reduced. Many important issues regarding path corrections for regional P/S discriminants remain the subject of continuing research efforts. Research questions to be addressed include: How can earthquakes and explosions be discriminated along paths with S-wave blockage and/or attenuation? Can universally transportable path corrections and discriminants be developed or does short-period regional P/S discrimination need to be investigated at every station separately? Future efforts will be directed at obtaining explosion data to test path correction strategies and discrimination at ABKT and seeking out the most important crustal waveguide effects for other monitoring stations in the Middle East and North Africa.

### **Acknowledgments**

Raw waveform data were obtained from the Incorporated Research Institutions for Seismology-Data Management Center (IRIS-DMC). Data were processed using the Datascope3.0 Seismic Application Package, developed by the University of Colorado, IRIS-Joint Seismic Project Center and SAC2000 developed by the Lawrence Livermore National Laboratory. Figures were made using the GMT3.0 software package (Wessel and Smith, 1991). We are grateful to Dogan Seeber and Mauwia Barazangi of Cornell University for providing the Former Soviet Union Institute of Physics of the Earth

basement and Moho depth models. Research was performed under the auspices of the U.S. Department of Energy by the Lawrence Livermore National Laboratory under contract W-7405-ENG-48. This research was supported in part by Phillips Laboratory Contract Number F19628-95-K-0014. Contribution number 343 University of California Santa Cruz Institute of Tectonics.

## References

- Barazangi, M., E. Fielding, B. Isaks and D. Seeber (1996). Geophysical and geological databases and CTBT monitoring: A case study of the Middle East, in *Monitoring a Comprehensive Test Ban Treaty*, E. Husebye and A. Dainty (Editors), Academic Publishers, Dordrecht, 197-224.
- Baumgardt, D. (1990). Investigation of teleseismic Lg blockage and scattering using regional arrays, *Bull. Seism. Soc. Am.*, **80**, 2261-2281.
- Baumgardt, D. (1996). Investigation of Lg blockage and the transportability of regional discriminants in the Middle East, Scientific Report No.1, PL-TR-96-2294, 11 November 1996, ENSCO Inc., Springfield VA. ADA323818
- Baumgardt, D. and C. Schneider (1997). Multivariate canonical correlations of P/S ratios and propagation path parameters for Iran, *Proceedings of the 19th Annual Seismic Research Symposium on Monitoring a Comprehensive Test Ban Treaty*, 23-25 September 1997, Defense Special Weapons Agency Report, 14-23.
- Bennett, T., and J. Murphy (1986). Analysis of seismic discrimination capabilities using regional data from western United States events, *Bull. Seism. Soc. Am.*, **76**, 1069-1086.
- Blandford, R. (1981). Seismic discrimination problems at regional distances, in *Identification of Seismic Sources-Earthquake or Explosion*, E. Husebye and S. Mykkeltveit (Editors), Reidel, Boston, 695-740.

- Fan, G. and T. Lay (1997a). Statistical analysis of irregular waveguide influences on regional seismic discriminants in China, in press *Bull. Seism. Soc. Am.*
- Fan, G. and T. Lay (1997b). Multivariate analysis of waveguide effects on regional seismic phases in western China, submitted to *Seismo. Res. Lett.*
- Fielding, E., B. Isacks, and M. Barazangi (1992). A geological and geophysical information system for Eurasia, Tech Report No. 2, F29601-91-K-DB08, Phillips Laboratory, Hanscom Air Force Base, MA.
- Hartse, H., S. Taylor, S. Phillips and G. Randall (1997a). A preliminary study of regional seismic discrimination in Central Asia with emphasis on western China, *Bull. Seism. Soc. Am.*, **87**, 551-568.
- Hartse, H., R. Flores and P. Johnson (1997b). Correcting regional seismic discriminants for path effects in western China, submitted to *Bull. Seism. Soc. Am.*
- Hearn, T. and J. Ni (1994). Pn velocities beneath continental collision zones: the Turkish-Iranian Plateau, *Geophys. J. Int.*, **117**, 273-283.
- Kadinsky-Cade, K., M. Barazangi, J. Oliver and B. Issacks (1981). Lateral variations of high-frequency seismic wave propagation at regional distances across the Turkish and Iranian Plateaus, *J. Geophys. Res.*, **86**, 9377-9396.
- Kennett, B. (1986). Lg waves at structural boundaries, *Bull. Seism. Soc. Am.*, **80**, 1133-1141.
- Kunin, N. (1987). Distribution of sedimentary basins of Eurasia and the volume of the Earth's sedimentosphere, *Int. Geol. Rev.*, **22**, 1257-64.
- Kunin, N. and E. Sheykh-Zade (1983). New data on lateral inhomogeneities in the upper mantle under western Eurasia, *Dokl. Akad. Nauk. USSR*, **273**, 1087-1091.
- National Research Council (1997). Research required to support comprehensive nuclear test ban treaty monitoring, National Academy Press, Washington, D.C., 138pp.
- Phillips, S., G. Randall, H. Hartse, S. Taylor and H. Patton (1997). Source and path effects on regional phases in China, Proceedings of the 19th Annual Seismic Research

- Symposium on Monitoring a Comprehensive Test Ban Treaty, 23-25 September 1997, Defense Special Weapons Agency Report, 125-134.
- Pomeroy, P., J. Best and T. McEvilly (1982). Test ban treaty verification with regional data - a review. *Bull. Seism. Soc. Am.*, **72**, S89-S129.
- Rodgers, A., J. Ni and T. Hearn (1997a). Propagation characteristics of short-period Sn and Lg in the Middle East, *Bull. Seism. Soc. Am.*, **87**, 396-413.
- Rodgers, A., T. Lay, W. Walter and K. Mayeda (1997b). Comparison of regional phase amplitude ratio measurement techniques, in press *Bull. Seism. Soc. Am.*
- Rodgers, A., W. Walter and T. Lay (1997c), Calibration of distance and path effects on regional P/S discriminants at station ABKT (Alibek, Turkmenistan): azimuthal sector regionalization, submitted to *Bull. Seism. Soc. Am.*
- Schultz, C, S. Meyers, S. Ruppert (1997). Event location in the Middle East and North Africa, Proceedings of the 19th Annual Seismic Research Symposium on Monitoring a Comprehensive Test Ban Treaty, 23-25 September 1997, Defense Special Weapons Agency Report, 291-300.
- Taylor, S., M. Denny, E. Vergino and R. Glasner (1989). Regional discrimination between NTS explosions and western U.S. earthquakes, *Bull. Seism. Soc. Am.*, **79**, 1142-1176.
- Taylor, S. (1996). Analysis of high-frequency Pg/Lg ratios from NTS explosions and western U.S. earthquakes, *Bull. Seism. Soc. Am.*, **86**, 1042-1053.
- Walter, W., K. Mayeda and H. Patton (1995). Phase and spectral ratio discrimination between NTS earthquakes and explosions. Part I: empirical observations, *Bull. Seism. Soc. Am.*, **85**, 1050-1067.
- Wessel, P. and W. Smith (1991). Free software helps map and display data, *EOS*, **72**, 445-446.
- Zhang, T.-R. and T. Lay (1994a). Analysis of short-period regional phase path effects associated with topography in Eurasia, *Bull. Seism. Soc. Am.*, **84**, 119-132.

- Zhang, T.-R. and T. Lay (1994b). Effects of crustal structure under the Barents and Kara Seas on short-period regional wave propagation for Novaya Zemlya explosions: empirical relations, *Bull. Seism. Soc. Am.*, **84**, 1132-1147.
- Zhang, T.-R., and T. Lay (1995). Why the Lg phase does not traverse oceanic crust, *Bull. Seism. Soc. Am.*, **85**, 1665-1678.
- Zhang, T.-R., S. Schwartz and T. Lay (1994). Multivariate analysis of waveguide effects on short-period regional wave propagation in Eurasia and its application in seismic discrimination, *J. Geophys. Res.*, **99**, 21,929-21,945.
- Zhang, T.-R., T. Lay, S. Schwartz and W. Walter (1996). Variation of regional seismic discriminants with surface topographic roughness in the western United States, *Bull. Seism. Soc. Am.*, **86**, 714-725.

**Affiliations:**

Lawrence Livermore National Laboratory, L-205, P.O. Box 808, Livermore, CA 94551  
(A.J.R. & W.R.W.)

University of California Santa Cruz, Institute of Tectonics and Earth Sciences Department,  
Santa Cruz, CA 95064 (T.L. & G.F.)



THOMAS AHRENS  
SEISMOLOGICAL LABORATORY 252-21  
CALIFORNIA INSTITUTE OF TECHNOLOGY  
PASADENA, CA 91125

AIR FORCE RESEARCH LABORATORY  
ATTN: VSOE  
29 RANDOLPH ROAD  
HANSCOM AFB, MA 01731-3010 (2 COPIES)

AIR FORCE RESEARCH LABORATORY  
ATTN: RESEARCH LIBRARY/TL  
5 WRIGHT STREET  
HANSCOM AFB, MA 01731-3004

AIR FORCE RESEARCH LABORATORY  
ATTN: AFRL/SUL  
3550 ABERDEEN AVE SE  
KIRTLAND AFB, NM 87117-5776 (2 COPIES)

RALPH ALEWINE  
NTPO  
1901 N. MOORE STREET, SUITE 609  
ARLINGTON, VA 22209

MUAWIA BARAZANGI  
INSTITUTE FOR THE STUDY OF THE CONTINENTS  
3126 SNEE HALL  
CORNELL UNIVERSITY  
ITHACA, NY 14853

T.G. BARKER  
MAXWELL TECHNOLOGIES  
8888 BALBOA AVE.  
SAN DIEGO, CA 92123-1506

DOUGLAS BAUMGARDT  
ENSCO INC.  
5400 PORT ROYAL ROAD  
SPRINGFIELD, VA 22151

THERON J. BENNETT  
MAXWELL TECHNOLOGIES  
11800 SUNRISE VALLEY DRIVE SUITE 1212  
RESTON, VA 22091

WILLIAM BENSON  
NAS/COS  
ROOM HA372  
2001 WISCONSIN AVE. NW  
WASHINGTON DC 20007

JONATHAN BERGER  
UNIVERSITY OF CA, SAN DIEGO  
SCRIPPS INSTITUTION OF OCEANOGRAPHY IGPP, 0225  
9500 GILMAN DRIVE  
LA JOLLA, CA 92093-0225

ROBERT BLANDFORD  
AFTAC  
1300 N. 17TH STREET  
SUITE 1450  
ARLINGTON, VA 22209-2308

LESLIE A. CASEY  
DEPT. OF ENERGY/NN-20  
1000 INDEPENDENCE AVE. SW  
WASHINGTON DC 20585-0420

CENTER FOR MONITORING RESEARCH  
ATTN: LIBRARIAN  
1300 N. 17th STREET, SUITE 1450  
ARLINGTON, VA 22209

ANTON DAINTY  
HQ DSWA/PMP  
6801 TELEGRAPH ROAD  
ALEXANDRIA, VA 22310-3398

CATHERINE DE GROOT-HEDLIN  
UNIVERSITY OF CALIFORNIA, SAN DIEGO  
INSTITUTE OF GEOPHYSICS AND PLANETARY PHYSICS  
8604 LA JOLLA SHORES DRIVE  
SAN DIEGO, CA 92093

DEFENSE TECHNICAL INFORMATION CENTER  
8725 JOHN J. KINGMAN ROAD  
FT BELVOIR, VA 22060-6218 (2 COPIES)

DIANE DOSER  
DEPARTMENT OF GEOLOGICAL SCIENCES  
THE UNIVERSITY OF TEXAS AT EL PASO  
EL PASO, TX 79968

MARK D. FISK  
MISSION RESEARCH CORPORATION  
735 STATE STREET  
P.O. DRAWER 719  
SANTA BARBARA, CA 93102-0719

LORI GRANT  
MULTIMAX, INC.  
311C FOREST AVE. SUITE 3  
PACIFIC GROVE, CA 93950

HENRY GRAY  
SMU STATISTICS DEPARTMENT  
P.O. BOX 750302  
DALLAS, TX 75275-0302

I. N. GUPTA  
MULTIMAX, INC.  
1441 MCCORMICK DRIVE  
LARGO, MD 20774

DAVID HARKRIDER  
BOSTON COLLEGE  
INSTITUTE FOR SPACE RESEARCH  
140 COMMONWEALTH AVENUE  
CHESTNUT HILL, MA 02167

THOMAS HEARN  
NEW MEXICO STATE UNIVERSITY  
DEPARTMENT OF PHYSICS  
LAS CRUCES, NM 88003

MICHAEL HEDLIN  
UNIVERSITY OF CALIFORNIA, SAN DIEGO  
SCRIPPS INSTITUTION OF OCEANOGRAPHY IGPP, 0225  
9500 GILMAN DRIVE  
LA JOLLA, CA 92093-0225

DONALD HELMBERGER  
CALIFORNIA INSTITUTE OF TECHNOLOGY  
DIVISION OF GEOLOGICAL & PLANETARY SCIENCES  
SEISMOLOGICAL LABORATORY  
PASADENA, CA 91125

EUGENE HERRIN  
SOUTHERN METHODIST UNIVERSITY  
DEPARTMENT OF GEOLOGICAL SCIENCES  
DALLAS, TX 75275-0395

ROBERT HERRMANN  
ST. LOUIS UNIVERSITY  
DEPARTMENT OF EARTH & ATMOSPHERIC SCIENCES  
3507 LACLEDE AVENUE  
ST. LOUIS, MO 63103

VINDELL HSU  
HQ/AFTAC/TTR  
1030 S. HIGHWAY A1A  
PATRICK AFB, FL 32925-3002

RONG-SONG JIH  
HQ DSWA/PMP/CTBT  
6801 TELEGRAPH ROAD  
ALEXANDRIA, VA 22310-3398

THOMAS JORDAN  
MASSACHUSETTS INSTITUTE OF TECHNOLOGY  
EARTH, ATMOSPHERIC & PLANETARY SCIENCES  
77 MASSACHUSETTS AVENUE, 54-918  
CAMBRIDGE, MA 02139

LAWRENCE LIVERMORE NATIONAL LABORATORY  
ATTN: TECHNICAL STAFF (PLS ROUTE)  
PO BOX 808, MS L-175  
LIVERMORE, CA 94551

LAWRENCE LIVERMORE NATIONAL LABORATORY  
ATTN: TECHNICAL STAFF (PLS ROUTE)  
PO BOX 808, MS L-208  
LIVERMORE, CA 94551

LAWRENCE LIVERMORE NATIONAL LABORATORY  
ATTN: TECHNICAL STAFF (PLS ROUTE)  
PO BOX 808, MS L-202  
LIVERMORE, CA 94551

LAWRENCE LIVERMORE NATIONAL LABORATORY  
ATTN: TECHNICAL STAFF (PLS ROUTE)  
PO BOX 808, MS L-195  
LIVERMORE, CA 94551

LAWRENCE LIVERMORE NATIONAL LABORATORY  
ATTN: TECHNICAL STAFF (PLS ROUTE)  
PO BOX 808, MS L-205  
LIVERMORE, CA 94551

LAWRENCE LIVERMORE NAT'L LABORATORY  
ATTN: TECHNICAL STAFF (PLS ROUTE)  
PO BOX 808, MS L-200  
LIVERMORE, CA 94551

LAWRENCE LIVERMORE NAT'L LABORATORY  
ATTN: TECHNICAL STAFF (PLS ROUTE)  
PO BOX 808, MS L-221  
LIVERMORE, CA 94551

THORNE LAY  
UNIVERSITY OF CALIFORNIA, SANTA CRUZ  
EARTH SCIENCES DEPARTMENT  
EARTH & MARINE SCIENCE BUILDING  
SANTA CRUZ, CA 95064

ANATOLI L. LEVSHIN  
DEPARTMENT OF PHYSICS  
UNIVERSITY OF COLORADO  
CAMPUS BOX 390  
BOULDER, CO 80309-0309

JAMES LEWKOWICZ  
WESTON GEOPHYSICAL CORP.  
325 WEST MAIN STREET  
NORTHBORO, MA 01532

LOS ALAMOS NATIONAL LABORATORY  
ATTN: TECHNICAL STAFF (PLS ROUTE)  
PO BOX 1663, MS F659  
LOS ALAMOS, NM 87545

LOS ALAMOS NATIONAL LABORATORY  
ATTN: TECHNICAL STAFF (PLS ROUTE)  
PO BOX 1663, MS F665  
LOS ALAMOS, NM 87545

LOS ALAMOS NATIONAL LABORATORY  
ATTN: TECHNICAL STAFF (PLS ROUTE)  
PO BOX 1663, MS D460  
LOS ALAMOS, NM 87545

LOS ALAMOS NATIONAL LABORATORY  
ATTN: TECHNICAL STAFF (PLS ROUTE)  
PO BOX 1663, MS C335  
LOS ALAMOS, NM 87545

GARY MCCARTOR  
SOUTHERN METHODIST UNIVERSITY  
DEPARTMENT OF PHYSICS  
DALLAS, TX 75275-0395

KEITH MCLAUGHLIN  
CENTER FOR MONITORING RESEARCH (SAIC)  
1300 N. 17TH STREET, SUITE 1450  
ARLINGTON, VA 22209

BRIAN MITCHELL  
DEPARTMENT OF EARTH & ATMOSPHERIC SCIENCES  
ST. LOUIS UNIVERSITY  
3507 LACLEDE AVENUE  
ST. LOUIS, MO 63103

RICHARD MORROW  
USACDA/IVI  
320 21ST STREET, N.W.  
WASHINGTON DC 20451

JOHN MURPHY  
MAXWELL TECHNOLOGIES  
11800 SUNRISE VALLEY DRIVE SUITE 1212  
RESTON, VA 22091

JAMES NI  
NEW MEXICO STATE UNIVERSITY  
DEPARTMENT OF PHYSICS  
LAS CRUCES, NM 88003

ROBERT NORTH  
CENTER FOR MONITORING RESEARCH  
1300 N. 17th STREET, SUITE 1450  
ARLINGTON, VA 22209

OFFICE OF THE SECRETARY OF DEFENSE  
DDR&E  
WASHINGTON DC 20330

JOHN ORCUTT  
INSTITUTE OF GEOPHYSICS AND PLANETARY PHYSICS  
UNIVERSITY OF CALIFORNIA, SAN DIEGO  
LA JOLLA, CA 92093

PACIFIC NORTHWEST NATIONAL LABORATORY  
ATTN: TECHNICAL STAFF (PLS ROUTE)  
PO BOX 999, MS K6-48  
RICHLAND, WA 99352

PACIFIC NORTHWEST NATIONAL LABORATORY  
ATTN: TECHNICAL STAFF (PLS ROUTE)  
PO BOX 999, MS K6-40  
RICHLAND, WA 99352

PACIFIC NORTHWEST NATIONAL LABORATORY  
ATTN: TECHNICAL STAFF (PLS ROUTE)  
PO BOX 999, MS K6-84  
RICHLAND, WA 99352

PACIFIC NORTHWEST NATIONAL LABORATORY  
ATTN: TECHNICAL STAFF (PLS ROUTE)  
PO BOX 999, MS K5-12  
RICHLAND, WA 99352

FRANK PILOTTE  
HQ AFTAC/TT  
1030 S. HIGHWAY A1A  
PATRICK AFB, FL 32925-3002

KEITH PRIESTLEY  
DEPARTMENT OF EARTH SCIENCES  
UNIVERSITY OF CAMBRIDGE  
MADINGLEY RISE, MADINGLEY ROAD  
CAMBRIDGE, CB3 0EZ UK

JAY PULLI  
BBN SYSTEMS AND TECHNOLOGIES, INC.  
1300 NORTH 17TH STREET  
ROSSLYN, VA 22209

DELAINE REITER  
SENCOM CORP.  
73 STANDISH ROAD  
WATERTOWN, MA 02172

PAUL RICHARDS  
COLUMBIA UNIVERSITY  
LAMONT-DOHERTY EARTH OBSERVATORY  
PALISADES, NY 10964

MICHAEL RITZWOLLER  
DEPARTMENT OF PHYSICS  
UNIVERSITY OF COLORADO  
CAMPUS BOX 390  
BOULDER, CO 80309-0309

DAVID RUSSELL  
HQ AFTAC/TTR  
1030 SOUTH HIGHWAY A1A  
PATRICK AFB, FL 32925-3002

CHANDAN SAIKIA  
WOODWARD-CLYDE FEDERAL SERVICES  
566 EL DORADO ST., SUITE 100  
PASADENA, CA 91101-2560

SANDIA NATIONAL LABORATORY  
ATTN: TECHNICAL STAFF (PLS ROUTE)  
DEPT. 5704  
MS 0979, PO BOX 5800  
ALBUQUERQUE, NM 87185-0979

SANDIA NATIONAL LABORATORY  
ATTN: TECHNICAL STAFF (PLS ROUTE)  
DEPT. 9311  
MS 1159, PO BOX 5800  
ALBUQUERQUE, NM 87185-1159

SANDIA NATIONAL LABORATORY  
ATTN: TECHNICAL STAFF (PLS ROUTE)  
DEPT. 5704  
MS 0655, PO BOX 5800  
ALBUQUERQUE, NM 87185-0655

SANDIA NATIONAL LABORATORY  
ATTN: TECHNICAL STAFF (PLS ROUTE)  
DEPT. 5736  
MS 0655, PO BOX 5800  
ALBUQUERQUE, NM 87185-0655

THOMAS SERENO JR.  
SCIENCE APPLICATIONS INTERNATIONAL  
CORPORATION  
10260 CAMPUS POINT DRIVE  
SAN DIEGO, CA 92121

AVI SHAPIRA  
SEISMOLOGY DIVISION  
THE INSTITUTE FOR PETROLEUM RESEARCH AND  
GEOPHYSICS  
P.O.B. 2286 NOLON 58122 ISRAEL

ROBERT SHUMWAY  
410 MRAK HALL  
DIVISION OF STATISTICS  
UNIVERSITY OF CALIFORNIA  
DAVIS, CA 95616-8671

DAVID SIMPSON  
IRIS  
1200 NEW YORK AVE., NW  
SUITE 800  
WASHINGTON DC 20005

JEFFRY STEVENS  
MAXWELL TECHNOLOGIES  
8888 BALBOA AVE.  
SAN DIEGO, CA 92123-1506

BRIAN SULLIVAN  
BOSTON COLLEGE  
INSITUTE FOR SPACE RESEARCH  
140 COMMONWEALTH AVENUE  
CHESTNUT HILL, MA 02167

TACTEC  
BATTELLE MEMORIAL INSTITUTE  
505 KING AVENUE  
COLUMBUS, OH 43201 (FINAL REPORT)

NAFI TOKSOZ  
EARTH RESOURCES LABORATORY, M.I.T.  
42 CARLTON STREET, E34-440  
CAMBRIDGE, MA 02142

LAWRENCE TURNBULL  
ACIS  
DCI/ACIS  
WASHINGTON DC 20505

GREG VAN DER VINK  
IRIS  
1200 NEW YORK AVE., NW  
SUITE 800  
WASHINGTON DC 20005

FRANK VERNON  
UNIVERSITY OF CALIFORNIA, SAN DIEGO  
SCRIPPS INSTITUTION OF OCEANOGRAPHY IGPP, 0225  
9500 GILMAN DRIVE  
LA JOLLA, CA 92093-0225

JILL WARREN  
LOS ALAMOS NATIONAL LABORATORY  
GROUP NIS-8  
P.O. BOX 1663  
LOS ALAMOS, NM 87545 (5 COPIES)

RU SHAN WU  
UNIVERSITY OF CALIFORNIA SANTA CRUZ  
EARTH SCIENCES DEPT.  
1156 HIGH STREET  
SANTA CRUZ, CA 95064

JAMES E. ZOLLWEG  
BOISE STATE UNIVERSITY  
GEOSCIENCES DEPT.  
1910 UNIVERSITY DRIVE  
BOISE, ID 83725

TERRY WALLACE  
UNIVERSITY OF ARIZONA  
DEPARTMENT OF GEOSCIENCES  
BUILDING #77  
TUCSON, AZ 85721

DANIEL WEILL  
NSF  
EAR-785  
4201 WILSON BLVD., ROOM 785  
ARLINGTON, VA 22230

JIAKANG XIE  
COLUMBIA UNIVERSITY  
LAMONT DOHERTY EARTH OBSERVATORY  
ROUTE 9W  
PALISADES, NY 10964